



Transparent Heaters: A Review

Dorina T. Papanastasiou, Amélie Schultheiss, David Muñoz-Rojas, Caroline Celle, Alexandre Carella, Jean-Pierre Simonato, Daniel Bellet

► To cite this version:

Dorina T. Papanastasiou, Amélie Schultheiss, David Muñoz-Rojas, Caroline Celle, Alexandre Carella, et al.. Transparent Heaters: A Review. Advanced Functional Materials, 2020, pp.1910225. 10.1002/adfm.201910225 . hal-02513426

HAL Id: hal-02513426

<https://hal.science/hal-02513426>

Submitted on 7 Jan 2021

HAL is a multi-disciplinary open access archive for the deposit and dissemination of scientific research documents, whether they are published or not. The documents may come from teaching and research institutions in France or abroad, or from public or private research centers.

L'archive ouverte pluridisciplinaire **HAL**, est destinée au dépôt et à la diffusion de documents scientifiques de niveau recherche, publiés ou non, émanant des établissements d'enseignement et de recherche français ou étrangers, des laboratoires publics ou privés.

Transparent Heaters: A Review

Dorina T. Papanastasiou, Amélie Schultheiss, David Muñoz-Rojas*, Caroline Celle, Alexandre Carella, Jean-Pierre Simonato*, Daniel Bellet*

* corresponding authors

Keywords: transparent electrode, Joule heating, film heater, composite, stability

D.T. Papanastasiou, Dr. D. Muñoz-Rojas, Pr. D. Bellet

Univ. Grenoble Alpes, CNRS, Grenoble INP, LMGP, F- 38000 Grenoble, France

Email : david.munoz-rojas@grenoble-inp.fr; daniel.bellet@grenoble-inp.fr

A. Schultheiss, Dr. C. Celle, Dr. A. Carella, Dr. J.-P. Simonato

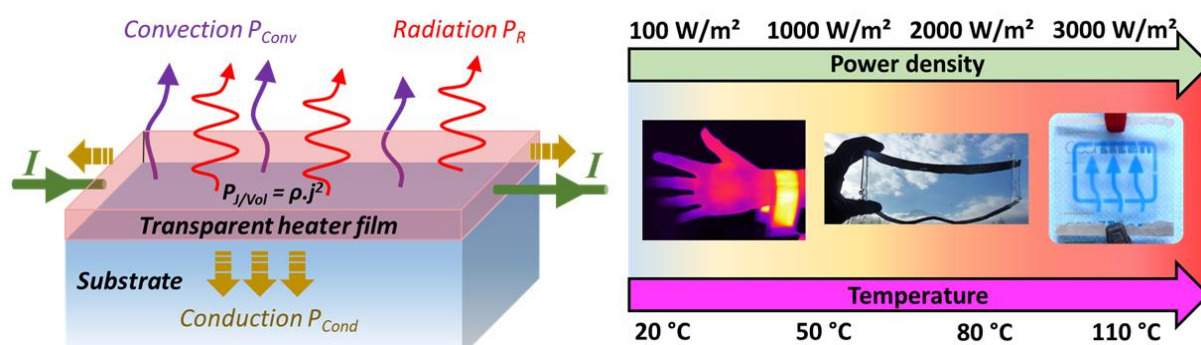
Univ. Grenoble Alpes, CEA, LITEN, DTNM, 17 avenue des Martyrs, F-38054 Grenoble, France

Email: jean-pierre.simonato@cea.fr

Short summary

Transparent heaters (TH) have attracted intense attention from both scientific and industrial actors due to the key role they play in many technologies, including smart windows, deicers, defoggers, displays, actuators and sensors. While transparent conductive oxides have dominated the field for the past five decades, a new generation of THs based on nanomaterials has led to new paradigms in terms of applications and prospects in the past years. Here we will review the most recent developments and strategies to improve the properties, stability and integration of these new THs.

Graphical abstract



1 Introduction

Transparent heaters (THs) are visually transparent devices that contain electrically conductive layers. When an electrical current flows across the transparent heater, it generates heat thanks to the Joule effect. This heat can be efficiently used in many devices. Consequently, numerous applications are concerned by THs, and the associated TH market is growing fast, comprising many types of devices (smart windows, deicers, defoggers, displays, thermotherapy pads, sensors...) for different industrial sectors (transport, buildings, healthcare, sport...). For instance, THs can provide the warmth required to extend the operating temperature of liquid crystal displays (LCDs) in cold environments or can increase the temperature for anti-fogging systems, anti-icing, deicing of optics and optical displays (very useful for transportation). Other applications include the heating of specific industrial processes, of microfluidic chips, of kiosks and handheld devices.^[1] Display technology and smart windows (used in transport or for interior architecture) are among the fastest growing markets related to THs. Importantly, defrosting windows in airplanes enables high-altitude flying.^[2] Smart windows can reduce energy loss in buildings, which currently account for over 40% of the energy consumed. This works thanks to special functional coatings which can regulate solar energy in response to heat (thermochromic material).^[3,4] This heat can be generated by THs within smart windows.^[5] While the required optical transparency depends upon the specific application, in this review we have considered THs having an optical transparency of at least 50%.

The fast control of temperature via the applied current or voltage makes THs a generally better choice when compared to conventional heating elements. This is enabled by the small thermal inertia of thin TH films.

The only technology used for TH before 1995 was based on transparent conductive oxides (TCOs), which were also broadly used as transparent electrodes in many applications including photovoltaics^[6], smart windows^[7], efficient lighting^[8] or displays.^[2,7,9,10] The three main TCO

materials are indium tin oxide (ITO)^[11–13], the most well-known and used TCO, fluorine-doped tin oxide (FTO)^[14,15] and aluminum-doped zinc oxide (AZO).^[16–19] TCOs are generally degenerately-doped n-type semiconductors which exhibit a high electrical conductivity of 10^3 – 10^4 S/cm.^[9] They are often fabricated as thin films of approximately 300 nm thickness in order to show high transparency (~90%). While TCOs can exhibit good or even excellent performances in terms of the trade-off between electrical conductivity and optical transparency in the visible range, their two main drawbacks concern their non-flexibility (due to their ceramic nature) and their intrinsic low optical transmittance in the near-infrared (NIR) spectrum due to plasmonic absorption^[13,20]. Therefore, great attention has been devoted to flexible and transparent electrodes^[21] or heaters for three main reasons: i/ the emergence of new-generation devices having flexible or nonplanar substrates, ii/ the potential scarcity of indium for ITO and iii/ the lack of transparency in the NIR. For some applications, even flexibility is not sufficient since stretchability could be a prerequisite, like for the integration of THs within wearable electronics.^[22] For example, flexible but also stretchable THs can be used in thermotherapy^[23,24], a popular treatment in physiotherapy which is particularly useful for the treatment of joint injuries and pain. For such applications, THs should also be soft and thin (and therefore light) so that comfort is not compromised.

It is also worth noting that even for non-flexible devices, we are looking for high throughput fabrication methods which are compatible with an economically viable technology, like the roll-to-roll (R2R) process. Indeed, R2R is a fast processing method associated with little or no loss of material, and which requires that both substrate and active layers be flexible.^[25,26] Therefore TCOs themselves are not compatible with such low-cost methods, except when integrated as very thin films with other materials such as oxides or metals, and thus alternative THs need to be developed.

Several emerging materials have recently been investigated for TH applications, including carbon-based nanomaterials, and mainly carbon nanotubes (CNT)^[27] and graphene^[28]. These

new materials are rather cheap and abundant and could therefore follow the fast-growing industrial demand. Moreover, THs made of these building blocks are flexible and can be processed in solution. In parallel, since 2009 metallic nanowire (MNW) networks have started to be more systematically investigated, notably following the seminal articles on: i) the synthesis of MNWs by the groups of Sun^[29] and Wiley^[30–32], among others; ii) the study of the physical properties of MNW networks by Coleman's group^[33,34]; and iii) the integration into efficient devices by Pei's group.^[35,36] Several recent reviews have summarized the main properties, challenges and integration of MNW networks^[20,37–41]. The first article showing that silver nanowire (AgNW) networks could act as efficient THs was published in 2012 by Simonato's group.^[42] As shown below, this ground-breaking paper was followed by many other studies focused on the physics of THs based on MNW networks^[43], on the integration of this type of TH into various devices^[22,44,45] as well as on a better understanding and enhancement of these THs.^[46–48] More recently, great progress has also been reported on conductive polymers which can now be considered as very efficient materials for THs.^[49] For instance, Simonato's group^[50] has also reported the very first efficient TH exclusively based on thin films of conducting polymers.

While many reports show an intense research activity on each of these TH technologies, there is also active research on multi-layered materials or nanocomposites which can combine the advantages of different materials. For instance, Ko et al. showed that high-performance and flexible R2R sputtered ITO/Ag/ITO multilayers can exhibit a high optical transmittance (88.2 %), low sheet resistance ($3 \Omega/\text{sq}$) and can be efficiently integrated in a TH device.^[51] Similarly, Park et al. reported that ITO/Cu/ITO multilayer materials can also show promising electrical and optical performances and good TH integration.^[52] The different technologies will be thoroughly discussed in section 3 of this review.

The main scientific and technological features associated with THs can be listed as follows: thermal response time, steady state temperature, homogeneity, mechanical properties (under

bending and/or stretching tests), cycling/thermal/electrical/environmental stability including ageing, electrical and optical properties, fabrication process of the TH (the temperature being a potential issue for some applications), the material used, TH size and, finally, the overall fabrication cost, including both materials and processes.

Expected requirements associated to the TH can drastically differ depending on the targeted applications. For instance, smart windows, windscreens or displays require that the THs and their associated substrates exhibit high optical clarity, i.e. high optical transparency and low haziness (defined as the ratio between diffuse and total transmittance of light). Optical engineering related to THs notably concerns matching the optical index to improve reflection and transmission properties in the desired wavelength band (i.e. visible and/or NIR spectra).

The thermal response time is also a crucial parameter. The targeted steady state temperature of THs can be very different depending on the application. For smart windows applications, the thermochromic transition (i.e. metal-insulator transition) associated to hybridized VO₂/Graphene is about 60 °C^[53]. A low temperature is generally required for de-icing or defogging uses (below 30 °C). Some other applications need much higher temperatures, like fast defrosting in automotive or for gas sensors (see section 4 of this review). In these cases the chosen material for the TH should exhibit a very good thermal and electrical stability. TH stability can be a serious issue, especially when numerous cycles are foreseen during the lifetime of the device. It is worth noting that stability is related to several other aspects, including potential cycling/thermal/time/electrical/environmental issues. These crucial aspects will also be addressed in this review. The homogeneity of THs plays a key role for many applications. For example, this is essential for eye comfort when THs are used in windscreens, while hot spots can potentially be at the origin of the TH degradation.^[54]

As for all industrial devices, cost is overwhelmingly important to propel the commercialization and large industrial production (e.g., adding a TH within a ski or motorcycle helmet visor should only cost a few euros), with only a handful of exceptions like spatial applications.

This review is organized as follows. The main physical mechanisms associated with THs are presented in part 2.1, as well as simple physical models developed to better understand TH behavior. The main experimental methods currently used to investigate and explore the critical properties of THs will be described in part 2.2. Stability issues are thoroughly considered in section 2.3, from their physical origin to the solution for stability enhancement. Each TH technology (i.e. associated to specific material) is detailed. A thorough comparison and critical discussion of the different active materials are reported in section 3. Part 4 focuses on the integration of THs in different devices with specific associated requirements and performances. Finally, part 5 gives an overview of the main challenges that lie ahead and the main prospects related to THs in terms of better physical understanding, better performances and stability, as well as their future integration into industrial devices.

2 Principle of transparent heaters (THs):

2.1 Introduction to the thermal physics of THs

As stated above, THs are based on the Joule effect. Joule's law, experimentally demonstrated by J.P. Joule (1818-1889), states that when an electrical current I crosses a homogeneous conductive material with an electrical resistance R , the amount of heat released is equal to I^2R per unit of time. The power dissipated in the material is directly related to the achieved steady-state temperature, through a balance between the Joule effect and heat loss. These thermal losses are schematically presented in **Figure 1a**: they correspond to the total heat transfer from the TH and are associated to three main physical origins: i/ thermal conduction to the substrate or through any conducting connections, ii/ convection to the surrounding air and iii/ radiation emitted from the hot surfaces. Figure 1b exhibits some TH applications (medical, defogging, thermochromic), with characteristic values of temperature and areal power density. Several TH

technologies do exist, and their corresponding temperature ranges are roughly presented in Figure 1b in dashed lines. That being said, these temperatures depend upon the TH fabrication process and the experimental conditions under which the TH is used for a given application. Figure 1c reports the typical performance of the main TH technologies in terms of optical transparency Tr (the substrate transparency being subtracted) versus the electrical sheet resistance R_{sh} . The ongoing efforts by the community are focused on fabricating THs which are, simultaneously, as transparent and as conductive as possible (i.e. with a low sheet resistance). There is a trade-off between these two properties since for a homogeneous transparent conductive layer, the thicker the layer the lower the sheet resistance, but also the lower the optical transparency. This trade-off can be approached thanks to a figure of merit (FoM). For transparent electrodes (TEs), two main figures of merit have been proposed thus far. The first one was derived by Haacke et al. in 1976 who proposed to consider the ratio between the 10th power of the total optical transmittance Tr divided by the sheet resistance R_{sh} : Tr^{10}/R_{sh} .^[55] Haacke's FoM is very often used when dealing with transparent electrodes applications (such as photovoltaic or displays) but also for TH investigations. Another figure of merit was later derived by Coleman's group, who considered the ratio between the electrical conductivity and the optical conductivity (equal to the optical absorption coefficient divided by the free space impedance Z_0 (the latter is equal to: $1/(c \cdot \epsilon_0)$, where c is the speed of light and ϵ_0 the permittivity of free space).^[33] Both these FoMs are used as guides for comparing TEs and THs. Although they make physical sense for homogeneous and continuous thin layers, they have to be considered with more caution for non-homogeneous layers **such as CNT networks, metallic grids, or MNW networks**. For example, in the case of very long 1D conductive objects, a very high FoM could be obtained even if it does not present high homogeneity or usefulness for device integration. Different values of Haacke's FoM are plotted in Figure 1c, showing that there is a good variety of TH technologies that exhibit very good electrical and optical properties, and that are therefore well suited for TH integration. Other parameters of TH

applications have to be taken in consideration as well; for instance, graphene appears to be less conductive and therefore it will not be used alone for fast TH operation, as discussed in section 3.5.4. Chen et al. reported recently copper grid TH with an outstanding Haacke's FoM over $7820 \cdot 10^{-3} \Omega/\text{sq}$ (see Figure 1c), and a fast heating rate at low voltage.^[56] This clearly illustrates the efficiency of such technology as TH.

Figure 1d exhibits the time-dependent temperature of graphene-based THs with two different doping agents, and an ITO-based TH for the sake of comparison.^[57] During the "ON" voltage state, the classical time-dependent behavior shows a linear increase at first, followed by a saturation to a steady-state temperature. The three different materials used have different initial R_{sh} and therefore exhibit different steady-state temperatures for the same applied voltage (here 12 volts).^[57]

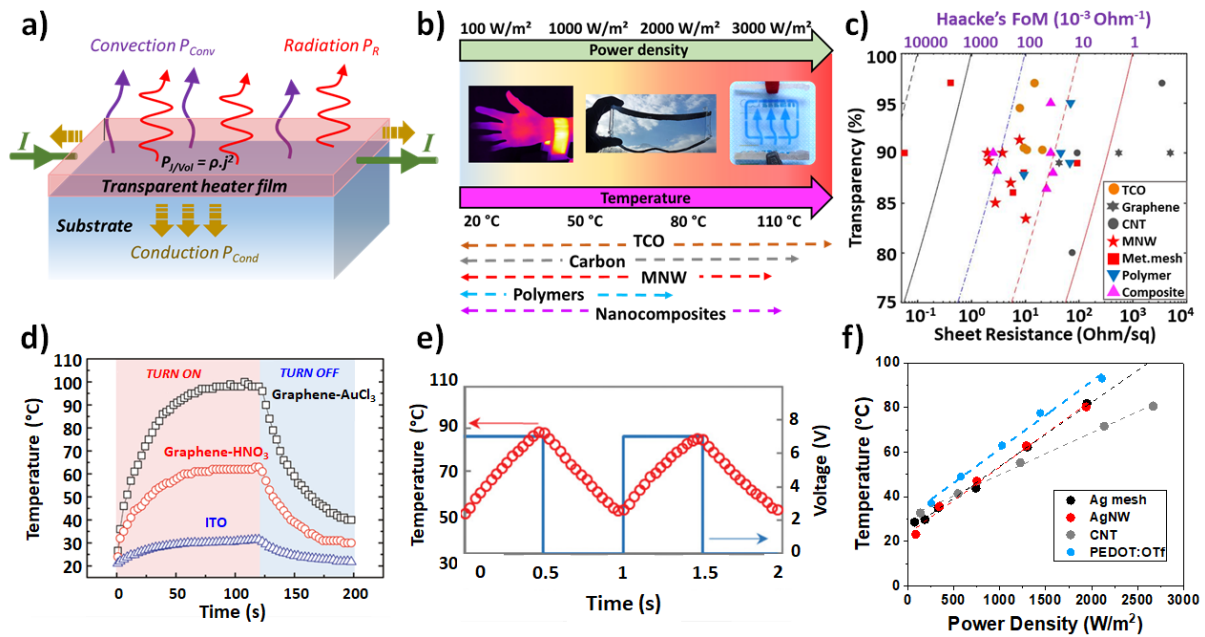


Figure 1. Main features of THs. a) Schematic of a TH: the thin TH is crossed by an electrical current, leading to heat production thanks to the Joule effect. A steady state is reached once this generated heat is equal to the sum of the heat losses shown with different colors. b) Main application domains of THs versus areal power density or temperature required. The arrows below represent roughly the typical maximum steady-state temperatures for the main TH technologies. c) Optical transparency versus sheet resistance diagram for different TH technologies based on: transparent conductive oxides (TCO)^[14,33,58–60], carbon nanotubes (CNT)^[27,33,61], graphene^[57,62,63], metallic nanowire (MNW) networks^[64–70], metallic grids-meshes^[56,71–76], conductive polymers^[49,50,77,78], nanocomposites^[22,48,51,79–81]. The dashed lines correspond to different values of Haacke's FoM: 10000, 1000, 100, 10, 1 times $10^{-3} \Omega/\text{sq}$. d) Time-dependence of temperature for graphene-based and ITO-based THs, showing the presence of a

transitional and steady-state regimes. The optical transmittance of ITO is 95.6% and those of graphene-based THs are 88.5% and 87.5%, respectively for AuCl₃ and HNO₃ doping protocols. Reproduced with permission.^[57] Copyright 2011, American Chemical Society. e) Time-dependence of temperature during voltage cycling showing a very fast thermal response when a TH (here composed of a carbon nanotube network) is deposited on a very thin substrate (12 Ω.m thick mica)^[61], in agreement with eq.4. Reproduced with permission.^[61] Copyright 2017, AIP Publishing f) Areal power density dependence of the stabilized temperatures measured for different TH technologies: a linear dependency is generally observed at least for temperatures lower than 100 °C (data for TH based on AgNW^[46], Ag mesh^[82], CNT^[61], PEDOT:OTf^[50]). The slope appears rather similar for the different TH technologies.

Sorel et al.^[43] gave a comprehensive and thorough description of the theory of Joule heating in a TH in general, and focused in more detail on THs based on silver nanowire networks. But similar approaches can also be found for other types of TH technologies, such as graphene^[83]. In general, the main key parameters for a TH are the steady-state temperature T_{stab} , and the time needed to approach T_{stab} . Most THs are supposed to reach the desired temperature by using a rather low voltage (< 12 V for standard uses) and after a relatively short response time (i.e. from a few seconds to a few minutes).

Considering that the temperature is uniform across the whole TH, the energy balance at a given time t can be written as follows (conduction losses due to external parts of the system are neglected)^[43]:

$$I^2 R = (m_1 C_1 + m_2 C_2) \frac{dT(t)}{dt} + A(h_1 + h_2)(T(t) - T_0) + \sigma A(\varepsilon_1 + \varepsilon_2)(T(t)^4 - T_0^4) \quad (1)$$

For each parameter, the indexes 1 and 2 correspond to the TH and the substrate, respectively; the instantaneous sample temperature is $T(t)$, while the ambient temperature is T_0 . In eq. 1, the term on the left is the dissipated heat per unit of time. The first term on the right is the sum of the heat per unit of time associated to the TH and to the substrate (transported via thermal conduction). This heat is responsible for the temperature elevation of the sample through the specific heat capacities C , with m_1 and m_2 being the mass of the TH itself and of the substrate respectively. The second term represents the heat losses per unit of time by convection, with h_1 and h_2 being the convective heat-transfer coefficients and A the film area, assumed to be equal to the substrate area. Finally, the third term stands for the heat losses by radiation, where σ is

the Stefan-Boltzmann constant and ε_1 and ε_2 the emissivity of the TH and of the substrate, respectively. Considering small temperature rises, allowing a linear expansion of eq.1 (the non-linear term associated to radiation losses being neglected) and with the hypothesis that the TH has a much lower heat capacity compared to the substrate ($m_1 C_1 \ll m_2 C_2$), the energy balance then has the following analytical formula^[43]:

$$\Delta T(t) = T(t) - T_0 \approx \frac{1}{\alpha} \frac{I^2 R}{A} \left[1 - \exp\left(-\frac{\alpha}{m_2 C_2 / A} t\right) \right] \quad (2)$$

where α is the heat transfer constant, which takes into account the parameters of heat losses expressed as follows:

$$\alpha = (h_1 + h_2) + 4(\varepsilon_1 + \varepsilon_2)\sigma T_0^3 \quad (3)$$

Eq. (2) shows that there is a transitional state for a short time, i.e. for a small t compared to the characteristic time τ , while for times much larger than τ , a steady-state temperature is achieved and the saturation temperature is then equal to: $\frac{1}{\alpha} \frac{I^2 R}{A}$. The expression of τ is given by:

$$\tau = \frac{m_2 C_2}{\alpha A} = \frac{\rho_{sub} t_{sub} C_{sub}}{\alpha} \quad (4)$$

where ρ_{sub} , t_{sub} and C_{sub} are, respectively, the density, thickness and specific heat (per unit of volume) of the substrate. After a time $t=\tau$, the temperature reaches 63% of the saturation temperature. Another characteristic time, called the response time, is also often used in the literature: it is defined as the time required to reach 90% of the steady-state temperature, its value being equal to $\ln(0.1) \tau$, i.e. 2.3τ .

The existence of both transitional and steady-state temperatures is validated by experimental observations, as shown in Figure 1d. τ is generally found to be between 10 and a few hundreds of seconds for the great majority of experimental reports. As a first approximation, this value does not depend much on the material that composes the TH. Accordingly, this range of τ values was observed for THs composed of AgNW networks^[45], CNT networks^[27], TCO^[84], conductive polymers^[50], electrospun nanofibers^[76,85] or graphene^[86]. For efficient THs, the τ

value mainly depends on the characteristics of the substrate: the thinner the substrate, the shorter the characteristic time. For example, the steady state temperature was achieved within 10 s when graphene films were deposited on a 50 μm thick polyimide (PI) film, while it took 80 s using 1 mm thick quartz as a substrate^[86]. This is coherent with equation (4). For very small substrate thicknesses τ can be very short too. Kim et al. demonstrated, as depicted in Figure 1e, that the use of single-walled carbon nanotubes (SWNTs) on a very thin polymeric substrate (12 μm thick) leads to a fast response: a temperature of 100 °C could be reached within 1 s with an input voltage of 7 V^[61]. Ke et al. used the same idea and obtained similar results on Al-doped zinc oxide deposited on 25, 65 and 100 micron thick mica substrates^[60].

According to equation (2), the steady-state temperature elevation, ΔT_{stab} , appears to be directly proportional to the applied areal power density and, as a first approximation, does not drastically depend on the TH type. Figure 1f presents the areal power density dependence of the stabilized temperatures measured for different TH technologies and demonstrates this trend. A linear dependency is generally observed (data for TH based on AgNW^[46], Ag mesh^[82], CNT^[61], PEDOT:OTf^[50]) at least for temperatures lower than 100 °C. The slope appears rather similar for the different TH technologies. These slopes depend on the different thermal losses which vary also according to the surface properties of the TH thin film and the substrate^[60]. The different thermal losses are convection, infra-red radiation and thermal conduction outside the TH itself (through the TH substrate/holder or the electrical connecting wires). Several investigations have tried to estimate the contribution of each thermal loss mechanism, which in turn depends on the substrate, temperature and TH material used. Sorel et al. discussed their dependence versus AgNW network density and showed that there is an increase in convection losses for denser networks which is caused by a higher surface roughness and higher internal area^[43]. The thermal conductivity and thickness of the substrate play a key role for thermal conduction losses. In general, radiative losses are negligible compared to conductive and/or convective losses, at least at low temperatures. Conversely, for high temperatures the radiative

losses can contribute significantly, and the linear approximation is not valid anymore. The linear dependence between the steady-state temperature and the areal power density is therefore not valid anymore. For instance, Ji et al. reported the fabrication of highly-stable THs based on ultra-long copper nanofiber networks that can be heated up to 800 °C^[87]. In this case, the steady-state temperature versus heat power does not show a linear dependence in the entire temperature range (as reported in the supplementary information of Ji et al).^[87] Interestingly, comparing the same TH in air and in vacuum conditions allows us to disentangle convective losses from conduction and radiation losses. Lagrange et al. performed similar experiments on AgNW networks deposited on glass^[46]: in air and in vacuum the temperature elevations increase linearly with the areal power density, but with different slopes. The difference between these two slopes (23.8 and 28.1 W.m⁻².K⁻¹ in vacuum and in air, respectively) allows us to deduce convective thermal losses: $h_{convective}$ could be estimated as 4.3 W.m⁻².K⁻¹.^[46] Another interesting discussion was also reported by Kang et al. regarding the influence of the CNT film density on the different types of heat-transfer losses.^[88] This can be understood through the heat-transfer losses that are directly related to the porous morphology of the CNT network.^[88] One can already classify THs into two different categories: on one side, the homogeneous layers like transparent conductive oxides (TCO), graphene, multilayers (composed of a thin metal surrounded by oxide layers) or conductive polymer films; on the other side, networks composed of carbon nanotubes, metallic nanowires, meshes and fibers. While the first category is supposed to heat homogeneously the whole TH surface, the second category can induce local heating due to its non-homogeneous nature, if heat does not diffuse along both the active material and/or the substrate quickly enough^[54]. These hotspots can induce local degradation within the TH and are therefore an issue to be dealt with. Das et al. investigated scaling in self-heated percolating networks and concluded that hotspot clustering appears to be a mechanism analogous to crystallization physics^[89]. The potential presence of hotspots will be discussed in this review, since their presence can lead to TH instability. In brief, the thermal stability of the

TH can be limited to the TH itself (e.g. degradation of the conductive polymer or morphological instability of silver nanowires^[90]) or to the substrate as well. Specifically, for polymeric substrates or low-quality glass substrates, heating can lead to local melting of the polymer or cracking of the glass substrate. For instance, Maize et al. recently used the thermo-reflectance technique to observe “super-Joule” heating hotspots in graphene and AgNW networks^[91], while the latter would have appeared homogeneous using a macroscopic infrared technique. This emphasizes the importance of spatial resolution in temperature observations and this point, among others, is discussed in the following section devoted to the experimental methods used to investigate the main properties of THs. It is worth mentioning that industrial needs require that a good heater should exhibit uniform thermal distribution over the heating area and achieve the target temperature often with a low voltage (i.e. below 12 V).

2.2 Experimental methods to investigate the main properties of THs

This section aims at introducing the main properties of THs and the experimental methods used to investigate them. Generally speaking, a TH is considered efficient if it shows low electrical resistance, high optical transmittance at least in the visible range, a controllable heating rate, good stability and a low haze factor. We will first focus on electrical resistance and optical transparency. Then, we will present the methods to investigate the basic operating modes of a TH, the heating performances, which are particularly studied by temperature measurements at different length scales. This enables us to measure characteristic features like the heating rate and the relationship between temperature and areal heat power density. Regarding the temperature, there are several ways to measure it through direct contact or contactless means, and with different spatial resolutions, as illustrated below. Since the market appeals prompt research for flexible (or even stretchable) TH, the methods to investigate their mechanical properties are also discussed. Thermal, electrical, humidity and/or mechanical stresses are also

reviewed. Finally, other TH features like haze factor, adhesion and roughness are briefly described, as well as their experimental investigation.

Electrical properties. Electrical resistance is a key property of THs, and is evaluated using several experimental methods. The sheet resistance R_{sh} (in Ω/sq) is traditionally used to characterize uniform thin films, since it provides a direct and local measurement of electrical properties, independent of specimen size. The four-point probe method allows a precise measurement of R_{sh} since it eliminates the contributions of electrical wiring and contacts to the global electrical resistance.^[92] This method is generally performed for emerging **Transparent Conductive Materials (TCMs)** such as thin films or metallic nanowire networks, despite being a direct contact method which can induce local damage. This electrical measurement is very valuable for estimating the electrical homogeneity of a sample by measuring its electrical performance in many different areas. As a first approximation and for a homogeneous layer, R_{sh} is equal to the ratio between electrical resistivity and layer thickness, the latter being often measured by an electronic microscope, a profilometer, Atomic Force Microscopy (AFM) or an ellipsometer. Basic two-point probes can also provide the electrical resistance on samples. In general, two parallel electrodes at opposite sides of the specimen are fabricated using silver inks or metallic layers deposited by evaporation or sputtering. This two-probe method is generally used to follow in-situ the electrical resistance measured during voltage or thermal ramps^[46,90]. For a homogeneous square layer with good electrical conductivity, the 4-probe and 2-probe methods are expected to provide similar results. Another tool to investigate electrical homogeneity is the one-probe electrical mapping, which draws up a cartography of voltage distribution.^[93] **In addition, terahertz spectroscopy has been used for non-contact measurement of the conductance of AgNW networks.**^[94]

Optical properties. A critical feature of THs is their optical transparency. As shown in **Figure 2a**, TCOs like FTO exhibit a very good transparency in the visible spectrum (390 to 700 nm). However, their optical transmittances decreases dramatically in the NIR spectrum due to plasmonic absorption (as described in section 3.1). Emerging TCMs such as metallic grids, or metallic nanowire and CNT networks, allow the incident light to be transmitted through the non-covered empty substrate spaces, and thus they remain transparent to a great extent in the whole VIS-NIR spectrum. The transmittance of an AgNW network is shown in Figure 2a: this network is still very transparent in the NIR region. In the case of THs, most applications are in the visible range, which explains why most reports present only visible light measurements. Total transmission can be measured precisely by UV-visible-NIR spectrophotometry with an integrating sphere, as schematically depicted in Figure 2b. There are also small and handy instruments like tint meters, which provide transparency values at a certain visible wavelength, usually 550 nm (light wavelength for maximum efficiency of human eyes). Generally speaking, the optical transparency is either reported in literature at this wavelength of 550 nm or averaged over a typical range of 370-700 nm (i.e. the visible range), but unfortunately it is not always reported whether authors refer to specular (i.e. direct) or total transmittance. The measurement of diffuse transmission is of crucial importance. It is generally expressed through the haze factor, defined as the ratio between the diffuse and total transmittances (Figure 2b). Figure 2c shows a typical example of a low and a highly diffuse/hazy FTO. The non-hazy FTO is the usual FTO layer deposited on a glass substrate, while the diffuse FTO was fabricated by depositing oxide nanoparticles before FTO deposition^[59,95]. The required haze factor values depend drastically upon the desired application. For displays or window defrosting, low haze values are mandatory. For other applications, however, this is less stringent. Although it is an important characteristic, TH haziness is not often reported, preventing the complete benchmarking of TH technologies. **In the case of AgNW networks, the haze factor is directly proportional to the areal mass density (usually expressed in mg m^{-2}).^[64] Moreover, it has been**

reported that decreasing the diameter or extending the length of AgNWs leads to lower haze factors.^[96,97]

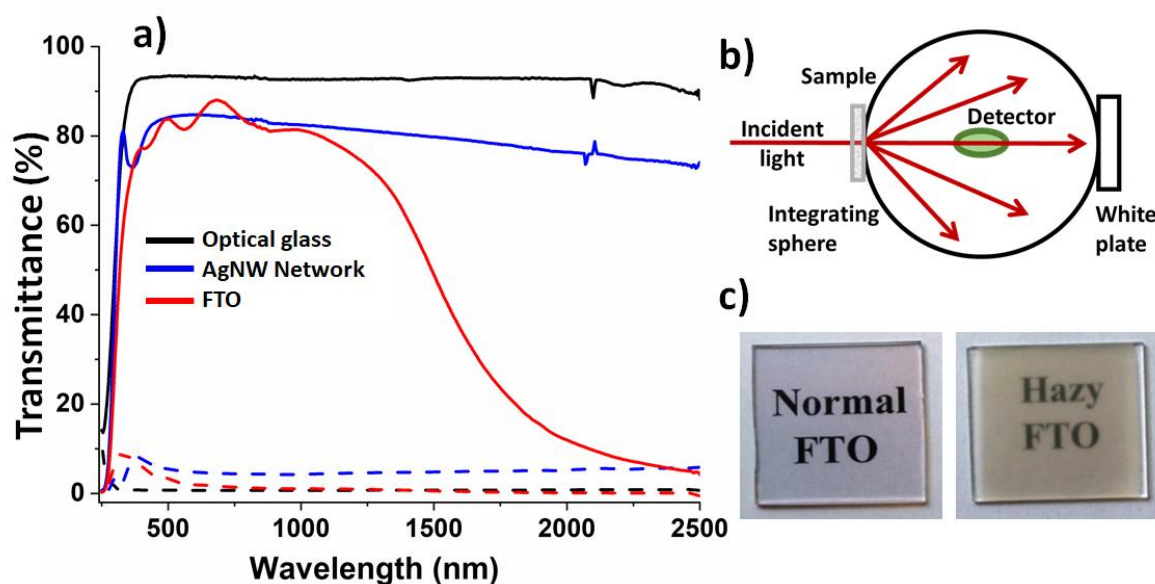
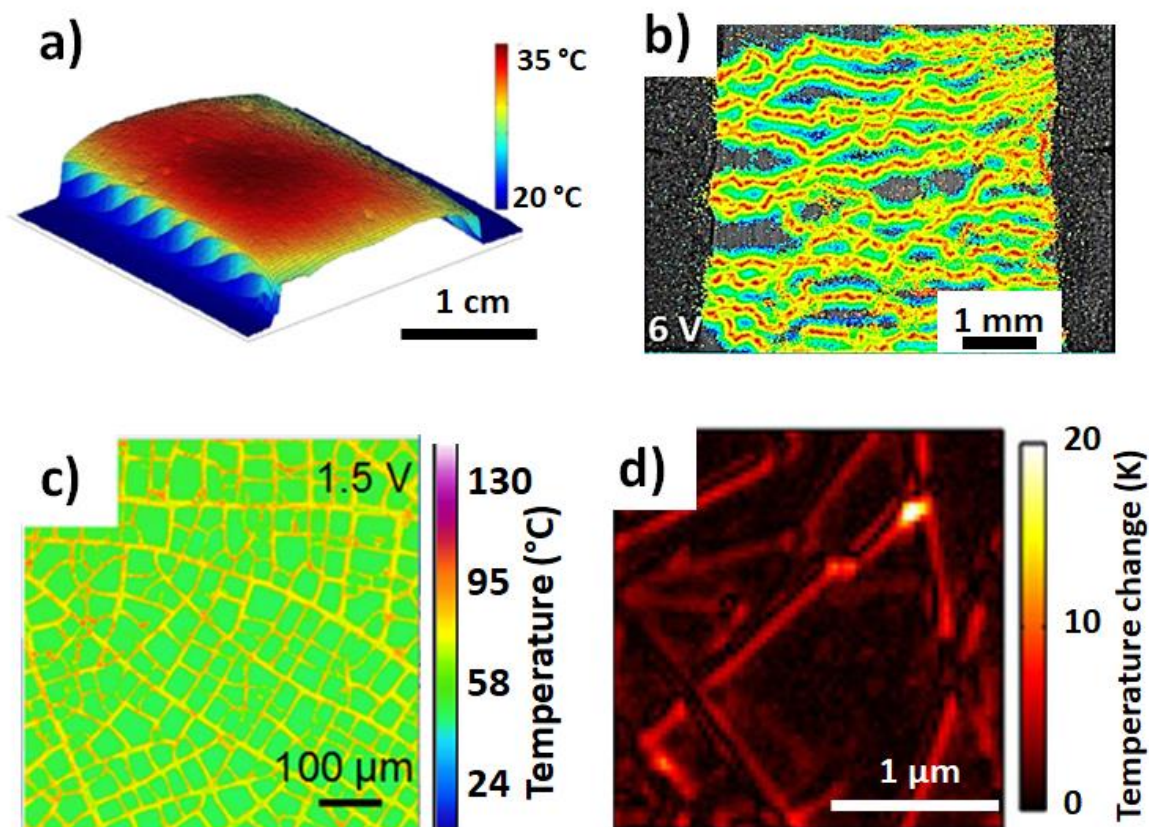


Figure 2. Optical transmittance of transparent heaters (TH). a) Total and diffuse transmittance, shown respectively in continuous and dashed lines, for an AgNW network and an FTO layer deposited on bare optical glass. Both layers have a sheet resistance close to 20 Ω/sq . Metallic nanowire networks are transparent in the NIR region. b) Schematic representation of the spectrophotometer with the integrating sphere. Total (diffuse) transmittance is measured with (without) the white plate to include (exclude) the specular transmittance. c) Pictures of non-hazy (left) and hazy (right) FTO layers on 25x25 mm² glass substrates.

Temperature measurement. The accurate measurement of temperature is essential for the fine characterization of THs. Measurements of the temperature produced by THs as a function of the input voltage or other tuned parameters is expected with high temporal and spatial resolutions. One can calculate and/or define other characteristic properties that were discussed in the previous section 2.1, such as steady-state temperature, heating rate, operating voltage, heat power density, thermal resistance or conductivity, heat transfer coefficient, etc. A common choice for measuring the temperature is the use of a thermocouple, directly connected to the studied sample or device. Thermocouples are cheap and cover a wide range of temperatures. There are several suitable types of thermocouples depending on applications and the temperature ranges.^[98] The most reported thermocouple in the case of THs is the type K

thermocouple. Another way to measure the temperature by direct contact is the use of resistance temperature detectors (RTD) which are based on the increasing electrical resistance of conductors with increasing temperatures. The platinum RTD in particular displays a superior stability and excellent repeatability, but is more expensive than common thermocouples, and has a narrower range of temperature measurement.^[99] Although these types of thermometers are accurate and easy to use, some studies on THs require a precise mapping of the temperature distribution that cannot be performed properly with the sensors described above. Thermal imaging IR cameras detecting radiations in the mid or long-IR range of the electromagnetic spectrum are appropriate. They have become an indispensable experimental tool for specific temperature measurements. The spatial distribution of temperature is an important advantage of IR imaging since it allows the investigation of heating homogeneity, reveals defects that are optically invisible, and moreover it provides the temperature distribution globally in a device and its environment. Radiative temperature measuring is a non-contact method that can be much more convenient when it is hard or impossible to contact with the studied TH. However, IR imaging gives access only to the surface temperature, which is a clear disadvantage, but this does not appear to be a problem for THs since the active films are very thin. Some key parameters for an IR camera are the temperature range and the thermal sensitivity, the spatial resolution and the frame rate. The pixel pitch of these cameras has decreased to 10 microns, and recent studies suggest that it can be lowered down to 5 microns.^[100] Other critical issues of IR imaging are emissivity and reflection. In modern IR cameras these parameters can generally be set by the operator. Almost all of the reported studies for THs use IR imaging. Emissivity is rarely investigated experimentally^[101,102]; that being said, Kim et al. showed that for AgNW-carbon hybrid THs, the emissivity of the tested film heater decreased linearly with the AgNW content^[102]. This information is useful for the quantitative assessment of thermal losses. Finally, another method with higher sensitivity and a submicron spatial resolution is thermoreflectance (TR). It detects temperature changes near the surface using the relationship between optical

437 reflectance and temperature.^[103] It is used for very specific temperature studies, and not to
438 record the temperature in large areas since it is difficult to define an accurate absolute
439 temperature., In the case of AgNW networks for example, TR imaging can record hotspots of
440 individual nanowire junctions in the 300x300 nanometer region size.^[91] In another case a
441 picosecond TR technique was used to study the thermal diffusivity of 30 to 70 nm thick ITO
442 thin films.^[104] **Figure 3** presents examples of IR and TR imaging with the corresponding size
443 scales. Figure 3a represents the temperature profile of AgNW-rGO (reduced graphene oxide),
444 measured by an IR camera with a low pixel resolution of 250 μm x 250 μm . This roughly
445 corresponds to an area with more than one hundred nanowires.^[54] A comparable technique used
446 to reveal defects in microelectronic devices is lock-in thermography (LiT).^[105] It can provide
447 an IR emission intensity and a heat timing map^[106] but does not include any thermal calibration
448 or numerical scale. However, as shown in Figure 3b, it appears very useful to visualize the
449 electrical and thermal distribution in the case of MNW networks. It enables us to investigate
450 the activation of efficient percolating pathways and the detection of hot spots under electrical
451 stress.^[107] In the case of the IR camera shown in Figure 3c, the higher resolution of 1.6 μm
452 helps identify the temperature of each channel of the metal crack template.^[108] Finally,
453 Figure 3d shows how advantageous TR can be to perform temperature studies, for example to
454 image hot spots and nanowire junctions.^[91]



455

456 **Figure 3.** Thermal imaging methods for characterizing THs at different length scales. a) 3D temperature
 457 profile measured using an IR camera with 250 μ m x 250 μ m pixels, for AgNW-rGO after applying an
 458 electrical current of 20 mA for 60 s. Reproduced with permission.^[54] Copyright 2017, IOP Publishing.
 459 b) LiT image of an AgNW network. The efficient percolating pathways can be detected in brighter
 460 colors with a camera of 640 \times 512 pixels resolution with 10 Hz “ON-OFF” voltage cycles of 6V.
 461 Reproduced with permission.^[107] Copyright 2016, American Chemical Society. c) Thermal map of a
 462 metal mesh network fabricated from a crack template under 1.5 V, with IR imaging with 1.6 μ m
 463 resolution. Reproduced with permission.^[108] Copyright 2017, American Chemical Society. d) Enlarged
 464 region of a nanowire network channel, showing representative hotspots using thermoreflectance (TR)
 465 imaging. Reproduced with permission.^[91] Copyright 2015, American Chemical Society.

466 The different types of temperature measurements are carried out and presented as a function of
 467 the electrical properties, since the Joule effect is responsible for the heating. As mentioned
 468 previously, the steady-state temperature (T_{steady}) is an important feature for THs and can be
 469 studied experimentally by applying a constant voltage or areal power density. The time
 470 necessary to reach the steady-state temperature is also measured, and the heating rate is usually
 471 calculated and reported with the corresponding value of the applied voltage. Plotting T_{steady}
 472 versus the input power density values shows a linear relationship, with the slope coefficient
 473 representing the thermal resistance per unit of area. Another typical experiment related to

performance measurements of THs is the cyclability or “ON-OFF” test, which consists of switching between the on and off states of the applied bias for a large number of operating cycles.^[102,109]

Mechanical properties. The first application of THs was during World War II, with the use of stiff tin oxide to defrost the cockpit windshields of aircrafts to allow them to fly at higher altitudes.^[2] These past years, the development of nanotechnology and advances in flexible electronics have given rise to a huge variety of applications that require excellent stability under mechanical stresses (flexibility and even stretchability). As explained hereinafter, TCOs cannot be integrated into very flexible devices, despite their excellent electrical and optical properties. The high temperature deposition process makes it rather impossible to use flexible and transparent polymers as substrates, because these do not have high thermal resistance.^[110] When they are deposited on flexible substrates, the electrical performance of TCOs is often limited due to deformations that appear on these thin films. On the other hand, the flexibility of emerging materials such as CNTs, metallic grids, MNWs and conductive polymers is one of the main reasons why their study is constantly increasing. The measurement of electrical resistance over thousands of bending cycles is a standard experiment reported in the literature. In general, the bending radius (usually of several mm) is provided. This value is important since it indicates to what extent the TH can be bent, sometimes crumpled. For THs, electrical conductivity must not be altered by mechanical stresses, and the thermal performance should remain stable. In order to estimate the mechanical behavior of THs, the temperature is usually monitored simultaneously to bending. IR imaging, as a contactless method, is particularly convenient for the direct evaluation of performances. **Figure 4a** presents typical examples of bending tests while Figure 4b exhibits stretching tests with concomitant temperature recording by IR camera. Twisting tests, as shown in Figure 4c, are also sometimes reported, depending on the specific application needs. High flexibility has become a common target for emerging

499 TCMs. Interest has also recently been focused on stretchability, which is intrinsically more
500 complicated. The loss of electrical conductivity can be either total, low or negligible depending
501 on several parameters such as the amount of conductive material or the choice of material itself.
502 Ongoing investigations on stretchable THs with an association of different materials (leading
503 to nanocomposites or hybrid materials, see section 3.5) lead to promising features.^[22,70,111]
504 Finally, the incorporation of TCMs into elastic substrates, and the adhesion to various types of
505 substrates is another issue concerning mechanical properties which could influence the
506 performance of TH applications. **Embedded structures can be a promising strategy to tackle**
507 **adhesion issues.**^[81] Measuring performance stability after repeating tape tests^[47,112,113] and
508 microscopic observations of the adhesion between the layers are useful techniques to determine
509 the key drivers that should be studied in depth.

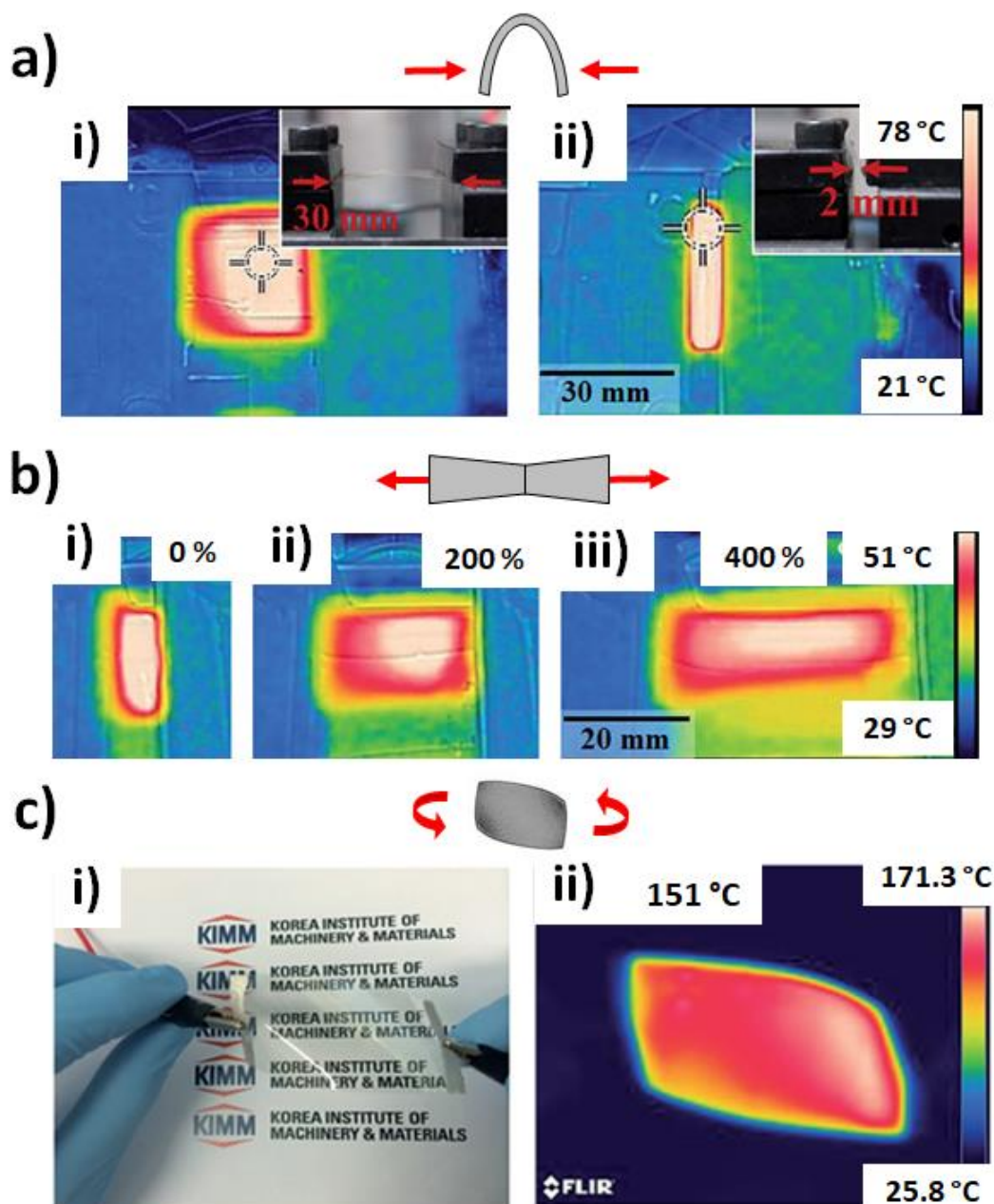


Figure 4. Infrared observations of THs when submitted to different mechanical stress modes. a) Photographs and IR images of an AgNW film during bending tests at i) the initial conformation and ii) the final conformation. The AgNW film ($R_{sh}=15 \Omega/\text{sq}$, $Tr=95\%$) was supplied with a voltage of 5 V. b) During the stretching experiment at: i) the initial state ($L=10 \text{ mm}$), ii) the intermediate stages of stretching with the strain values in percentage shown in the insets, and iii) the final state ($L=50 \text{ mm}$). The substrate was a stretchable eco-flex. a,b) Reproduced with permission.^[114] Copyright 2017, Royal Society of Chemistry. c) Mechanical flexibility and stability of a CuNi TH on a polymer substrate: i) picture and ii) IR image of the heater at 9 V bias under twisting conditions. Reproduced with permission.^[115] Copyright 2017, Royal Society of Chemistry.

Stability. Electrical, thermal, mechanical and chemical stabilities are key parameters for TH performance. Firstly, it is necessary to verify that electrical conductivity and heat emitted

remain stable in the long run when THs undergo electrical stresses. Several tests can be performed, like a voltage ramp and/or plateau cycles with resistance and temperature recordings. The “ON-OFF” test described above is another typical stability experiment that is performed in most TH studies. The application of a constant voltage/power for hours in order to check if the temperature remains stable^[116] is also usually carried out. In other cases, constantly increasing voltage ramps are applied until the breakdown of the heating performance, followed by the application of lower voltages to investigate potential reversibility.^[46] These experiments have proven that the encapsulation of heating materials with protective coatings is an excellent choice to improve stabilization. Thermal stability is crucial for THs and it is linked to the potential degradation of active materials or surrounding materials due to high operating temperatures and fast heating/cooling rates. A way to study this is to measure electrical resistance under thermal stress (thermal ramps or plateaus) without applying any electrical power (except a very small current for the resistance measurement). It is also important to investigate the intrinsic heat stability of the substrates used to fabricate a TH, especially in the case of flexible polymers, which are known to limit the stability of flexible THs. Regarding chemical oxidation and ageing, typical measurements are carried out in environmental chambers and involve the simultaneous exposure to controlled humidity and temperature, combined with light irradiation^[48,117]. Generally, the relative humidity chosen is over 80 %, and the temperature between 45°C and 90°C, which covers most of the harshest use conditions.^[70,93,118–121] Study durations varies strongly, and usually depends on the anticipated stability of the TH and on the expected lifetime of its components. For example, stability studies for copper nanowire (CuNW)/NPs usually last minutes^[120] or hours^[118,119], while for AgNW the duration of the study can be days^[70] or months^[121]. Of note, there are some large discrepancies in terms of MNW network stability from one research group to another, probably originating from differences in MNW growth conditions and purification processes, leading to different surface chemistries, and consequently to more or less stable MNW networks.

549

550 3 The investigated materials technologies for transparent heaters

551 Several material technologies for TH applications have been thoroughly investigated. The very
552 first type of thin layers were TCOs, which have been investigated for several decades^[2,9,14,17,59].
553 These thin films of metal oxide have been studied for several applications, including transparent
554 electrodes for solar cells or touch screens, and have already been widely integrated in industrial
555 devices.^[7,10] For THs, like for transparent electrodes, industrial needs have prompted research
556 into other materials^[21]. There are several reasons for this. TCOs, for instance, are ceramic and
557 therefore do not usually withstand any mechanical stress; this makes them incompatible with
558 flexible applications. Moreover, lowering the cost is a strong argument against the vacuum-
559 process and/or the use of indium in the classical indium tin oxide (ITO), due to the scarcity of
560 indium. Likewise, the search for properties that are better adapted to industrial requirements
561 necessitates the exploration of other materials. The goal of this part 3 is to present the main
562 materials categories and their related properties when used for THs. Each type of materials will
563 then be discussed in more detail below, starting with metallic oxide-based materials, then
564 carbon-based nanomaterials (graphene and CNTs), metallic-based materials, conductive
565 polymers and finally nanocomposites or hybrid materials. In this review we consider that
566 *nanocomposites* are materials for which the nanostructures are within a continuous phase such
567 as a matrix, while *hybrid* nanomaterials refer to combination of materials of different natures
568 such as organic-inorganic.

569

570 3.1 Metallic oxide-based materials

571 Among all the different types of TCMs, TCOs were the first to be developed and studied. They
572 have been used industrially for a long time and in many different applications. ITO thin films,
573 in particular, have been employed for the production of THs to defrost aircraft windshields. The
574 basic properties of TCOs have been extensively described in previous works, and we refer the

reader to those for additional details^[9,122,123]. Of note, the morphology and structure of TCO thin films play a key role in their conductivity. These thin films usually exhibit polycrystalline structures, as shown in **Figure 5a**, with crystal sizes that depend on the deposition method used and other parameters like film thickness. The latter can easily reach hundreds of nanometers.^[14] Twins are often observed (for FTO for instance), and as in the case of grain boundaries, they are detrimental to charge mobility^[14,59,124]. The fact that grains often become bigger as the film thickness increases has a direct impact on the conductivity of the layers, since the number of grain boundaries and twins decreases (Figure 5b). Another important aspect of TCOs is the fact that transparency in the IR region of the spectrum falls rapidly with film thickness or with carrier concentration due to plasmonic absorption as shown, respectively, in Figure 5c and 5d.^[20] For TH applications where IR transparency is important, e.g. night vision applications for glasses and binoculars, the TCO technology is therefore not perfectly adapted compared to other TH technologies.

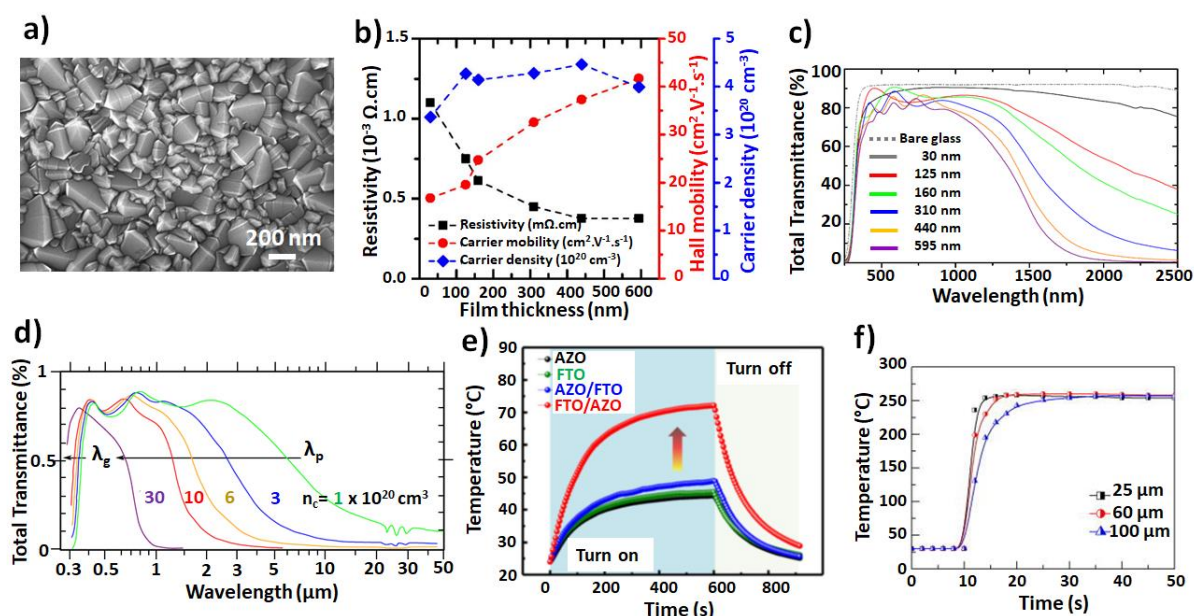


Figure 5. Transparent conductive oxides (TCO) used as THs. a) SEM image of a typical 400 nm thick FTO layer showing the grain-boundary structure of the thin polycrystalline film. b) Main electrical characteristics of FTO layers vs film thickness: electrical resistivity, carrier mobility and carrier density. Reproduced with permission.^[14] Copyright 2013, AIP Publishing. c) Total optical transmittance for different FTO film thicknesses: the thicker the film, the lower the transmittance, specifically in the near infra-red region due to plasmonic absorption. d) Computed spectral normal transmittance of ITO. The values correspond to electron density. Reproduced with permission.^[125] Copyright 1986, AIP

Publishing. e) Time dependence of temperature when a 12 V voltage is applied to a TH composed of either an AZO layer (black), a single FTO layer (green), an AZO/FTO (blue) or a FTO/AZO (red) double-layer film on glass which shows different electrical properties. This clearly illustrates the strong influence of the TH electrical properties on the heating performance. Reproduced with permission.^[84] Copyright 2014 John Wiley and Sons. f) Measured temperature vs time for a 100 nm-thick AZO-based TH, deposited on mica substrates of different thicknesses, illustrating the role played by the thermal inertia of the substrate in terms of response time. Reproduced with permission.^[60] Copyright 2018, AIP Publishing.

Despite TCOs being the oldest studied TCMs, there are surprisingly few reports in the literature dealing with the application of TCOs as THs. The studies reported so far involve ZnO-based materials, Ga-doped ZnO (GZO)^[126–128] and Al-doped ZnO (AZO)^[60,84,127,129], FTO^[84] and ITO^[130–133]. Indeed, TCOs have been mainly investigated in the framework of industrial research and development, which is generally not associated with scientific publications.

In industry, ITO is routinely deposited by sputtering, a vacuum method that is generally associated with higher costs compared with solution process technologies. Im et al. explored the utilization of ITO nanoparticle (NP) solutions to process ITO thin films^[130] as an alternative to vacuum processing. The films were fabricated by spin-coating the ITO NP solution on a glass substrate, followed by annealing up to 400 °C. The main effect of the annealing step is to sinter the particles. Using these films, a temperature of 163 °C was achieved for a bias voltage of 20 V, and dry-ice was used to demonstrate the defrosting capabilities of the TH.^[130] More recently, Kim et al. used the same approach. However, by increasing the annealing temperature of the deposited ITO NP and by using different atmospheres during the annealing step, they demonstrated that the oxygen vacancies in the film can be controlled^[131]. In this case, temperatures up to 215 °C were reached for a 15V bias, with a thermal efficiency of 162.9 °C/(W/cm²) being obtained for optimized samples. In another study, Yang et al. demonstrated that by adding organic additives such as polymethyl methacrylate and terpineol to the ITO NP solution, the obtained heaters are more efficient and homogeneous. The authors made micro-heaters using this approach, and could reach temperatures of 445 °C for a bias voltage of only 12 V.^[132]

Kim et al. explored the use of bilayers by combining AZO and FTO deposited by sputtering and Chemical Vapor Deposition (CVD), respectively.^[84] They observed that both conductivity and transparency improved for bilayers with respect to single layers of the same thickness, as demonstrated in Figure 5e.^[84] This is attributed to the higher overall particle size in the film, which affects both mobility and transparency. The best results, reported in Figure 5e, were obtained for FTO/AZO bilayers for which temperatures above 70°C were obtained for a bias voltage of 12 V.^[84] Roul et al. studied rigid and flexible AZO-based TCOs by depositing AZO on glass and polyethylene terephthalate (PET) substrates by magnetron sputtering.^[129] The films deposited on glass reached temperatures of approximately 100°C for a 12 V bias for the samples deposited at 200 °C. Flexible heaters made on PET reached 50°C for bias voltages of 8 V. Nevertheless, stability results are only shown for AZO/glass samples, and no study of the effect of bending on the properties of the flexible TH is reported. It is also worth mentioning that ZnO-based TCOs may not be the best candidates for high temperature applications, since ZnO tends to absorb oxygen species in the grain boundaries, which has a detrimental effect on mobility, as explained and modelled recently.^[19] It has been shown that the absorption of oxygen species increases rapidly with temperature^[134], thus most likely limiting the applications of THs based on AZO.

Ke et al. showed that despite the ceramic nature of ITO, flexible THs can be obtained by using mica substrates as thin as 15 µm, thanks to their layered structure.^[133] ITO layers of up to 500 nm were deposited by pulsed laser deposition (PLD) at room temperature and annealed at up to 500°C. Flexible THs were fabricated, exhibiting fast ramping. Temperatures of up to 438°C were reached in less than 15 s at a bias voltage of 19 V. The same approach was used by the same authors to make flexible THs based on AZO/mica.^[60] Figure 5f shows the measured temperature versus time for a 100 nm-thick AZO-based TH deposited on mica substrates of different thicknesses: this illustrates the role played by the thermal inertia of the substrate,^[60] in agreement with equation (4). Record heating rates of 200°C/s were obtained in this case. The

occurrence of van der Waals epitaxy between the mica substrate and the grown AZO film reasonably explained this superior performance.

Gallium has also traditionally been used to dope ZnO. Jayathilake et al. deposited ZnO co-doped with Al and Ga (AGZO) by aerosol-assisted chemical transport, which showed a lower conductivity than AZO or GZO films^[127]. The films were prepared by dispersing previously prepared AGZO powders (by microwave synthesis) in a methanol solution containing formic acid and cellulose. Then aerosol generated from this suspension was carried by N₂ gas to a glass substrate at 400 °C. Temperatures above 132 °C were achieved in 10 min for bias voltages of 18 V. Older reports on physically deposited GZO films were performed by Kim et al.^[128] and Ahn et al.^[126] In the first case, the films were deposited by rf-magnetron sputtering on glass substrates^[128] and reached 90 °C after 22 s for a bias voltage of 48 V. In the second case, PLD was used to deposit the films on glass substrates, and reached over 88 °C after 48 s for a 12 V bias.^[126]

Thus, while TCOs, and in particular ITO, are the most prominent transparent materials today, with a broad range of industrial applications, fundamental studies involving promising approaches are still being carried out in order to push the limits of these materials in terms of performance and mechanical flexibility. These studies are framed in a wider research that involves the exploration of competing materials, such as carbon-based nanomaterials, which are described in the next section.

3.2 Carbon-based nanomaterials (CNTs & graphene)

Carbon-based thin film heaters were first described in 2007.^[27] Carbon fibers, carbon nanotubes (CNTs) or graphene derivatives have been widely reported in the literature to address several fields of applications including defogging,^[135] anti-icing, de-icing,^[83,136,137] wearable electronics,^[138,139] thermochromic displays^[140,141] or thermomechanical sensors.^[62]

Most published studies report the use of carbon-based thin film heaters for the assessment of non-transparent devices. Their high flexibility and stretchability are, without doubt, advantages that make them very interesting for various type of heaters thanks to their remarkable mechanical properties, while conversely they exhibit low transparency.^[57] Since this review focuses on THs, only devices or active materials with good transparency are discussed hereinafter.

Active parts of carbon-based THs can be processed either by dry or solution-based routes, the latter being often more suitable for many supports (PEN, PET, PC, PI or cotton fabrics for example). CNT devices can be produced either through percolative networks implying printing processes^[61], or thanks to CNT forest (aligned CNTs, usually prepared by chemical vapor deposition (CVD) / transfer protocol). For the first method, **Figure 6a** shows an SEM image of a transparent and flexible single wall carbon nanotubes (SWCNT) heater prepared on a plastic substrate, along the associated IR images at various applied voltages.^[61] Regarding graphene and its derivatives, exfoliation of graphite or chemical reduction of GO were reported. Recently, unusual and interesting approaches based on the use of carbon nanosheets from the carbonization of polymers or from natural carbonaceous by-products of ethylene production were published by Souri et al.^[142] and by Morris et al.^[143], respectively.

Both the deposition processes and the intrinsic properties of the material strongly impact the performances of carbon-based THs. For CNT networks, the trade-off between transparency and conductivity can also be controlled by nanotube types (e.g. single-walled vs multi-walled MWCNT). SWCNTs generally exhibit high transparency and low haze, but rather low conductivity due to the presence of poorly conductive semi-conducting CNTs and resistive CNT-CNT junctions.^[61,144] MWCNT-based electrodes (100% of metallic behavior tubes) are more conductive but less transparent due to their larger size, and exhibit a higher haze value.^[145] Figure 6b exhibits optical and infrared pictures of graphene-based THs illustrating both flexibility and uniformity.^[57] In the case of percolative networks of graphene flakes, each

graphene layer decreases the transparency by $\sim 2\text{-}3\%$. However, devices made of a graphene monolayer obtained by dry deposition keep a very high level of transparency, but this technique is somewhat limited to small surfaces. Improvement is still required in terms of uniformity of highly conductive graphene layers and larger surface coverage. Due to the higher electrical contact resistances between the conductive objects of carbon-based networks (CNTs, Carbon flakes) compared to MNW networks, most carbon-based THs require denser systems to reach the same level of conductivity, at the expense of the transparency.

As input voltage and surface temperature are strongly correlated to sheet resistance, in most cases, carbon-based THs are addressed with high input voltages from 10 to 100V for at most a few cm^2 samples. Indeed, transmittances higher than 70% are achievable at several hundreds of $\Omega/\text{sq.}$ ^[146] On polyimide substrates, temperatures higher than 350°C have been reached.^[142] Considering that surface power densities of a few kW/m^2 are required for both thermal comfort and heating, the lifetime and stability of carbon-based materials are a true asset of carbon-based THs.

In the case of carbon-based THs, transparency is clearly impaired if one intends to reach low sheet resistance for high heating performance. New developments using carbon nanostructures hybridized with metallic nanowires could provide an interesting alternative since carbon-based materials can significantly enhance the stability of metallic nanowires (See section 3.5.1).

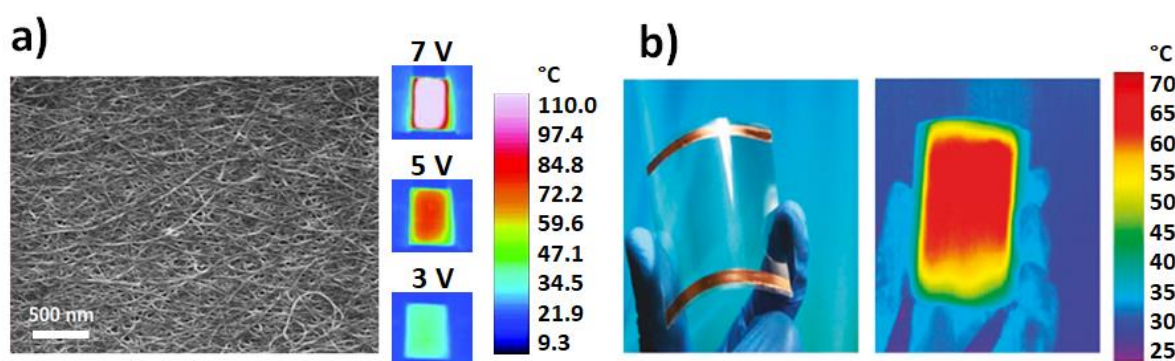


Figure 6. Performances of carbon-based transparent heaters on flexible substrates. a) SEM pictures and infrared pictures of SWCNT-based transparent electrodes when submitted to applied voltages of 3, 5 or 7 volts. Reproduced with permission.^[61] Copyright 2017, AIP Publishing b) Highly flexible graphene-

based TH with optical and infrared pictures illustrating both flexibility and uniformity. Reproduced with permission.^[57] Copyright 2011, American Chemical Society.

3.3 Metallic-based materials: metallic grids, metallic meshes, MNW random networks

While TCOs have been largely studied for several decades to be used as transparent electrodes (TEs) or THs, other materials such as metallic-based nanostructures have been considered since the year 2000 approximately^[21,147]. They present additional properties when compared with TCOs, since many of them can be deposited at low temperatures and exhibit good mechanical flexibility. Metals indeed appear attractive as potential TH active materials since they possess very high electrical and thermal conductivities. For instance, silver exhibits the highest conductivities among all materials at room temperature. However, ultrathin metallic films generally do not show an interesting trade-off between optical transparency and sheet resistance, due to both strong light absorption and electron scattering at surfaces or interfaces. As such, the only way to take advantage of metals for TH applications is to engineer metal nanostructures. This can provide interesting opportunities to manipulate photons and electrons in order to achieve electrical, optical and mechanical properties that are not reachable with TCOs. The main metallic patterns that can be efficiently used for TH production are metallic meshes, MNW networks and metallic grids. The difference between metallic grids and meshes in the literature is sometimes confusing. In this review we will consider that *metallic meshes* do not contain privileged directions in terms of conductive lines, while *metallic grids* are constituted by a periodic arrangement of metal lines, generally with a 3- or 4-fold symmetry. In this section, we will briefly examine the different investigated metallic-based materials, by describing their main features, properties and their potential integration into TH devices. Progresses toward low-cost TH fabrication, wire-wire junction resistance, physical properties, adhesion and stability will also briefly be discussed.

Metallic meshes can exhibit some interesting features as THs. As shown by Kiruthika et al. interconnected crackles can be obtained thanks to the spreading of low cost crackle wall paint

752 by using the drop coating technique.^[82] Interconnected Ag meshes can be fabricated by
753 depositing a thin metal layer on top of the obtained crackles and then removing the template.
754 **Figure 7a** shows a typical optical image of an Ag mesh fabricated on glass, while the inset
755 corresponds to the optical profiler image (the thickness is approximately 300 nm).^[82] This type
756 of metallic mesh network exhibits interesting physical properties on large areas. Kiruthika et
757 al. reported a sheet resistance of 1 Ω/sq on an 18x15 cm^2 area, associated to an optical
758 transmittance of 77%.^[82] Thanks to the low electrical resistance, the use of metallic meshes as
759 THs requires a rather low voltage: an 8.5 V bias was used to reach uniformly heated surfaces
760 of up to 170°C. This efficient defrosting device successfully withstood an ultra-sonication test,
761 as well as many defrosting cycles.^[82] Metallic mesh networks have been the subject of many
762 studies lately, with various metallic species being evaluated, like copper,^[148] silver,^[149,150]
763 nickel,^[151] cupronickel,^[115] gold^[152] and platinum.^[72]

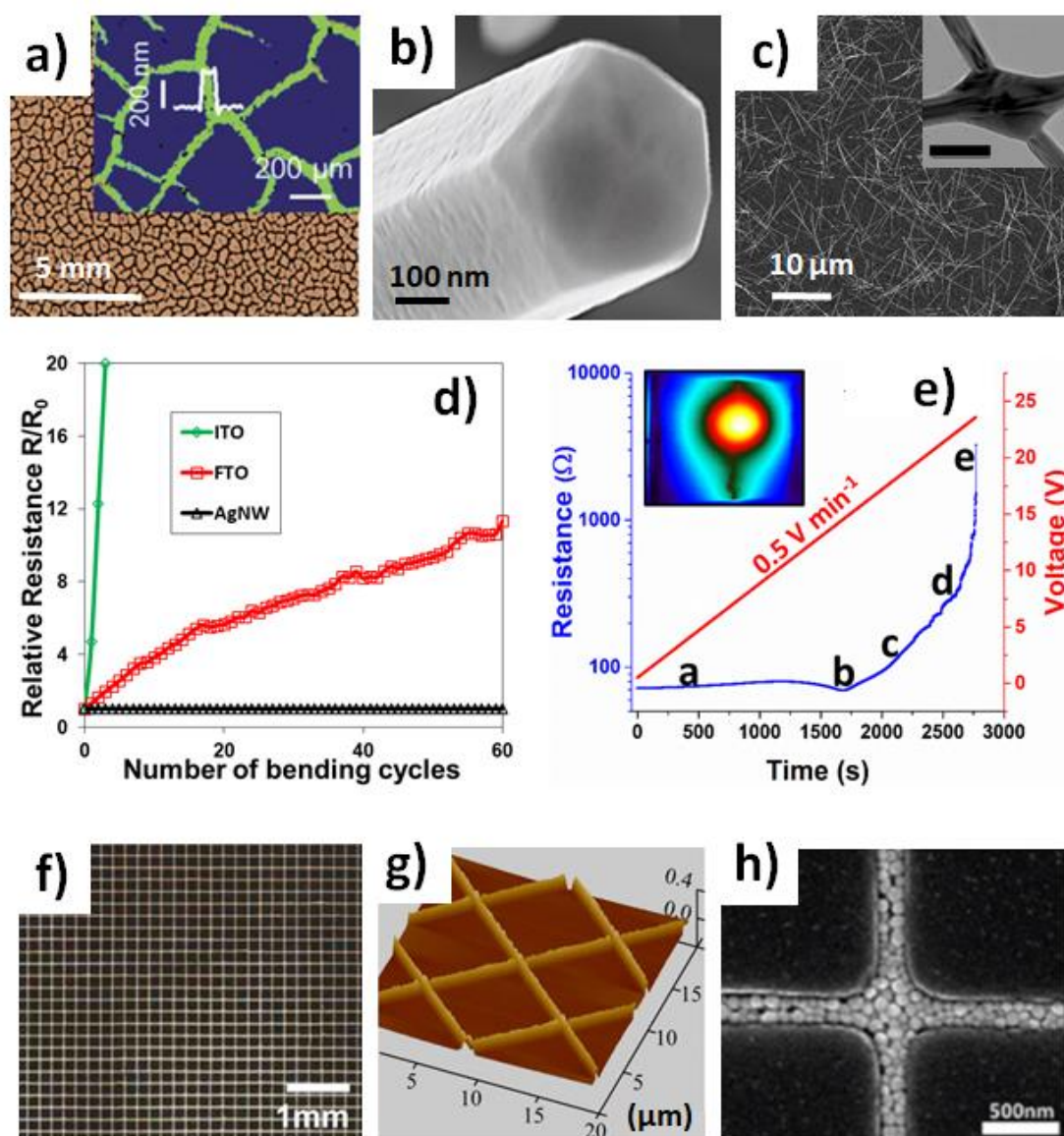


Figure 7. Main features of metallic-based THs. a) Optical image of an Ag mesh fabricated on glass; the inset corresponds to the optical profiler image (thickness of about 300 nm). Reproduced with permission.^[82] Copyright 2014, Royal Society of Chemistry. b) High-resolution SEM image of a copper nanowire (CuNW) with a 5-fold symmetry. Reproduced with permission.^[66] Copyright 2017, John Wiley and Sons. c) Typical SEM picture of an AgNW random network. The inset shows a TEM picture of a sintered junction between two nanowires (bar scale: 100 nm).^[153] d) Relative electrical resistance of different types of TH materials (ITO, FTO and AgNW) versus the number of bending cycles at 5 mm radius of curvature. Reproduced with permission.^[20] Copyright 2016, John Wiley and Sons. e) Evolution of the electrical resistance of an AgNW network during a voltage ramp of 0.5 V/min. The electrical resistance exhibits a drastic increase associated to the appearance and propagation of a crack, as revealed by the IR image in the inset (the width of the IR image corresponds to 25 mm). Reproduced with permission.^[93] Copyright 2018, American Chemical Society. f) Optical microscopy image of a flexible transparent Au grid electrode with the following geometrical features: grid width: 4.5 μm ; grid spacing: 200 μm ; Au thickness: ~ 90 nm. Reproduced with permission.^[154] Copyright 2014, American Chemical Society. g) AFM profile sections of a silver grid fabricated by femtosecond laser writing of a silver aqueous solution. The profile shows a good uniformity of the grid. Reproduced with permission.^[155] Copyright 2016, AIP Publishing. h) SEM image of the silver nanoparticle (AgNP)-based metallic grid fabricated by capillary assembly of AgNPs. Reproduced with permission.^[156] Copyright 2016, Royal Society of Chemistry.

784

785 MNW networks have been the subject of a lot of research lately, with a focus on the industrial
 786 integration of the networks as transparent electrodes into opto-electronic devices, as recently
 787 reviewed by several authors.^[20,38,39,157,158] Among the possible MNW materials, silver has been
 788 the most investigated^[33,34,39,159–162], while CuNW networks constitute an interesting
 789 alternative.^[48,66,76,163,164] Figure 7b exhibits a high-resolution TEM image of a CuNW showing
 790 the 5-fold symmetry.^[66] Figure 7c reports a typical SEM picture of a random AgNW network.
 791 The inset shows a TEM picture of a well-sintered junction between two AgNWs,^[153] knowing
 792 that an efficient local sintering of the junction between the different AgNWs leads to lower
 793 junction's electrical resistance and, therefore, to lower overall network electrical resistance.^[90]
 794 While the most used deposition techniques are spin-coating and spray-coating, several original
 795 methods have been proposed lately to fabricate AgNW networks with good performances. For
 796 instance, Hu et al. proposed a versatile agitation-assisted assembly approach that induces an
 797 orientation of AgNWs. This leads to excellent performances with a R_{sh} value of 2.8 Ω/sq , an
 798 optical transparency of 85% and a high stretchability of up to 40%.^[68] The electrical resistance
 799 of junctions between AgNWs can be reduced by several methods, such as thermal annealing,^[90]
 800 UV treatment^[165] or as shown recently by Huang et al. using a self-limited nano-soldering
 801 method. This method can decrease R_{sh} from 18.6 to 7.7 Ω/sq while preserving a constant optical
 802 transmittance of 90%.^[166] The first demonstration of AgNW networks being efficiently used as
 803 THs was published in 2012 by Celle et al..^[42] These authors showed that the intrinsic features
 804 of AgNW random networks made it possible to combine bendability, transparency and high
 805 heating performances at low voltages (below 12 V), which constitutes a clear asset for
 806 integration in many applications.^[42] This demonstration, on both glass and polymeric
 807 substrates, was followed by numerous publications. Sorel et al..^[43] published in 2014 a
 808 comprehensive physical approach of AgNW network-based THs, including the different

regimes associated with low network density (percolative regime) and high network density (bulk-like regime). The authors also provided critical considerations related to electrical conductivity, optical transparency and heat dissipation for efficient THs. Figure 7d shows the relative electrical resistance of different types of TH technologies (ITO, FTO and AgNW) versus the number of bending cycles with a radius of curvature of 5 mm. AgNW networks are much more flexible than TCOs.^[20] However, one of the main issues with MNW networks is their relative low stability under electrical and/or thermal stresses, even at device-operating conditions, as reported in several studies.^[46,54,90,167,168] This is illustrated in Figure 7e, which displays the evolution of the electrical resistance of an AgNW network during a voltage ramp of 0.5 V/min. The electrical resistance exhibits a drastic increase associated to the appearance and propagation of a crack, as revealed by the IR image in the inset (the width of the IR image corresponds to 25 mm).^[93] As reported below (section 3.5.3), the deposition of a thin oxide layer on top of MNW networks drastically enhances their stability or their adhesion.^[47,48,167] These nanocomposites can lead to efficient and stable THs,^[44,46,47,117,169] as discussed further in section 3.5.

Metallic grids have been the subject of a lot of research since they appeared as promising transparent electrodes, with both optical transmittance and sheet resistance being well controlled by adjusting the period and width/thickness of the patterns.^[147,170] The metal lines are thin enough (~few μm) to provide a low sheet resistance, while the period of the grid is large enough (~5-200 μm) to provide sufficient transparency but not too large, to ensure heating uniformity over the entire TH. Figure 7f shows a typical optical image of a flexible transparent Au grid electrode with the following geometrical features: grid width of 4.5 μm , grid spacing of 200 μm , Au thickness of ~90 nm.^[154] This Au grid electrode exhibits an optical transmittance of 92% at 550 nm and a sheet resistance of 97 Ω/sq .^[154] The fabrication of metal mesh electrodes was originally performed using vapor deposition processes, which require vacuum and generate metal waste. Consequently, many studies have investigated other reliable fabrication methods,

and in particular large area printing methods like flexography, slot-casting, screen printing and others. Figure 7g exhibits an AFM profile section of a silver grid, fabricated by femtosecond laser writing of a silver aqueous solution, which shows the good uniformity of the grid.^[155] This fabrication method possesses advantages in terms of flexibility and adaptability compared to alternative techniques like the combination of metal evaporation and lithography. Figure 7h shows an SEM image of a silver nanoparticle-based (AgNP) metallic grid fabricated by capillary assembly of AgNP.^[156] Of note, metallic grids can exhibit excellent flexibility.^[147] However, one of the potential weaknesses of metal grids is the weak adhesion to the substrate. Lee et al proposed to enhance this adhesion through colloidal deposition and silver enhancement steps. This improves the adhesion of the metal mesh thanks to an intermediate adhesion layer based on 3-aminopropyltriethoxysilane.^[112] This approach results in an optical transmittance of 97.7% and a sheet resistance of 71.6 Ω /sq, and its use as a TH enables to homogeneously reach a temperature of 245°C under an applied voltage of 7 V, showing a clear enhancement of adhesion.^[112] Another very promising strategy to tackle adhesion issues relies on embedded structures since they can: i/ enhance the surface smoothness, ii/ improve drastically the mechanical stability and iii/ induce strong adhesion to the substrate. Khan et al. demonstrated a cost-effective electrodeposition solution process of embedded metal-mesh with excellent mechanical, optical and heating performances.^[74] Of note, metallic fibers (with diameters much larger than nanowires) can exhibit interesting properties. Wang et al. recently demonstrated that percolating networks of Ag nanofibers fabricated by blow-spinning constitute efficient THs.^[73] This TH technology can indeed exhibit good optical and electrical properties, as demonstrated with Ag nanofibers networks that were obtained with an optical transmittance of 95% and a sheet resistance of 16 Ω /sq, enabling to reach temperatures larger than 285°C with a 10 V bias.^[73] Singh et al. reported a TH with low operating voltage based on embedded PVA@Ag nanofiber network. This TCM structure has a smooth surface topology and excellent bending stability after 10 000 bending cycles at 1.0 mm bending radius.^[81] In the

case of copper based fibers, Jo et al. demonstrated a highly stretchable and transparent TH with ultra-low sheet resistance that can keep the working temperature constant up to 300 % stretching.^[76]

3.4 Polymer-based materials

Conductive polymers present attractive features for TH fabrication in terms of flexibility/stretchability, cost and processability. However, only few of them exhibit an electrical conductivity suitable for TH applications.

Recently, a breakthrough was performed in TH fabrication with the first demonstration of a 100% polymeric TH. Gueye et al. demonstrated the ability of poly(3,4-ethylenedioxythiophene) (PEDOT)-based thin films to be efficient THs, without the need for metal or conductive fillers.^[50] Three conductive polymers were studied (i) PEDOT doped with polystyrene sulfonate (PSS) and with ethylene glycol (EG): PEDOT:PSS-EG, (ii) PEDOT doped with trifluoromethanesulfonate CF_3SO_3^- (OTf): PEDOT:OTf, and (iii) PEDOT:OTf thin films treated with dilute sulfuric acid to further enhance conductivity: PEDOT:Sulf. The chemical structures are displayed in **Figure 8a**. These conductive polymers show excellent optoelectronic and heating properties^[50], and are flexible, as shown in Figure 8b. The electrical resistance and heating properties of the polymer-based TH remain stable under strong mechanical stress (1000 cycles with a 9 mm bending radius), as shown in Figure 8c. Temperatures higher than 100 °C can be reached in a few minutes with a bias of less than 12 V (Figure 8d). Transparencies higher than 87% are generally obtained with extremely low light diffusion, the haze value being typically under 1%. This aspect is very important because haziness is a critical parameter for most optoelectronic applications, and such low values are hardly ever achieved with other non-TCO materials.^[38] This polymer-based technology made it possible to reach high power densities, up to 10 000 W/m² (Figure 8d). Heating homogeneity,

measured by IR imaging, and extended mechanical stability were demonstrated. Chemical instability could have been anticipated because PEDOT-based materials are known to be sensitive to light and moisture. However, after encapsulation with a barrier film, a loss of only 1°C was measured after 200 h under continuous heating at 55°C, compared to 9°C without encapsulation, which indicates that encapsulation methods should be developed and optimized for the long term durability of these THs.

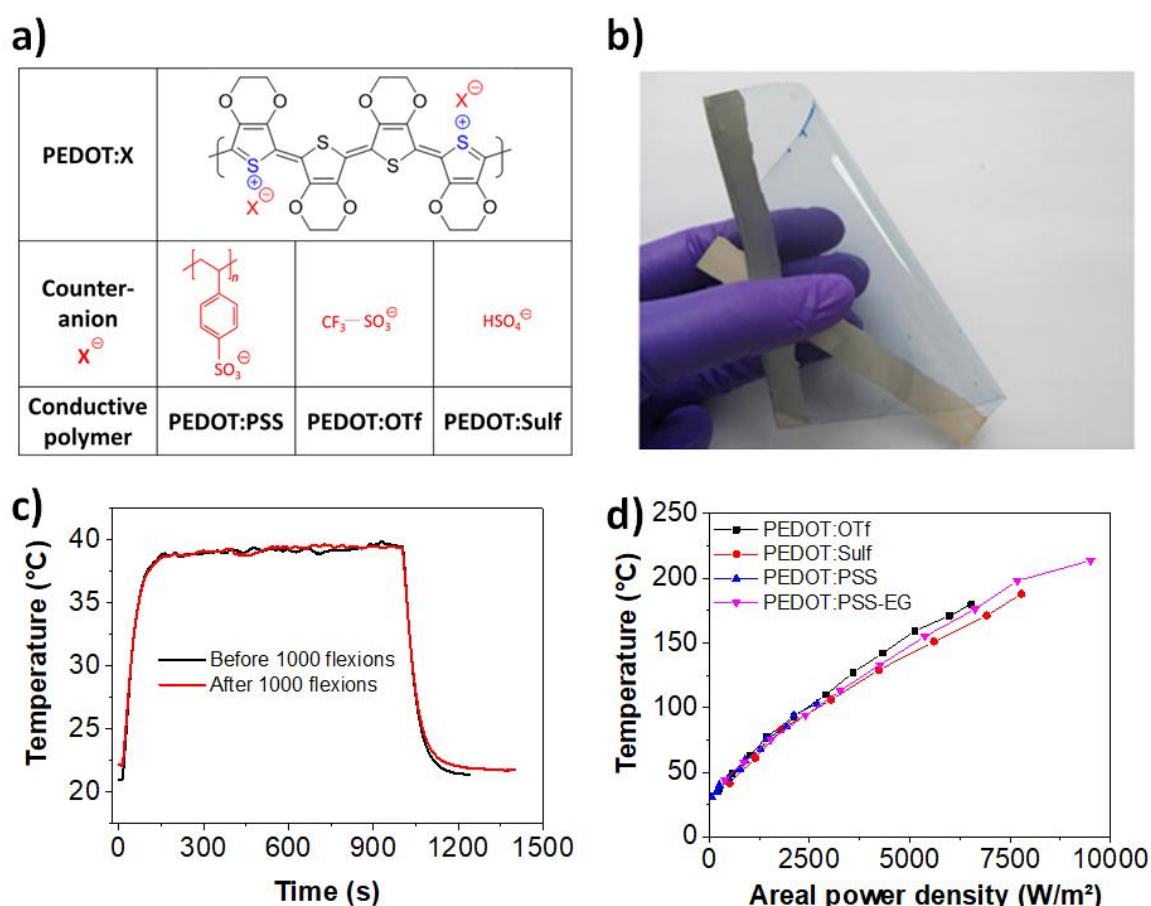


Figure 8. Main features of conductive polymer-based transparent heaters. a) Chemical structures of PEDOT and three main counter-ions forming respectively: PEDOT:PSS-EG, PEDOT:OTf and PEDOT:Sulf. b) Picture of a PEDOT-based TH illustrating its flexibility. c) Temperature increase of PEDOT:PSS-EG-based THs before and after 1000 bending cycles (9 mm radius of curvature) showing its good mechanical stability. d) Temperature increase versus areal power density for conductive polymer-based TH. b-d) Reproduced with permission.^[50] Copyright 2017, American Chemical Society.

Another recently reported approach is based on the use of nanofibers of conductive polymers to form a mesh, which can be used as a TH. An effective and cost-friendly method to produce such nanofibers is electrospinning, which allows the polymer to be deposited onto any curved or flexible surface. Some

experiments were carried out on polycaprolactone/carbon black (PCL/CB), polyethylene oxide/polyaniline (PEO/PANI) and PEO/PEDOT:PSS systems.^[85,171] The best results were obtained with the PEO/PEDOT:PSS blend. These polymeric THs show moderate performances in terms of heating properties, requiring a 60V bias to reach 70 °C, at 84 % transparency.^[85]

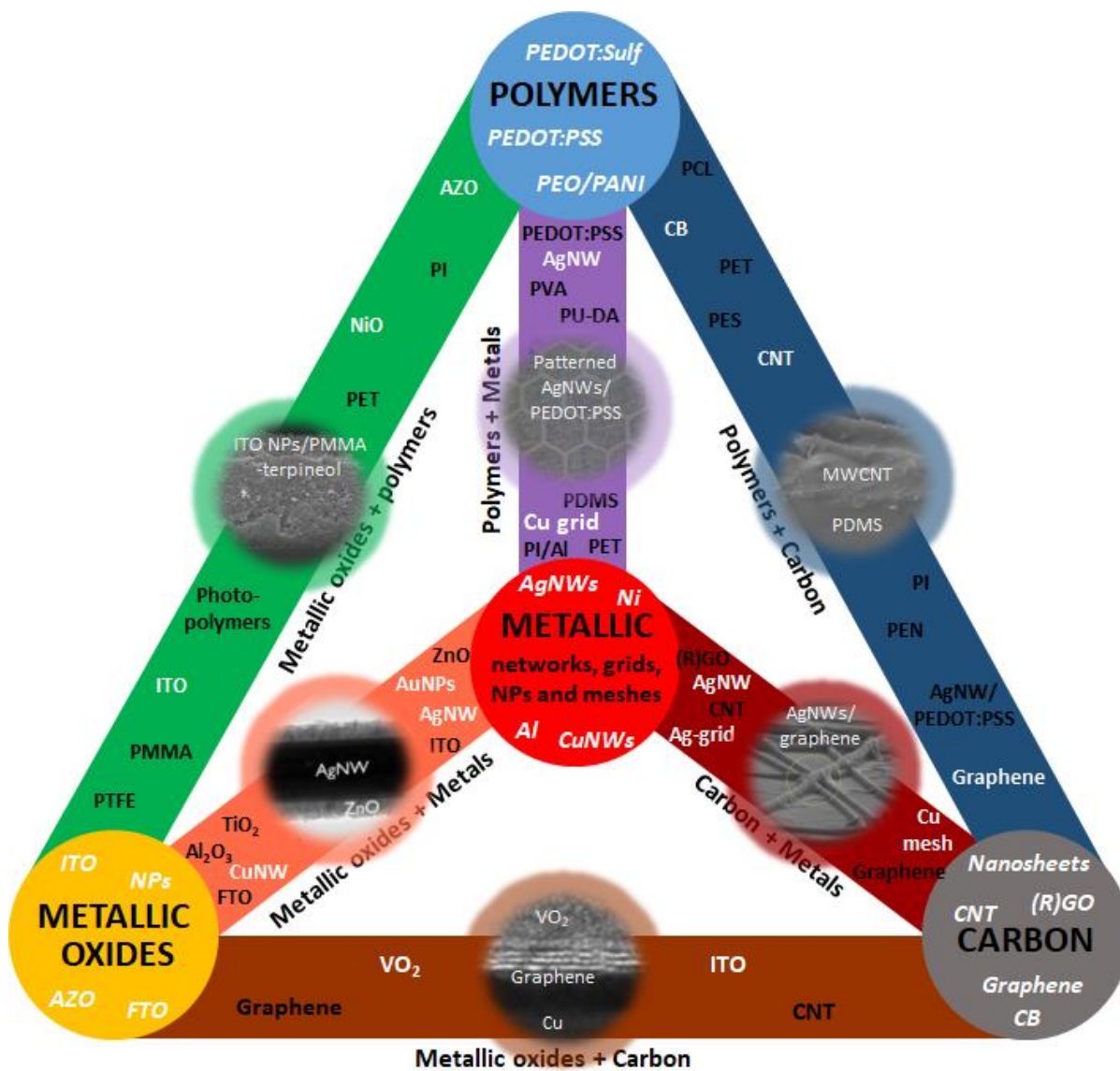
PEDOT:PSS films can also be patterned using a microfluidic post treatment with solvents. The conductivity is locally boosted by several orders of magnitude, making it possible to obtain localized heating with microscale resolution^[172].

These recent developments based on thin films of intrinsically highly conductive polymers open the way to new high performance and purely organic THs.^[173]

3.5 Nanocomposites and hybrid transparent heaters

THs have gained a constantly increasing attention in research and industry these past years with a recent focus on multilayers, hybrids and nanocomposites. Matching materials with TH requirements is promising since it combines the best properties and advantages of each material, and generally offers much better performances than THs composed of a single material type. In other words, each conductive nanomaterial (TCO, metallic-based materials, carbon-based materials or conductive polymers) has its own advantages and disadvantages, but satisfying all industrial requirements with a single material is nearly impossible. The combination of several of these nanomaterials, however, can offer enhanced properties or better stability. This trend is observed in other modern domains in advanced materials science. This can be illustrated with the case of 1D carbon-based nanocomposites used in electrochemical energy storage devices; these have attracted intensive research interests lately, as an effective way to store energy from renewable energy sources. These aspects have been reviewed recently by Shi et al.^[174] who showed that 1D carbon-based nanocomposites (where CNT are either embedded, coated, encapsulated or supported) can be efficiently integrated into batteries and supercapacitors.

A large family of these hybrids for TH applications includes metallic nanowire networks or grids/meshes coated with protective layers of graphene derivatives or TCOs. These composites exhibit the very high electrical conductivity characteristic of metallic nanomaterials, and the coatings offer higher electrical and thermal stability. Other structures include thin TCO layers and metal nanowires ^[47], or MNWs combined with conductive polymers^[175]. The emerging hybrids/nanocomposites based on nanomaterials open the way for flexible devices fabricated using low-cost and up-scalable processes, and leads to a wide variety of modern applications with futuristic shapes and everyday life uses. These nanomaterials can then be successfully integrated into devices since they exhibit an interesting trade-off between electrical and mechanical properties, stability, transparency and haze value. **Figure 9** illustrates the richness and diversity of the materials investigated for TH applications. These materials have been classified according to the main investigated TH technologies: they are composed of either the four primary material types (metallic oxides, metals, conductive polymers and carbon) or of hybrids/nanocomposites composed the combination of these primary materials. The primary material is the main material, while the secondary material is usually present in lesser amounts, and generally added afterwards. The main materials used in each case (primary and hybrids/nanocomposites) are represented in white letters. Each picture illustrates an example of a hybrid category: (from left to right, clockwise) 1) metallic oxides/polymers, 2) polymers/metals, 3) polymers/carbon, 4) carbon/metals, 5) metallic oxides/carbon, 6) metallic oxides/metals. The color code used in Figure 9 applies to the rest of the figures of this review.



949

Figure 9. Schematic classification of main TH technologies investigated: they are either composed of the four primary material types (metallic oxides, metals, conductive polymers and carbon) or of hybrids/nanocomposites through combinations. This illustrates the richness and diversity of TH-related advanced materials. The main materials used in each case (primary and hybrid) are represented in white letters. Each picture illustrates an example of a hybrid category: (from left to right, clockwise) 1) metallic oxides/polymers; SEM image of an ITO NP/polymethyl methacrylate (PMMA)-terpineol mixture. Reproduced with permission.^[132] Copyright 2015, Elsevier. 2) polymers/metals; optical micrograph of printed AgNW/PEDOT:PSS composite grids with an hexagonal pattern. Reproduced with permission.^[176] Copyright 2019, MDPI. 3) polymers/carbon; cross-section SEM images of a MWCNT/polydimethylsiloxane (PDMS) bilayer film. Reproduced with permission.^[177] Copyright 2015, Elsevier. 4) carbon/metals; Tilted cross-section SEM image of single-layer graphene/AgNW/glass. Reproduced with permission.^[178] Copyright 2019, John Wiley and Sons. 5) metallic oxides/carbon; HR-TEM of the cross section of graphene-supported VO₂ on a copper substrate which will eventually be etched. Reproduced with permission.^[53] Copyright 2013, American Chemical Society. 6) metallic oxides/metals; TEM image of a 30 nm thick ZnO-coated AgNW. Reproduced with permission.^[47] Copyright 2018, American Chemical Society.

966

To show the recent evolution of TH technologies related either to emerging materials or to nanocomposites, we have investigated the relative number of publications per TH technology. **Figure 10a** shows, through pie-charts, the percentage of scientific articles associated to the different TH technologies, gathered every 4 years since 2004. This shows that before 2008 TCOs related to TH were almost the only technology reported in the literature, while carbon materials (graphene and CNTs) were starting to be well studied. From 2009 on, metallic nanowires, meshes and grids have attracted much more attention. These past years, nanocomposites/hybrids were the focus of many articles, and excellent performances and stability have been reported. Of note, conductive polymer-based THs started to be explored around 2017.^[50] The growing size of the pie-charts with time illustrates the fact that the number of articles per year has been multiplied by 10 between the first period (2004-2008) and the more recent one (2014-2018). It clearly shows the growing interest in THs from the scientific community, driven by the industrial needs. In parallel, there is a strong industrial activity in the TH field, which is not reflected in scientific publications due to intellectual property strategies. Similar trends as those shown in Figure 10a can be surveyed in terms of patent application numbers linked to TH technologies.

To illustrate the versatility of nanocomposites, Figure 10b and 10c illustrate a typical example where properties can be tuned if the AgNW content is varied in hybrid conductive films composed of CNTs and AgNWs.^[102] Figure 10b shows the influence of AgNW content on optical transmittance and haze value, while Figure 10c shows the emissivity versus AgNW film content of similar film heaters prepared by roll to-roll coating.^[102] Figure 10d shows the enhancement of the stability of AgNW networks thanks to thin oxide layer (ZnO) coatings. The voltage failure observed during voltage ramps increases from 9 to 18 V for, respectively, bare AgNWs to 30 nm ZnO-coated AgNWs, showing a clear electrical stability enhancement.^[47]

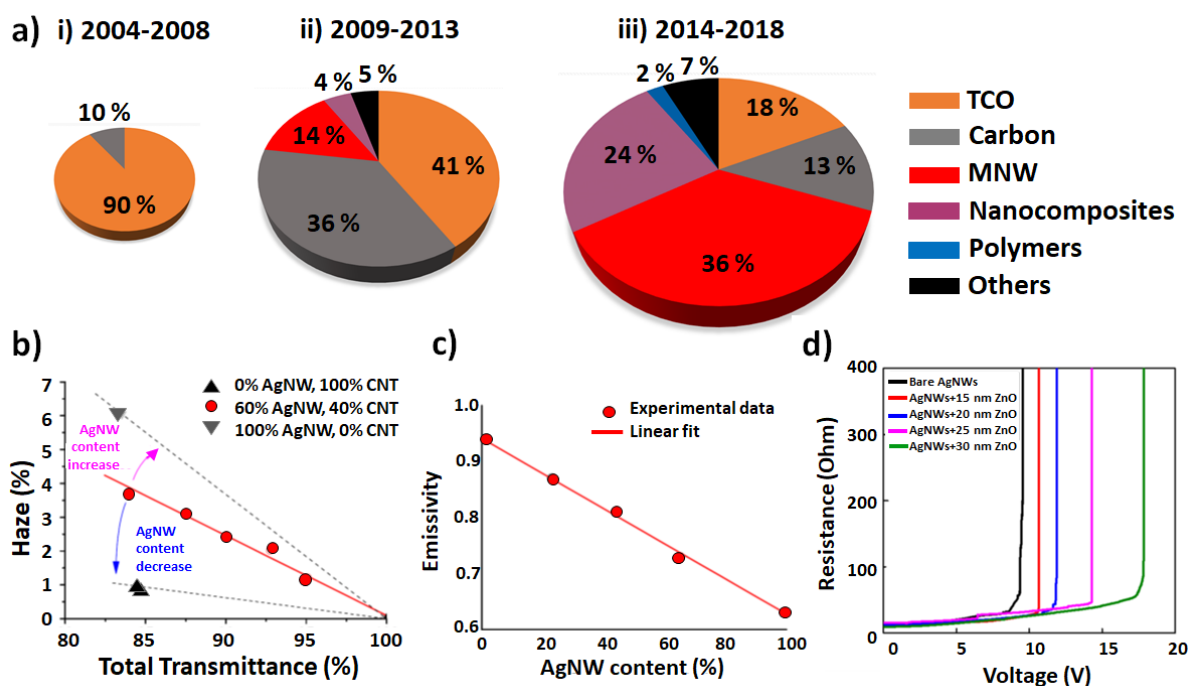


Figure 10. Emergence and examples of the assets of nanocomposite TH technologies. a) Pie-chart representing the percentage of scientific articles associated to the different TH technologies, showing that before 2008 mostly TCOs were mentioned in TH literature, while a small proportion of carbon materials (graphene and CNTs) were starting to be studied. Since 2009 MNW, meshes and grids have attracted much more attention. These past years, nanocomposites have been the focus of many articles, while conductive polymer-based THs have been explored since 2017. The pie-charts are growing with time to illustrate the fact that the number of articles per year has been multiplied by 10 between the first period (2004-2008) and the more recent one (2014-2018), demonstrating a clear growing interest in THs by the scientific community, driven by industrial needs (Sources: Scopus and Web of Science). b) Influence of AgNW content on optical transmittance and haze factor of hybrid conductive films composed of CNTs and AgNWs. c) Emissivity versus AgNW film content of similar film heaters prepared by roll to-roll coating. b,c) Reproduced with permission.^[102] Copyright 2013, Elsevier. d) Variation of electrical resistance versus voltage for bare and ZnO-coated AgNW networks subjected to voltage ramps of 0.1 V/min: the stability of the hybrid composite is clearly enhanced since the failure voltage increases with ZnO thickness. Reproduced with permission.^[47] Copyright 2018, American Chemical Society.

The next sections of 3.5 will focus in more detail on the properties of nanocomposites, discussed per combinations of materials.

3.5.1 Higher thermal efficiency of metallic nanowire and carbon-based materials

Carbon-based materials and MNW hybrid materials have been widely developed for transparent properties enhancements like haze tuning^[102,179,180], but also to improve stability^[181–183] or adhesion.^[184] These hybrids are mainly comprised of 2D MNW networks (copper or silver)

combined with CNTs, graphene, GO or rGO. As reported in section 3.2, carbon-based THs suffer from their poor conductivity at high levels of transparency. For heating applications, strong synergies are evidenced when combining the properties of carbon materials and MNWs for efficient, stable and highly flexible THs.

The carbonaceous species (CNTs or Graphene) of the NW-based hybrids significantly improves stability and heat dissipation^[116] of the MNW networks for better thermal efficiency.^[185] Indeed, a more effective spreading of the heat with a small amount of SWCNTs improves the overall thermal stability of the NW network by improving resistance to current shocks.^[185] Moreover, the excellent thermal contact between nanowires and graphene, estimated at 0.5 m.K/W by Gupta et al. prevents Joule heating at the NW/NW junctions.^[186] Sadeque et al. focused their work on thermal transport behaviors in 2D networks of hybrid materials, especially graphene/AgNW composites.^[187] They disentangled contributions from local self-heating (hotspots) and heat spreading from the contacts, using thermoreflectance measurements.^[187]

Figure 11a shows SEM pictures of a CNT-AgNW hybrid heater. Highly stretchable and stable hybrid THs were developed, with a very low haze (under 1% at 95% transparency) and elasticity as high as 20%.^[80] As reported very recently by Wang *et al.*, a tri-layer film-based heater of rGO-AgNW-GO, as shown in Figure 11b, exhibits far better chemical, mechanical and thermal performances than pure AgNWs.^[188] They report a significant improvement in long-term stability, with fewer failures on the sandwich-structured film heater.

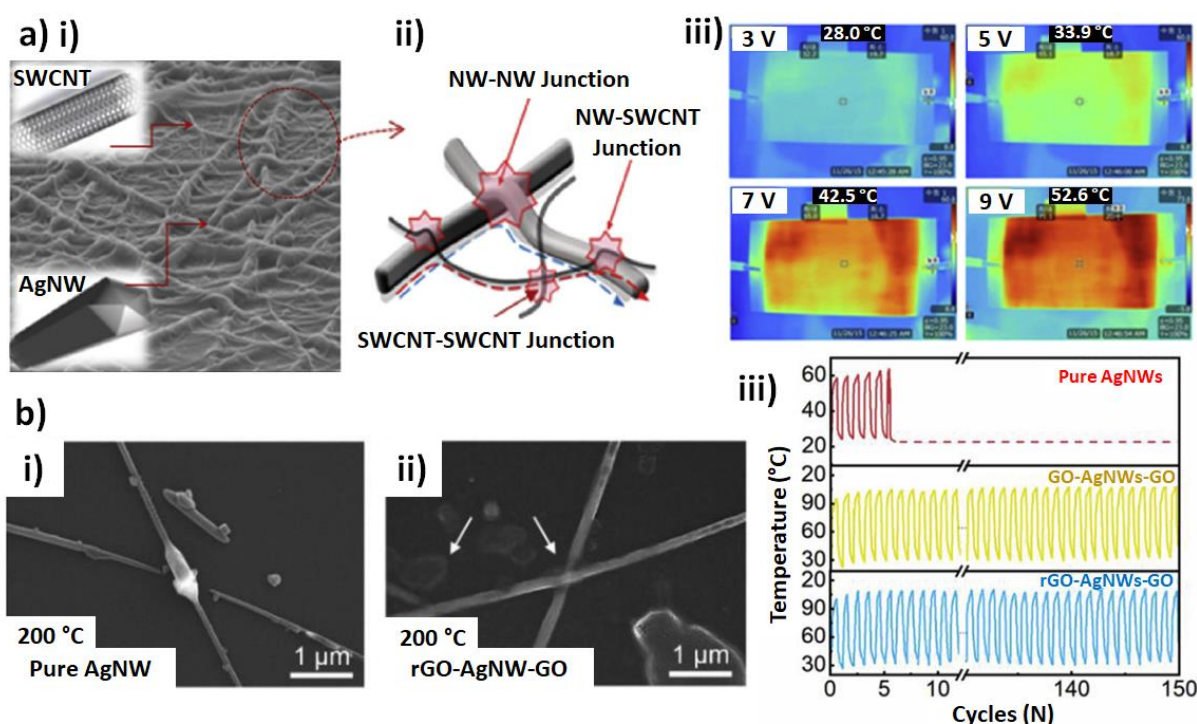


Figure 11. Carbon and MNW-based hybrid THs. a) AgNW-SWCNT hybrid composite layer on TPU: i) FESEM surface image of the hybrid composite layer. ii) schematic representation showing the current pathways. iii) IR thermal images of the SWCNT–AgNW hybrid TH, with a sheet resistance of 30 Ω/sq , under different applied input voltages (3, 5, 7 and 9 V). Reproduced with permission.^[80] Copyright 2018, Elsevier. b) Tri-layer rGO-AgNW-GO composite film i) SEM pictures of pure AgNWs, ii) tri-layer composite film heated at 200°C, iii) heating and cooling tests of pure AgNW, GO-AgNW-GO and rGO-AgNW-GO THs under ON/OFF current cycles of 60 s. Reproduced with permission.^[188] Copyright 2019, Elsevier.

3.5.2 Adhesion enhancement within metallic nanowire/polymer hybrid transparent heaters

As previously mentioned, polymers are extremely attractive in terms of flexibility/stretchability and processability. Nanocomposite materials relying on MNWs and polymers combine the high conductivity of a MNW network with the desirable mechanical properties of polymers, like flexibility,^[189] stretchability,^[190] and adhesion^[175].

Thanks to the addition of conducting elements in polymer matrices, it is possible to enhance the conductivity while preserving processability. Most of these composite-based THs take advantage of metallic nanofillers, often made of silver or copper. Nanospecies with high form factors are preferred, to favor percolation for the electron pathways. In particular, metallic

nanowires can provide efficient networks at low densities, as described by the stick percolation theory.^[191,192] PEDOT:PSS, Polyimide (PI), polydimethylsiloxane (PDMS), PET, polyester (PE), poly(methyl methacrylate) PMMA, and even healable polyurethane (PU-DA) are the most reported matrices for the fabrication of composites for THs.^[79,112,114,175,189,193–204] Biopolymers like chitosan are interesting emerging materials for medical TH applications because of their biocompatibility and biodegradability.^[205] For composites, the choice of the polymer-conducting filler couple depends on the specific properties that are targeted. Polymers generally act as binders to ensure good contacts between nanoparticles and substrate, or they can serve as flexible/stretchable substrates to provide these properties to the system. They do not improve the heating properties, but are interesting nonetheless because of their optical properties (thin film transparency), their potential ability to allow the homogeneous dispersion of conducting nanoparticles, and for their mechanical performances. PEDOT:PSS is also often used as a host for the fabrication of conducting composites, and has mainly been used to improve the adhesion with the substrate. The comparison of film adhesion before and after peeling of 3M Scotch tape is demonstrated in **Figure 12a** and 12b for a pristine AgNW (Figure 12a) and PEDOT:PSS composite film (Figure 12b).^[175] The optical transmittance (measured at 550 nm) was increased from 75% to 81% for the AgNW film, while it remains at 79% for the composite film, demonstrating the enhanced adhesion of the composite.

PEDOT:PSS can also enhance the conductivity by creating conductive pathways between spatially separated nanowires.^[206] In some cases, the conductive polymer can be doped with graphene to improve heating stability.^[116]

Nearly all reported polymer/AgNW hybrid systems show similar performances with a maximal temperature of 100-150 °C, a transparency around 85 % at an operating voltage between 10 and 40 V. Large differences in haze factor are observed, with values ranging from 3% ^[189] to 30 %.^[194] Screen printing, doctor-blading and drop coating are the main methods reported for the deposition of AgNWs, which are then coated with the polymer. ^[175,189,194] AgNWs can be

1079 embedded to improve the contact and stability in flexion, with a stable resistance after 1000
1080 bending cycles (with a 500 μm radius of curvature).^[189] Another way to stabilize the system is
1081 to add a thin transparent protective layer of poly(vinyl alcohol) (PVA) or insoluble PI.^[194,196]
1082 Healable polymers, based on the Diels-Alder reaction, can be cured by simple heat
1083 treatment.^[202] Figure 12c shows that after deliberate damage by a knife cut, the
1084 AgNW/polyurethane-based TH can heal and recover its original conductivity thanks to a simple
1085 heat treatment at 120 °C.^[202]
1086 Hybrid materials with a copper/alumina/PI combination are interesting, with a high and stable
1087 temperature of 300°C reached for a 10 V bias, associated with 91% transparency.^[201] Alumina
1088 limits the diffusion and oxidation of Cu, while PI is an effective binder to improve the adhesion
1089 strength between the Cu wires and the substrate. Heating stability was demonstrated for 100
1090 cycles with a substantial pulsed current of 1.5 A. Mechanical properties were investigated with
1091 bending (1000 cycles, 2 mm radius) and stretching (30 % stretchability on PDMS) experiments,
1092 and no significant change in conductance was observed. **Similar improvement of adhesion**
1093 **properties of AgNW networks to the substrate due to the use of PI was demonstrated by Lu et**
1094 **al.**^[204]

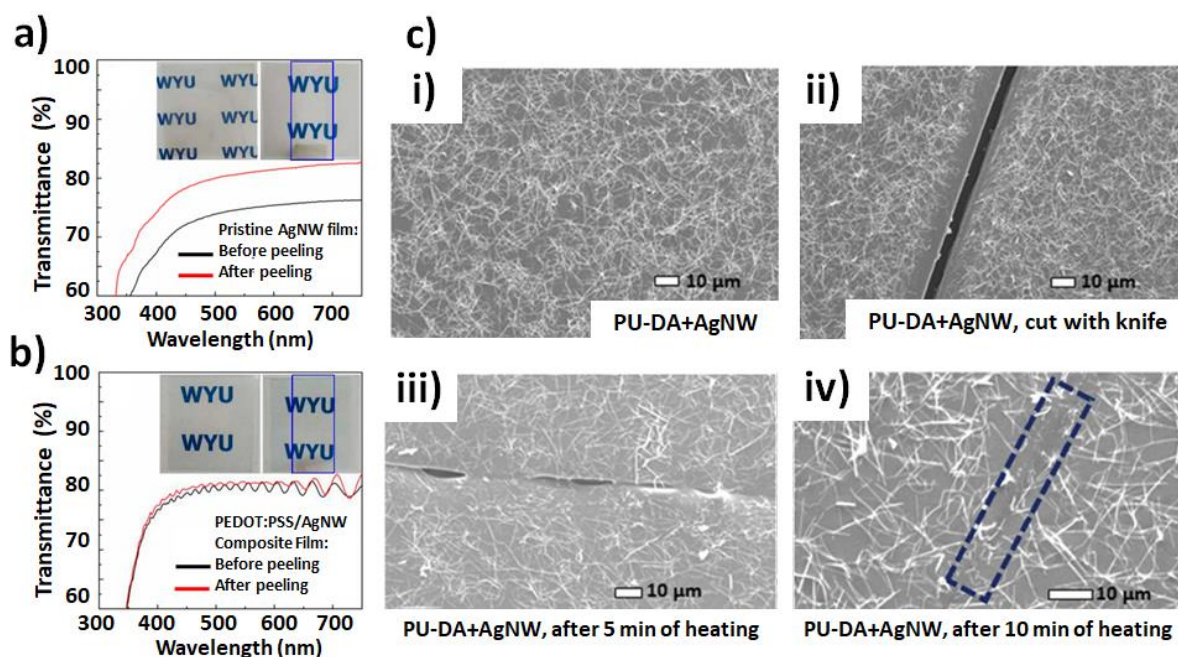


Figure 12. THs based on nanocomposites with AgNW networks and polymers. a) Peeling test of a pristine AgNW film showing a large increase in optical transparency. b) Similar experiment with AgNW and PEDOT:PSS composite showing no increase in optical transparency, associated to a clear improvement in adhesion thanks to the polymer. Reproduced with permission.^[175] Copyright 2017, MDPI. c) FESEM images of the transparent, flexible and healable material with AgNWs and polymers: i) The healable TH as deposited, ii) after a cut with a knife, iii) healing of the electrode at a temperature of 120 °C for 5 min, and (iv) healing of the electrode at a temperature of 120 °C for 10 min. The dotted box indicates the location of the previous cut. Reproduced with permission.^[202] Copyright 2017, Royal Society of Chemistry.

3.5.3 Stability enhancement of metallic nanowires with oxide material

Percolating MNW networks have been shown to act as efficient transparent electrodes^[20,33,34] and can be used in solar cells^[40] and as THs^[42]. The most studied MNWs are AgNWs since their synthesis and properties exhibit strong advantages: silver is the material with the highest thermal and electrical conductivity at room temperature, and the synthesis of AgNWs is well-mastered. However, these metallic nanowire networks suffer from stability issues. MNW thermal instability leads to spheroidization (associated to the loss of the percolating nature of the networks^[90]). Furthermore, electrical instability is observed when the networks undergo electrical stress^[93,168]. CuNW networks are interesting^[30,31] since the price of Cu is much lower than Ag. However, Cu is much more prone to oxidation than Ag and thus the chemical stability

of CuNWs is a more critical issue. To enhance the stability of MNWs in general, several solutions have been investigated. The coating of MNWs by a thin oxide layer has shown clear improvements in stability. This strategy has been reported for AgNW/TiO₂^[46], AgNW/ZnO^[47,207], CuNW/Al₂O₃^[48,169], CuNW/ZnO.^[208] **Figure 13** shows SEM (a,b) and TEM (c,d) images of AgNW networks before (a,c) and after (b,d) the deposition of a thin layer of ZnO using atmospheric pressure spatial atomic layer deposition (AP-SALD)^[47]. This technique appears as an ideal approach to protect MNWs since it is a rapid, atmospheric and cheap method for thin film conformal deposition, and therefore does not compromise the low-temperature, atmospheric pressure fabrication of MNW networks.^[208–210] A 25 nm thick coating of ZnO drastically enhances the stability of the TH, as shown in Figure 13e.^[47] Figure 13f shows the relative electrical resistance of the bare AgNW network and the ZnO:Al/AgNW nanocomposite versus time when the samples were subjected to voltage ramp cycles (between 2 V and 6.5 V). The electrical stability is clearly enhanced thanks to the conformal coating when compared to bare AgNWs.^[208] Similarly, Tigan et al. recently reported an extensive study relating CuNW network density and oxide nature (Al₂O₃, ZnO) with electrical and optical properties, as well as stability. These authors were able to reach thermal stability up to 273 °C for CuNW with a thin Al₂O₃ coating, and a remarkably high heating rate of 14 °C/s.^[169]

In addition to improving the network stability, oxide coatings give rise to materials with a much higher adhesion than bare nanowires. Figure 13g shows an optical picture of the peeling off test of a CuNW/Al₂O₃/polyimide(PI) composite film using 3M scotch tape.^[201] Figure 13h reports the variations in optical transmittance (blue) and sheet resistance (black) for Cu wire/Al₂O₃/PI (black circles) and Cu wire/Al₂O₃ (black square) network composite films versus the number of performed tape tests. The composite film (Cu wire/Al₂O₃/PI) clearly exhibits an enhanced adhesion compared to the Cu wire/Al₂O₃, which became insulating after the third tape test.^[201]

Of note, an approach has recently been used to enhance the transmittance of AgNW networks coated with protective metal oxide bilayers thanks to an anti-reflective coating.^[211]

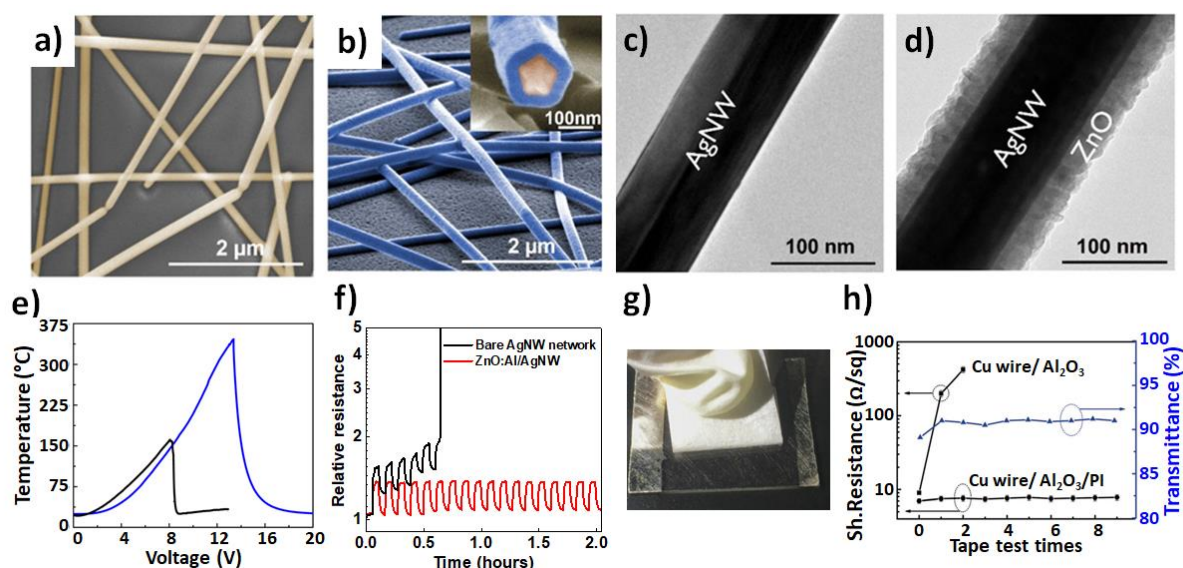


Figure 13. THs based on nanocomposites of MNWs and thin oxide layers. SEM (a,b) and TEM (c,d) observations of AgNW before (a,c) and after (b,d) deposition of a thin layer of ZnO layer using atmospheric pressure spatial atomic layer deposition (AP-SALD). A 25 nm thick ZnO coating drastically enhances the electrical stability of the TH, as shown in e), with the measured temperature during a voltage ramp for a bare and a coated silver nanowire network, in black and blue lines respectively. a-e) Reproduced with permission.^[47] Copyright 2018, American Chemical Society. f) Relative electrical resistance versus time of the bare AgNW network and ZnO:Al/AgNW nanocomposite when the samples were subjected to voltage ramp cycles (between 2 V and 6.5 V): the electrical stability is enhanced thanks to the conformal coating. Reproduced with permission.^[208] Copyright 2019, Royal Society of Chemistry. g) Optical picture showing the peeling off test for the Cu wire/ Al_2O_3 /polyimide (PI) composite film by 3M scotch tape. h) Variations of sheet resistance (black) versus the number of performed tape tests for Cu wire/ Al_2O_3 /PI and for Cu wire/ Al_2O_3 network composite films; optical transmittance values (blue) Cu wire/ Al_2O_3 /PI are also plotted. g,h) Reproduced with permission.^[201] Copyright 2016, Royal Society of Chemistry.

While the positive effects of thin oxide coatings on the performance of MNW networks have been reported several times, coating with metallic or oxide nanoparticles (NP) can also be an efficient method. For example, Morgenstern et al. showed that full encapsulation of the AgNW network by a layer of ZnO-NP drastically enhances thermal stability.^[207] Cheong demonstrated that AgNW and AZO can lead to efficient and flexible THs: the AZO coating enables to reach a higher average film temperature of 100 $^{\circ}\text{C}$ (30 $^{\circ}\text{C}$ higher than uncoated AgNWs) as well as a greater heating uniformity.^[212] Cheng et al. also showed that AgNWs can be decorated with gold nanoparticles, leading to a greatly enhanced thermal stability.^[213] Sharma et al. demonstrated that highly stable THs can be obtained with AgNWs decorated with cobalt

nanoparticles (CoNPs). It was found that an optimum AgNW-CoNP ratio of 50-50 wt% leads to good performances of the corresponding TH, with a thermal stability up to 350 °C.^[214]

3.5.4 Metallic grids and transparent conductive oxides or graphene

Hybrids based on metallic grids combined with graphene exhibit a superior electrical and mechanical stability. Kim et al.^[148] fabricated copper grid meshes by photolithography and deposited a graphene layer on top of the meshes (**Figure 14a**), while Kang et al.^[215] used electro-hydrodynamic jet printing to write silver grids on a large-area graphene layer. In both cases the hybrids showed improved and more uniform heating performances^[215] compared to each separate material, even after thousands of bending or twisting cycles.^[148] In the case of the Cu grid/graphene, the excellent flexibility is also due to the corona treatment of the PET substrate. Another study on metallic grid-based hybrid THs combined Ag meshes with a thin layer of ITO (Figure 14b). In this study, Kwon et al showed a 12% increase in optical transmittance, followed by a lower power consumption compared to the as-deposited ITO films^[149].

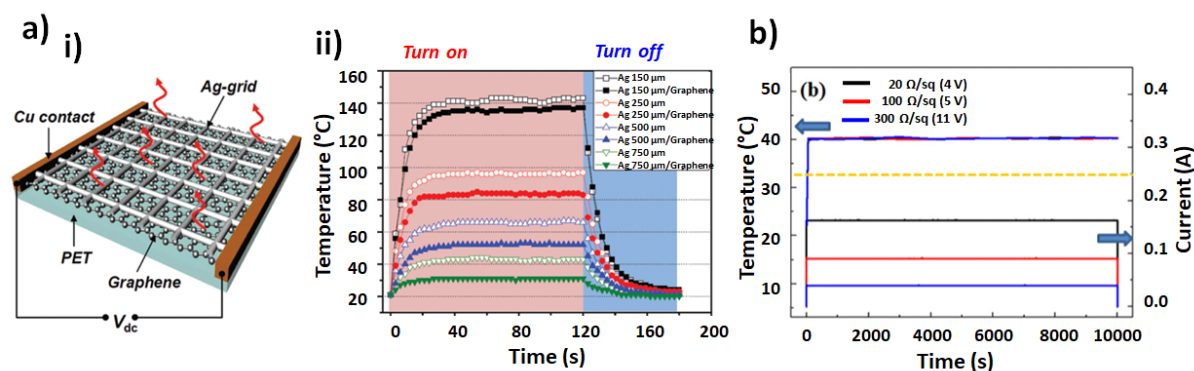


Figure 14. Transparent heaters from metallic grid-based hybrids. a) Ag-grid/graphene heaters: i) schematic illustration of the Ag-grid/graphene film heater connected to Cu electrodes. The size of the heating area was $5 \times 5 \text{ cm}^2$ and ii) time-dependent temperature response of the Ag-grid and Ag-grid coated with graphene heaters. Reproduced with permission.^[215] Copyright 2015, Royal Society of Chemistry. b) Ag mesh-ITO hybrid heaters with sheet resistances of 20, 100, and 300 Ω/sq . The temperature remains very stable for 10,000 s while a voltage of 4, 5 and 11 volts is applied, respectively. Reproduced with permission.^[149] Copyright 2014, IOP Publishing.

3.5.5 Transparent heaters based on metallic or transparent conductive oxide multilayers

Other combinations of materials have been reported in the literature, including multilayers of TCOs or polymers with metallic thin films, or by combining different TCOs and nanoparticles. Several studies deal with the combination of a metallic thin film that is sandwiched between two TCO layers. Kim's group demonstrated that it is possible to make high-performance and flexible THs using continuous roll-to-roll (R2R) sputtering.^[51] In their studies, Ag or Cu was sputtered, from metallic targets, in between 40 nm thick ITO layers. They used a pilot scale system capable of coating 700 mm wide PET substrates at room temperature. In the case of ITO/Ag/ITO films, a transmittance of 88.2% and a sheet resistance of 3 Ω/sq were achieved.^[51] 50 x 50 mm² THs were then fabricated, reaching a steady-state temperature of 100 °C by applying 5 V. In this case, the Ag layer was 12 nm thick and took around 100 s to reach 100 °C. In the case of ITO/Cu/ITO layers, an optical transmittance of 73.9% and a sheet resistance of 11.8 Ω/sq were obtained.^[52] In this study, the best figure of merit was obtained for 12 nm thick Cu layers, and temperatures above 100 °C were obtained under a bias of 8 V. In another study, the ITO layers were replaced by InZnSiO, in combination with Ag, using the same R2R sputtering approach.^[216] The electrodes showed a transmittance of 91.91% and a sheet resistance of 7.83 Ω/sq for a 8 nm thick Ag layer. The electrodes reached 110 °C for a bias of only 2.4 V. The amorphous nature of the oxide yielded a high thermal stability upon cycling, as well as mechanical stability (no degradation of performance after 10,000 bending tests with a 10 mm bending radius).^[216] The same group presented a similar approach in which ITO was replaced by SnO₂ and the metal layer was composed of a AgPdCu alloy.^[217] In this case, these flexible In-free electrodes were deposited by thermal evaporation, and showed a minimum sheet resistance of 9.42 Ω/sq with transmittance values above 91% for 50 nm thick SnO₂ layers and a 10 nm thick metallic layer.^[217] The metallic layers alone showed a poorer performance than the tri-layer in terms of both conductivity and transmittance, due to the antireflective effects of

the multiple coatings. THs made of $\text{SnO}_2/\text{AgPdCu}/\text{SnO}_2$ multilayers reached different temperatures for different SnO_2 thicknesses. For 10 nm thick oxide layers, temperatures above 110 °C were obtained under a 5.5 V bias, with heating response times between 100 and 200 seconds.^[217] Finally, in a similar approach, Roul *et al.* reported AZO/Ag/AZO electrodes made by sputtering, on PET substrates.^[218] The structural, electrical and optical properties were evaluated as a function of Ag layer thickness. The best results were obtained for a thickness of 5 nm, for which temperatures above 100 °C were obtained for a bias voltage of 10 V.^[218] In another case of a multilayer transparent electrodes, Kang *et al.* proposed the study of polymer/Ag/polymer and polymer/Ag/inorganic (ITO or SiN_x) tri-layer electrodes.^[219] The electrodes were produced by an R2R sputtering system, and the addition of a fluorocarbon polymer led to a higher flexibility, with the electrodes sustaining bending up to a radius of 3 mm, with a sheet resistance of less than 5 Ω/sq and a transmittance of 68%. The use of fluorocarbon polymer also yielded water-repelling electrodes, preventing wetting and removing contamination. THs based on fluorocarbon/Ag/ SiN_x reached 180 °C for a bias voltage of 13 V.^[219] Kim *et al.* have presented an asymmetric multilayer TH based on a GZO seed layer, an Ag metallic layer and a GZO optoelectronic control layer.^[220] The electrodes were deposited by sputtering at room temperature, and they showed an optimum sheet resistance of 5.4 Ω/sq for a transmittance of 81.6% (50 nm GZO/12 nm Ag/50 nm GZO). The electrodes were deposited on glass substrates of different thicknesses, in order to evaluate the effect of heat loss through the substrate. The temperature reached on the film and the substrate, as well as the rising time, both depended on the substrate thickness. Heat loss due to conduction needs to be considered for substrates ≥ 3 mm. A model is presented that allows the calculation of heating rates and deicing times.^[220] In a different approach, Im *et al.* proposed THs based of CNT sheets with granular metal (Pd).^[221] The addition of these metal particles boosted the heating efficiency by a factor of 3.6, from 99.9 to 27.3 °C cm^2/W . This improvement is attributed to electron-lattice interaction and heat loss suppression. Finally, Hudaya *et al.* reported THs based on FTO

with scattered metal nanodots (Cr, NiCr and Ni). The FTO layers were deposited by sputtering, while the metallic nanodots were deposited by electron cyclotron resonance CVD.^[222] The electrodes showed transmittance values over 85% and reached saturation temperatures over 80 °C for a bias voltage of 12 V.

These and other approaches, like TiO₂/Ag/TiO₂ multilayers, have been explored in recent years.^[223] While only the examples described above have been evaluated as THs, it is expected that more electrodes based on the combination of different materials will also be evaluated for TH applications.

3.6 Synthetic comparison between the different TH technologies

As previously described, there are different TH technologies which exhibit diverse characteristics. We have briefly reminded the main features for each technology, and will compare them in more detail in this section. TCOs are the most investigated/used TH technology in industrial devices,^[10] and were discussed in section 3.1. They certainly are the most stable technology, at least in terms of electrical and thermal stability, but they are not compatible with flexible devices nor with solution-based fabrication processes. Moreover, due to indium scarcity, technologies using more abundant or cheaper materials, have been investigated.^[21] Carbon-based materials are mainly represented by carbon nanotubes and graphene, which have already been integrated in TH devices by several research teams (see section 3.2).^[27,61,143] Lately there has been a clear interest in metallic-based THs (as reported in section 3.3). MNW random networks have been well investigated these past years, in particular AgNW^[20,39] and to a lesser extent CuNW.^[48,66,169,224] Interesting properties in terms of TH behavior have been reported with this technology, along with promising flexibility and cost-effective solution process fabrication. MNW-based THs appear compatible with large scale industrial fabrication such as roll-to-roll technology.^[42,44,45] In parallel, metallic mesh networks and grids also exhibit good physical properties and constitute efficient THs.^[72,112,148] However,

the thermal and electrical stability of these metallic-based THs can be a severe issue. However, as shown by Chen et al.,^[56] Cu based grids made from a Ag seed layer and a subsequent electroplating of Cu imprinted microgrooves exhibit very good performances. Indeed, sheet resistance down to 0.03 Ω/sq associated with a transmittance of 86% was demonstrated. Furthermore these TH exhibit good stability. The possibility to fabricate them by roll-to-roll manufacturing appears promising for industrial integration. Metal nanofibers present also interesting physical properties in recent studies.^[75,87] Additionally, very recent efforts have led to drastically improve the properties of conductive polymers^[49], reaching the conductivity of state-of-the-art FTO layers (i.e. $3 \cdot 10^{-4} \text{ S/cm}$)^[14]. By investigating different dopants for poly(3,4-ethylenedioxythiophene) (PEDOT)-based materials, Gueye et al. reported thin polymer films with a R_{sh} of 57 Ω/sq , a transparency of 87% and a very low haze factor (i.e. <1%). The use of these conductive polymers enables the fabrication of all-polymer-based THs with excellent performances^[50], with steady-state temperatures exceeding 100 °C when subjected to a 12 V bias.

As described in section 3.5, the association of the different aforementioned materials leads to nanocomposites and/or hybrids, constituting a very rich family of TH technologies that offer a large panel of properties/performances with clearly enhanced electrical and thermal stabilities. The ongoing efforts by the community to fabricate, better understand and optimize THs is notably driven by the growing desire for low-cost, more stable and efficient THs. These efforts can efficiently address several challenges for many applications, the latter being described below in section 4.

The comparison of these different technologies is represented in **Figure 15**, with several criteria being considered. It is worth mentioning that these criteria and the marks associated to each criterion and for each TH technology are subject to discussion, therefore only general trends should be considered. Depending on experimental TH synthesis and usage, a range of figures of merit with minimum and maximum values are proposed. Exceptions ruling out these trends

do exist. The flexibility criterion refers to the capacity of a TH technology to withstand bendability or, for some applications, stretchability tests. TCOs are generally not flexible since oxides belong to the ceramic family, which are brittle materials (see Figure 7d), while other TH technologies are highly flexible. This is the case of all emerging TH technologies. Another critical issue is thermal stability: TCOs are very stable compared to other TH technologies. Thin oxide layers are even used as coatings for other TH technologies, forming efficient and stable nanocomposite THs. Conductive polymers are the least thermally stable among all TH technologies due to their organic nature. Nevertheless high temperatures (above 100°C) can be maintained for a long time, which is sufficient for most applications. The cost of a TH technology depends on several parameters, including the industrial production chain. The learning curves generally show a power law dependency between the cost of a device and the total cumulative production amount. Spatial uniformity is an application-dependent criterion. Homogeneous and continuous thin layers (such as TCOs, conductive polymers or some nanocomposites) are uniform by nature, while networks of carbon nanotubes or metallic nanowires, tiled graphene-based sheets or metallic grids can appear non-homogeneous, as demonstrated by the appearance of hot spots in the worst case.^[187] The use of nanocomposites combining both continuous and discontinuous THs can prevent this non-uniformity. Haacke's figure of merit (FoM) was used (Tr^{10}/R_{sh}): generally speaking, apart from graphene and CNT networks this FoM has rather high values for all TH technologies. Finally, the technological readiness level (TRL) criterion was used. The highest TRL value belongs to the TCO family, which has been investigated and used in industrial devices for several decades. The lowest TRL value is for the conductive polymers, for which the drastic progresses of conductivity making them very promising are only recent.^[49,50]

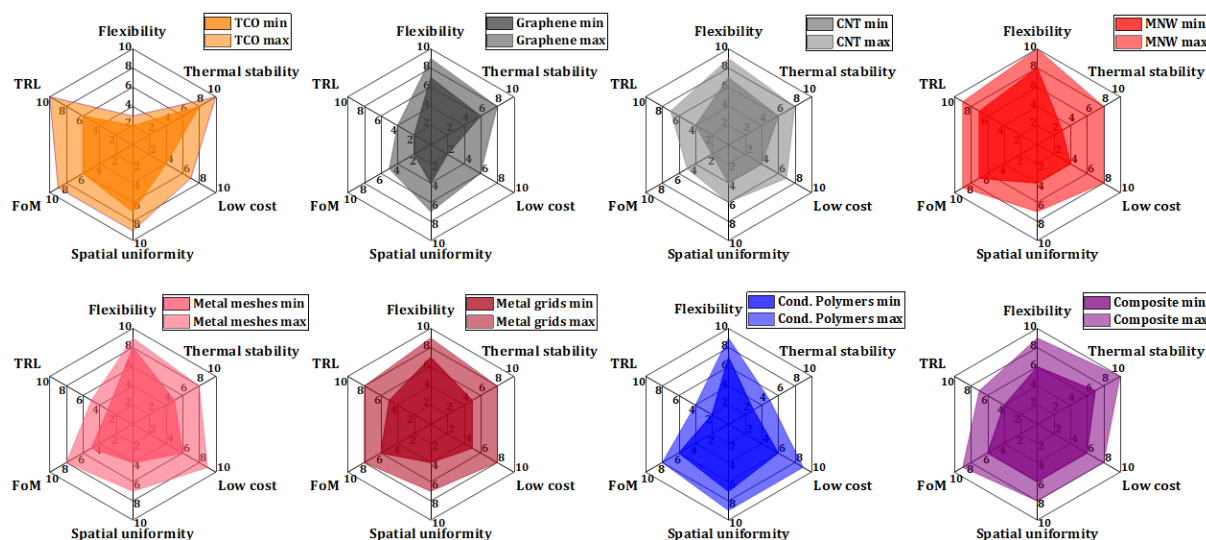


Figure 15. Comparison of THs fabricated with the different technologies. This figure shows the general trends with six criteria (clockwise from the top): flexibility, thermal stability, low cost (of both material and process), spatial uniformity, figure of merit (FoM) and technological readiness level (TRL). Depending on the synthesis and usage of experimental THs, a range of figures of merit with minimum and maximum values is proposed. The marks for all criteria for each TH technology are only general indications, since the actual marks are application-dependent.

Other characteristics could also be of interest. This is the case for the haze factor, which should be low (typically below 2 or 3%) when a TH is placed on windscreens, visors or displays to ensure eye comfort (preventing blurriness). The haze factor is typically low for TCOs, while it can vary drastically for other TH technologies. For instance, small MNW diameters are preferred to decrease the haze factor^[96] of MNW-based THs. Recently, Ji et al. reported a study of ultra-long copper nanofibers covered with a shell of carbon black, which can provide a high-clarity view (i.e. with low haziness) associated to a transparency of 91% and a sheet resistance of $0.8 \Omega/\text{sq}$.^[87] This once again shows that nanocomposite THs can exhibit excellent properties through efficient combinations of key assets from different TH technologies.

4 Integration of transparent heaters in devices:

As described above, THs concern numerous applications. TH fabrication is generally carried out with the goal of implementation in a specific device and for a particular application. As such, active material choice and device design must be considered according to specifications

related to the operational use of the device. After pointing out some issues related to TH fabrication (part 4.1), we will describe examples of technical uses. The first one deals with THs for deicing, defrosting or defogging systems (4.2). Then we show how THs can be relevant for thermochromic devices (4.3), medical applications (4.4) and other niche applications (4.5).

4.1 Integration of THs within devices: generalities and potential issues

Even though the intrinsic performances of the materials developed for THs are generally very good, their integration into functional devices can encounter some difficulties. Integration will depend on the nature of the active and support materials, and in general on the environment close to the heating film. In some cases, adhesion can be an issue if the deposited active layer does not stick well to the substrate. This can occur with metallic nanowires, which usually show limited adhesion and can be removed by a simple finger sweep. Layers of graphene- or PEDOT-based materials can be very thin (i.e. less than 20 nm) and thus very fragile and sensitive to mechanical stress. An encapsulating layer needs to be deposited on top of these materials to ensure a good adhesion to the surface, to avoid mechanical damage while preventing the release of the nanomaterials towards end-users. This encapsulation can be carried out through different techniques, like wet processes for transparent polymers, physical deposition of TCOs by atomic layer deposition, lamination with thin glass sheets or transparent adhesive films.

As mentioned earlier, haziness must be finely controlled during the fabrication process since the haze value can vary significantly for some materials. Low haze values are mandatory for TH applications for windscreens or displays, whereas haziness may not be critical for other applications. This means that the fine control of the material itself (e.g. metallic nanowire diameter^[97] or layer thickness of carbon-based material) is crucial to reach the desired specifications and homogeneity on large surfaces. Depending of the TH application, tints induced by the materials should be considered (from a blue- or greenish hue for conductive

1365 polymers, blackish for CNTs, metallic greyish or a slight orange color for silver and copper
1366 nanowires, respectively, to yellowish with iridescence for TCOs).

1367 Despite their importance, electrical contacts are seldom mentioned in the reported works
1368 dealing with TH integration. The fabrication of good and reliable electrical contacts between
1369 the active layer and the voltage generator is usually not straightforward. Silver-based inks or
1370 pastes are often used for lab-scale demonstrations, but these materials are not always stable in
1371 the long term, and their homogeneous deposition can be tricky. Many other techniques and
1372 materials can be envisaged, like vacuum-deposited metals (gold, silver, copper, nickel, etc.),
1373 metallic ribbons or wires (usually copper-based materials), liquid metals (e.g. eutectic gallium-
1374 indium), or even materials with similar chemical natures to those used in THs, taking into
1375 account that these contact electrodes must be much less resistive than the active layers of the
1376 TH in order to avoid hotspots and Joule heating at unexpected locations.

1377 Beyond the nature of the electrical contacts, the geometry and patterns of contact electrodes are
1378 very important. They will define the heating zones. Depending on their design and voltage
1379 input, specific areas can be heated at different areal power densities. In a basic case study with
1380 two opposite electrodes on a square TH, the distance between the electrodes must be well
1381 designed with respect to the available bias supply. Indeed, the voltage must be increased when
1382 the distance between the electrodes is increased to keep good heating properties (generally at
1383 least a few hundreds of W/m²). If this distance increases too much, then high voltages must be
1384 used, which can seriously damage the active materials.

1385 TH production should also consider the end-user application requirements. For highly flexible
1386 substrates for example, TCOs will not be suitable and polymer materials or metallic nanowires
1387 will be preferred. This choice of active material will also define the relevant and available
1388 deposition techniques, which are active material-dependent. For large area deposition
1389 techniques, special care should be taken to ensure homogeneous deposition, and ideally online
1390 analysis techniques should be implemented to check deposition uniformity.

1391

1392 **4.2 Deicing, defrosting and defogging**

1393 The first application of THs was to avoid condensation in aircraft windshields to increase
1394 visibility in warplanes during military actions. At that time, the TCM used was tin oxide , but
1395 in modern airplanes it has been replaced by ITO, which is more conductive and thus allows a
1396 lower operating voltage (24V).^[2]

1397 The heat produced by THs can also be used for defogging or defrosting applications. Defogging
1398 of car headlights is a recent need. Indeed, since the invention of cars, headlights have been
1399 based on incandescent bulbs, which inherently produce heat, preventing headlight condensation
1400 when they are on. Light-emitting diodes (LEDs) are now gradually replacing conventional
1401 incandescent lamps, because of their reduced energy consumption.^[225] Despite this obvious
1402 advantage, this new kind of headlight does not produce enough heat to avoid condensation or
1403 frosting at the surface of the headlights or inside the headlight housing. This situation creates a
1404 new risk, since fog or frost on the headlights can change light refraction and increase light
1405 diffusion, which degrades road illumination and thus visibility for the driver.

1406 There is a market for defogging devices based on THs in food distribution, with refrigerated
1407 showcases using transparent windows^[2]. Indeed, when products are refrigerated, there is a risk
1408 of condensation because of the temperature difference between the two faces of the case.
1409 Consumers not being able to see products behind the windows can be detrimental to the store;
1410 THs offer an efficient solution to this problem, and patents linked to this topic have existed
1411 since the 90s, with ITO technologies.^[226]

1412 LCD panels are used for outdoor applications. A limitation of LCD displays is liquid crystals
1413 freezing and electronic performance degradation at low temperatures^[227,228,61]. An ultra-thin
1414 film heater at the surface of the screen is an easy and lightweight method to heat the display
1415 and avoid degradation linked to low temperatures.

For car windows (windshield and side windows) and external side mirrors, or even for motorcycle helmet visors, the operating voltage should ideally not exceed 12 V, which is the current standard voltage for cars and motorcycles. This is one of the reasons for the demand for new transparent coatings with lower resistances and similar transparency. The development of the 48 V vehicle will allow, in the near future, to reduce the pressure on the power management of large surface THs and will open up new prospects. Other reasons behind the demand for new transparent coatings concern flexibility and the ability to coat curved surfaces. As previously mentioned, some technologies meet these requirements, especially AgNWs, CNTs, graphene and conducting polymers.

Many demo products have been fabricated, like defoggers/defrosters for car windows or side mirrors (**Figure 16a,b**), made of patterned AgNWs,^[229,230] AgNFs,^[231] Cu grids^[56] or Ni/Ag microgrids.^[195] A demo motorcycle visor (Figure 16c) dip-coated with PEDOT:PSS-EG was fabricated and can be defrosted in a few seconds with a low voltage.^[50] Zn-Sn-oxide(ZTO)/Ag/ZTO was also demonstrated to be of interest for small area defoggers (Figure 16d), as well as for larger areas like the windshield of a commercial car.^[232] Since these systems require low voltages, even sport glasses/ski masks could integrate these new technologies in the coming years.

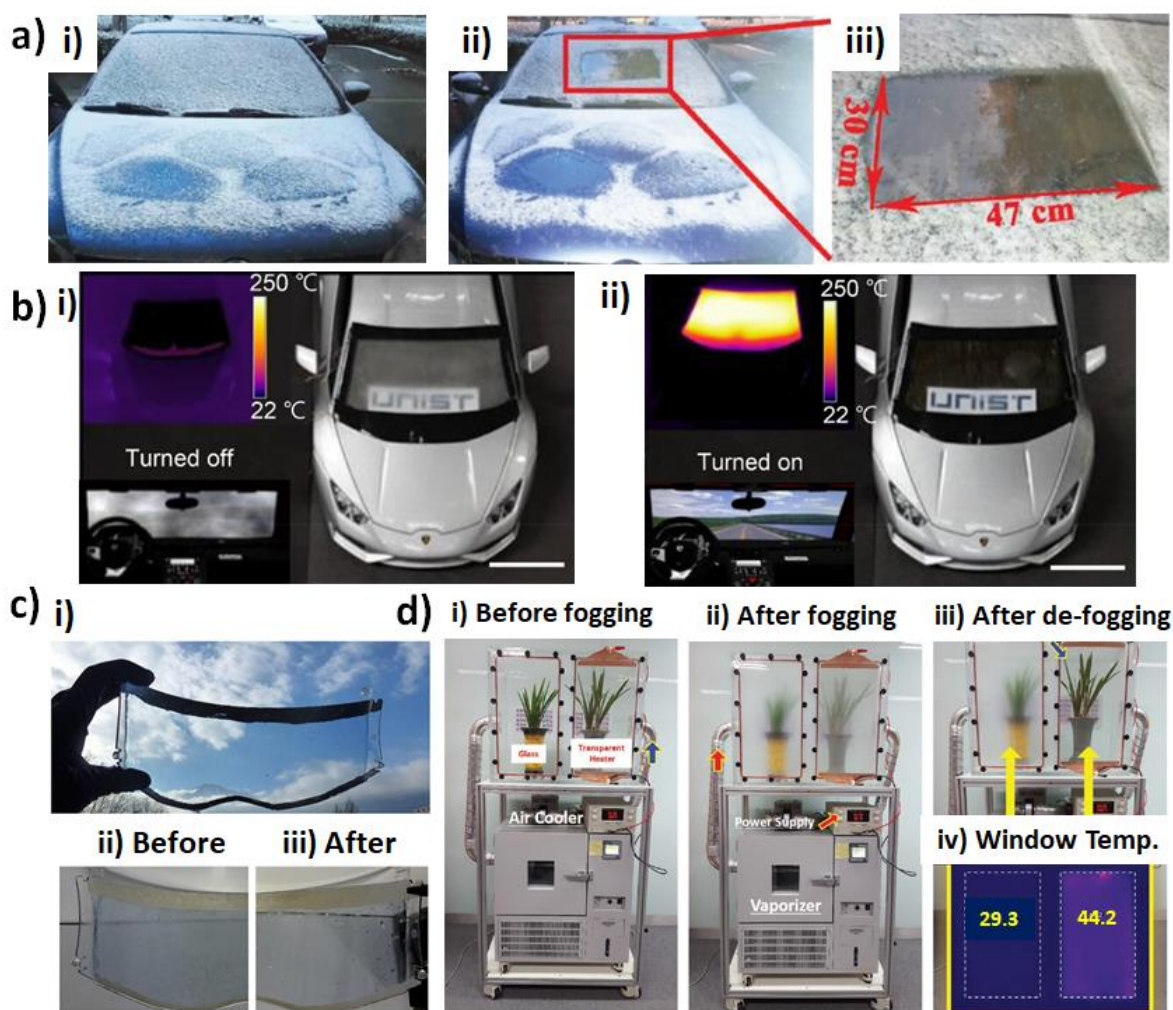


Figure 16. Defrosting and defogging transparent heater applications. a) A car windshield i) before and ii)-iii) after defrosting by applying 20 V for 5 min to a large-size Cu metal-mesh (30 x 47 cm²). Reproduced with permission.^[56] Copyright 2019, John Wiley and Sons. b) Photographs of the Ag/Ag₂O-NF/(index matching layer)IML heater-integrated automobile windshield at i) turn-off and ii) turn-on modes. The applied dc bias was 6 V. The insets show a driver's view through the windshield (lower) and an image captured with an IR camera displaying the temperature distribution of the windshield (upper). Reproduced with permission.^[231] Copyright 2018, American Chemical Society. c) i) a motorcycle visor with a PEDOT:PSS transparent heater, ii) iced in a freezer at -26 °C and iii) after defrosting by the TH. Reproduced with permission.^[50] Copyright 2017, American Chemical Society. d) Pictures describing the quality test of a Zn-Sn-oxide(ZTO)/Ag/ZTO transparent heater (52 x 31 cm²); i) general setting of the test with a normal glass and transparent heater glass placed in front of each orchid before running a test, ii) fog was generated on both windows using a moisturized hot air flow, iii) defogging was carried out on the heater glass for 50 s at 12 V, and (iv) temperature profile of the two glasses during defogging. Reproduced with permission.^[232] Copyright 2019, John Wiley and Sons.

4.3 Thermochromic applications

The alteration of the color or transmittance of thermochromic materials induced by changes in temperature can be used in a large variety of applications such as smart windows and green

buildings, aerospace and military, textile and food packaging.^[233] Thermochromic smart windows are attractive because they are visibly transparent and can intelligently control the amount of solar heat (mainly in the near-infrared region) in response to changes in ambient temperature.^[234] Thermochromic applications are attracting more and more scientific and industrial interests, with efforts being devoted to their successful integration into modern devices. The research discussed in this part shows the Joule effect-based TH influence on thermochromic performance, the associated issues like layer adhesion, and the integration in devices. Vanadium oxide VO₂ materials are often presented, because they exhibit the greatest potential for thermochromic devices and energy-efficient systems^[235] thanks to their electronic structure modification from semi-conducting to metallic behavior when the temperature exceeds 68 °C. Emerging TCMs like CNTs^[236], graphene^[53], AgNWs^[109,200,237,238], conductive polymers^[50] and hybrids^[102,203] have been investigated as the heating elements.

Liu et al.^[236] developed a CNT-based flexible microheater on PET for local heating into a thermochromic display, and tuned the thickness of the materials in order to optimize the thermochromic performance. A first approach was to decrease substrate thickness in order to obtain a good trade-off between mechanical robustness and thermal response. The thermal response of CNT-based films from room temperature to 100 °C was reduced to a few seconds thanks to the use of a 70 µm thick PET layer and with lower CNT coverage.^[236] Indeed, heat dissipation increases inversely with CNT coverage. Finally, a thermochromic display coupled to a driving circuit was made, and Chinese characters were displayed thanks to local heating by the CNT microheater on PET.

In parallel, Kim et al.^[53] reported interesting progress related to the fabrication of flexible VO₂/Graphene-based thermochromic films for energy-saving windows. Graphene acts as a very thin (i.e. atomic film), flexible but robust substrate for the formation of stoichiometric VO₂ crystals. The transfer of the graphene-supported VO₂ onto a plastic substrate enables the

formation of a flexible thermochromic film which shows a decrease of in-house temperature under infrared irradiation in a mock-up house.

In the case of AgNW-based THs, Li et al.^[237] studied the influence of AgNW networks on the VO₂ nanoparticle-based thermochromic performance. The infrared response of this VO₂/AgNW-based device can be controlled thanks to the applied voltage, and the dependence is shown to be highly stable and reversible. **Figure 17a** shows the square-like shape of the dynamic infrared response to the pulse voltage. The response of the VO₂/AgNW-based device exhibits a step variation. The transmittance in the infrared region can therefore quickly be altered when applying either rising or falling input voltage.

Huang et al.^[238] fabricated a flexible AgNW/PI TH with faster and higher heating temperatures at lower power consumption compared to TCO heaters. The flexible and stable TH was successfully used in a thermochromic device. The obtained AgNW/PI-based TH exhibited a heating temperature of 96°C under a bias of 6V, and a response time of 40 seconds.^[238]

Recently, Huang et al.^[200] fabricated a large-area flexible, transparent thermochromic window based on AgNW nylon-meshes. This thermochromic textile could be produced cheap and fast, i.e. 20 minutes for 7.5 m² and a cost of \$15.03.

Another interesting and recent study presented by Kim et al.^[109] used AgNW-based THs as a color-shifting anisotropic soft actuator with a very large bending curvature of 2.5 cm⁻¹ at a low temperature of 40 °C. The transient behavior of the curvature and temperature of the color changing actuators based on AgNW Joule heating is shown in Figure 17b as well as digital camera images of the color of the actuator. The devices have demonstrated a superior long-term stability for more than 10,000 operating cycles. Shi et al.^[203] demonstrated a SiO₂/AgNW/colorless PI composite film heater with an improved transparency of 3.5 % due to the antireflective SiO₂ coating. The haze of both bare and SiO₂-coated AgNW/cPI films are the same, as well as their heating performance. The composite shows good mechanical properties, and was tested in a thermochromic device with a purple to blue color change after 10 s of

applied voltage. Kim et al.^[102] fabricated a CNT/AgNW hybrid TH with reduced haze and improved flexibility at 1.5 mm bending radius. The haze of the hybrid film is tuned by AgNW content, and its heating performance is monitored by the color change of a thermochromic dye inside a beaker wrapped with the CNT/AgNW TH film.

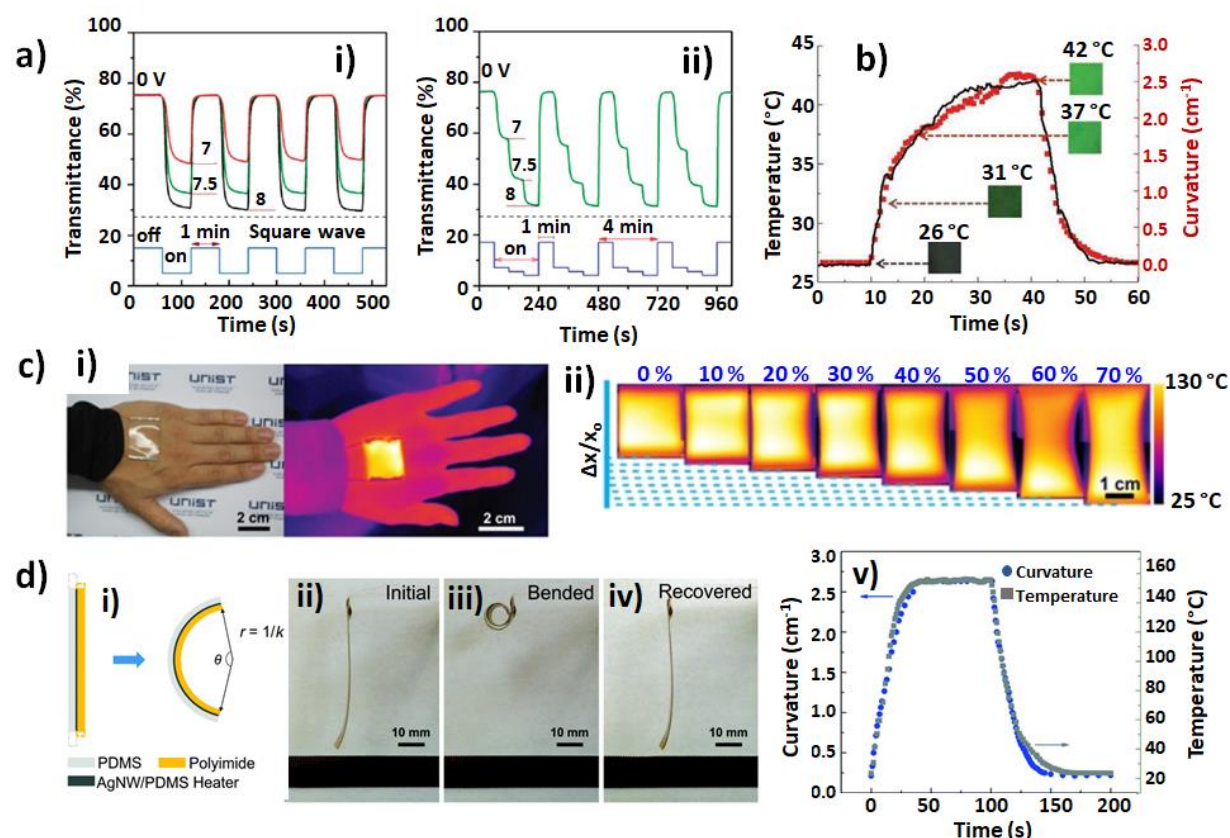


Figure 17. Thermochromic, medical and other transparent heater applications. a) Infrared response at 1.5 mm of a VO₂ NP-electrothermochromic film device based on AgNWs upon input of a pulse voltage with i) a square wave and ii) a square wave with a step variation. The dashed line denotes the lowest transmittance at a constant voltage of 8 V. The pulse wave pattern and its application method are shown below the dashed line, along with the wave parameters. Reproduced with permission.^[237] Copyright 2014, Royal Society of Chemistry. b) The transient behavior of the curvature and temperature of a color-shifting anisotropic soft actuator based on an AgNW network TH. Insets are digital camera images of the actuator's color changes with respect to temperature. Reproduced with permission.^[109] Copyright 2018, John Wiley and Sons. c) Transparent and wearable heaters using nanotrough network of CuZr metallic glasses; i) photograph and IR image of the heater attached to a human hand. The black strap is the custom-made electronic band for a power supply and temperature controller. ii) IR images of the CuZr nanotrough heater under various tensile strains. Reproduced with permission.^[70] Copyright 2016, American Chemical Society. d) Bending and heating performance of the PI/AgNW/PDMS bimorph actuator; i) schematic of the electrothermal bimorph actuation mechanism. k : bending curvature; r : radius of curvature, ii) the initial state, iii) the bent state with the maximum curvature and iv) the recovered state of the U-shaped actuator. One end of the actuator is fixed and the other end can bend freely and reversibly under an applied DC voltage of 4.5 V. v) Curvature and temperature of the actuator as a function of time. Reproduced with permission.^[239] Copyright 2017, Royal Society of Chemistry.

4.4 Transparent heaters for Medical applications

This last decade has seen the emergence of new flexible and stretchable electronics to fabricate sensors and actuators with properties similar to skin (namely deformation of up to 15 % and elastic modulus between 10 kPa and a few hundred kPa^[240]). These kinds of devices can be found under several names, namely “electronic skin”, “e-skin”, “epidermal electronics“ and “electronic tattoos”.^[241] They present the advantages of being skin-mountable and thus relevant for continuous health monitoring, drug delivery, thermotherapy, human motion detection, human-machine interfaces and soft robotics.^[241–243]

Since 2013, Webb et al.^[244,245] have worked on the continuous thermal characterization of the skin by using ultrathin arrays of sensors and heaters. Combining sensing and heating allows to monitor physical and chemical parameters (like body temperature, glycemia, blood pressure and oxygen, elastic modulus of the skin^[241]) and potentially immediately diagnosing and delivering a medical treatment by cutaneous contact, keeping in mind that skin permeability or healing can be improved by local heating^[246].

Epidermal drug delivery systems are attractive because of the reduced side effects of topical administration. Bagherifard et al.^[243] used flexible heaters in dermal patches to control the release rates of drugs encapsulated into a thermo-responsive hydrogel (N-Isopropylacrylamide, NIPAM).

Currently, sensor heaters are generally made of a bilayer of chromium and gold^[243–245], which are not transparent. Nevertheless, the nanometric thickness of the circuit results in a quasi-transparent device and highlights this line of research.

The most important application of electronic skins is thermotherapy, which is a new but expanding field. Indeed, heating pads are commonly used for a wide range of medical functions, like relieving pain^[247,248], preventing inflammation and improving blood circulation.^[121]

1553 Aside from pain relief, beneficial effects of a local heating treatment can be explained by the
1554 vasodilation, allowing blood vessels to supply more oxygen and nutrients to the surrounding
1555 area. Heating also prevents chronic inflammation by expelling inflammatory exudates.^[249]
1556 Moreover, heating pads can be useful in physiotherapy to help tendons, ligaments and muscles
1557 gain flexibility.^[250] The two currently available technical solutions for thermotherapy are heat
1558 packs and wraps.^[250,251] Heat packs are bulky and heavy and must be pre-heated in water or in
1559 a micro-wave, often compromising the fine control of the temperature. Heating wraps allow a
1560 better control of the temperature thanks to the Joule heating of resistors, but are usually rigid
1561 and heavy, which limits their wearability and their use in hospitals.^[23]
1562 New lightweight and autonomous devices combining a controlled temperature, fast response
1563 and high transparency are gaining interest. Using THs for thermotherapy pads would allow to
1564 see the heated parts of the body, potentially healing wounds, and to adjust more efficiently the
1565 treatment. Different techniques are under development to meet these requirements. The average
1566 values of temperature/voltage should be around 40-50 °C/3-5 V, to avoid burning the skin and
1567 to operate the devices with common batteries. Two methods are mostly studied: patterned
1568 nanocomposites and hybrid films with a network of metallic conductors and an elastomeric
1569 substrate.

1570 In 2015, Choi et al.^[23] developed a patterned nanocomposite made of AgNWs and a
1571 thermoplastic elastomer (styrene-butadiene-styrene, SBS). In order to obtain a highly
1572 conductive nanocomposite, a ligand-exchange reaction was carried out to homogeneously
1573 incorporate the AgNWs within the elastomeric matrix. This serpentine mesh-structure allows
1574 stable heating (+40 °C, 1 V) while being stretched (17% and 26% for extension or flexion of
1575 the wrist and the knee, respectively). The resistance remains stable after 5000 cycles at 30%
1576 strain and 48 h under UV exposure. Unfortunately, the device transparency value was not
1577 reported.

Other techniques being developed use conductive networks based on MNWs or metallic glasses, coated on elastomeric substrates. CuZr metallic glasses on PDMS display excellent optoelectronic properties, with a resistance of 4 Ω/sq for 90% transparency, combined with a high stretchability (only 30% change in resistance for 70% strain, Figure 17c)).^[70] Moreover, a temperature of 60 °C can be reached for a bias of only 3 V. In terms of stability it is demonstrated that the heating performance of the film is stable for 10 days under relatively harsh conditions (85 °C for 85% RH). CuNW-based hybrids also present good performances, with 96 Ω/sq for 91% transparency, using a poly(methyl methacrylate) (PMMA) coating.^[252] To obtain a stretchable device, the elastomer Ecoflex® (blend of cellulose, lignin, poly(lactic acid), poly(hydroxy alkanate) and starch) was used as a replacement for PMMA, and enabled a stretching of 80% with a constant DC bias of 1.5 V. Under these conditions, however, the maximal reported temperature reached only 30 °C. If the stretching is kept low, a temperature of 50°C can be reached while applying 3 V, which is sufficient for thermotherapy. Percolated AgNW networks deposited on PDMS and encapsulated with PVA were shown to have adequate properties for thermotherapy pads, with high transparency (90%), low sheet resistance (20 Ω/sq and a low operating voltage (3.5 V to reach 45 °C)).^[121] Stability under severe thermal (80 °C) and humidity (80% RH, 45°C) conditions was demonstrated for an extended period of 6 months, in addition to mechanical stability over 10,000 bending cycles (1 mm radius).

Recently, the impact of skin surface heating has been evaluated thanks to tests on porcine skin, to evaluate the efficacy of thermotherapy. A 12 °C temperature raise of the subcutaneous tissue (5 mm beneath the skin surface) was measured.^[190]

Stretchable TCMs demonstrate promising potential for thermotherapy. The stretchability of THs for thermotherapy is an added value. Many research projects on these materials have emerged in recent years, often in strong relationship with the development of flexible and transparent electronics.^[253] Based on the growing interest in wearable devices and the wide

range of medical applications, there is no doubt that the research on this topic will gain further momentum.

4.5 Other niche applications

Besides the main applications previously described, THs are clearly interesting for other niche fields like actuators, gas sensors or refractive index tuning. Actuators are devices which are able to convert different types of energy, such as light^[254], electric fields^[255], magnetic fields^[256], pneumatic pressure^[257] or thermal energy, into mechanical energy. Among them, electrothermal actuators are based on either the thermal expansion of a single material or on the difference in thermal expansions between two materials. Their competitive advantages over other actuators are their low actuation voltage, as well as their lightweight and electrolyte-free design. Zhu et al. demonstrated the use of graphene in bimorph actuators.^[258] Graphene contracts upon heating due to a negative thermal expansion coefficient, which is opposite to the common behavior of nearly all materials. This asymmetric thermomechanical response leads to a large bimorph actuation. More recently, transparent electrothermal actuators using CNT-based THs^[259,260] and AgNW-based THs^[109,239] have been reported. Yao et al. demonstrated a remarkable 2.6 cm^{-1} curvature at a very low actuation voltage of 0.2 V/sq (4.5 V) in electrothermal actuators using AgNW THs (Figure 17d).^[239]

Several studies mention the use of thermal stimuli to address different functions. Zhang et al. developed a transparency-switchable electrothermal actuator using aligned CNT-based THs.^[260] In this paper, the authors used a paraffin wax/polydimethylsiloxane composite. At room temperature, the composite is opaque due to the light scattering induced by the paraffin wax crystallites. Upon heating, actuation occurs simultaneously with wax melting, which results in a dramatic increase in transmittance. Kim et al. demonstrated the use of MNW-based THs for simultaneous actuation and thermochromic color change.^[109]

Transparency becomes an important feature for gas sensors. Since heating gas sensors can improve their performances, the use of Joule heating with THs was reported to improve sensitivity and/or recovery time.^[62,261] Choi et al. developed graphene-based gas sensors, in which graphene was used for both sensing and heating.^[62] They reduced the recovery time of the NO₂ sensor by two orders of magnitude by heating the system up to 250°C. Similarly, Walia et al. improved the response time (from 41 to 13 s) and recovery time (from 112 to 35 s) at 1% H₂, with a moderate Joule heating at 75°C of the transparent conducting palladium network used for sensing.^[261]

In another niche application, Heo et al. demonstrated the use of ITO-based THs for the development of lenticular lenses with a thermally tunable focus, using liquid crystals.^[262] The temperature can alter the birefringence of a liquid crystal-based lens by changing the refractive index between the active component and the polymer layer. Increasing the temperature from 25 °C to 55 °C altered the focal length from 5.5 mm to 8.5 mm. These lenticular lenses have potential in optical devices like phone cameras.

Finally Won et al.^[263] showed an original concept of stretchable kirigami TE consisting of ultrathin and flexible AgNWs/colorless polyimide cPI composites with laser patterned kirigami structure. A coating thin gold layer enables biocompatibility and enhances electrical stability. The laser patterning technique provides digital and rapid process (without patterning masks) allowing to design kirigami structures.^[263] This leads to achieve tunable stretchability, up to strain of 400%, which extends the scope of applications. Such a soft, thin and highly stretchable features can pave ways for multifunctional transparent and wearable electronic skin applications.

5 Prospects, future challenges and conclusive remarks

Since the first use of THs approximately eighty years ago, tremendous progress has been made in this field. TCOs were the first materials developed and produced at the industrial scale to fabricate efficient THs. These materials have been highly improved over the past decades, and now reach outstanding properties, in particular thanks to an excellent transparency-conductivity trade-off. Although TCOs have been the materials of choice until now, new scientific breakthroughs and new market needs have opened the way for innovative developments, notably based on nano-enabled technologies. The driving forces to search for (improved) substitutes to TCOs not only rely on cost issues, but also on geostrategic considerations, which can be a game-changer, and on the technological evolution of devices. Many devices will require flexibility and stretchability (displays, PV cells, touch screens...), which requires new performances and abilities. The development of these transparent materials could offer an additional value to existing opaque film heaters and permit to see through the active layer. This could be of interest applications in health (*e.g.* patches for thermotherapy) or safety (*e.g.* control of heating elements such as automotive gas pre-heater pipes).

Several relevant approaches appear very promising for TH production with improved functionalities. The recent development of nanomaterials has revealed unforeseen possibilities through the achievement of macroscopic performances relying on ordered or random assemblies of nanospecies, whether carbon-based or metallic. When electrically conductive nanoparticles are assembled on a surface above the percolation threshold, they give access to conductive surfaces at very low coverage values, which allows light to pass through, and to reach both high conductivity and high transparency. Another relevant possibility that needs to be further studied is the recent development based on the use of very thin films of highly conductive polymers. The performances are very promising, and these films have an intrinsically very low haze value.

All these new technologies have managed to meet the expectations at the prototype stage, but certainly need further development to ensure reproducibility, cost-efficiency and stability at the industrial stage. Reproducibility mainly relies on the constant quality and chemical purity of the raw materials (CNTs, graphene, MNWs, polymers), but also on stable large-scale production tools and multiscale characterization techniques. Stability aspects are also particularly important, and they should be tackled while taking into account the targeted operational conditions. The stability will depend on many parameters like the structure of the device (including chemical compatibility with other layers), the applied voltage, the cyclability, high temperature long-term operating modes, and many others.

Concerning the use of nanomaterials, an in-depth nanotoxicity assessment needs to be carried out to ensure the safe use for both the manufacturers' operators and the end-users. Some studies have already been reported^[97,264–268], but further understanding of all the possible toxicity aspects and long-term effects is needed.

To conclude this review, the current production of THs still relies essentially on an “old” technology which has been improved upon over the years, i.e. TCOs. Many existing and future applications will keep using this technology because it is a reliable and well-proven process. However, various ongoing technical developments will provide THs with additional properties (controlled haze factor, flexibility, stretchability, low-cost deposition processes...). We expect that there will not be a single winner among them, but rather several new TH technologies that will find specific industrial applications in the near future.

Acknowledgments:

This project was partially supported by the French National Research Agency in the framework of the “Investissements d’avenir” program (ANR-15-IDEX-02) through the project Eco-SESA. This work was also performed within the framework of the Centre of Excellence of

1701 Multifunctional Architected Materials "CEMAM" n° ANR-10-LABEX-44-01 through the
1702 project Earth. This work was funded by the Agence Nationale de Recherche (ANR, France) via
1703 the program [ANR-16-CE05-0021](#) (DESPATCH), ANR-18-CE09-0041 (Meaning) and ANR-
1704 18-CE09-0036 (Panassé). This work was also supported by the Région Auvergne Rhône-Alpes
1705 through the project Pack Ambition Recherche 2018 Eternité. The Carnot Energies du Futur is
1706 acknowledged through the project FREE. The authors would like to warmly thank Vincent
1707 Fitzpatrick for fruitful discussions.

1708

1709

1710 **References:**

- 1711 [1] R. Gupta, K. D. M. Rao, S. Kiruthika, G. U. Kulkarni, *ACS Appl. Mater. Interfaces*
1712 **2016**, 8, 12559.
- 1713 [2] R. G. Gordon, *MRS Bulletin* **2000**, 25, 52.
- 1714 [3] S. Long, X. Cao, G. Sun, N. Li, T. Chang, Z. Shao, P. Jin, *Applied Surface Science*
1715 **2018**, 441, 764.
- 1716 [4] L. Long, H. Ye, *Scientific Reports* **2015**, 4, DOI 10.1038/srep06427.
- 1717 [5] S. T. Heinilehto, J. H. Lappalainen, H. M. Jantunen, V. Lantto, *Journal of*
1718 *Electroceramics* **2011**, 27, 7.
- 1719 [6] J. You, L. Meng, T.-B. Song, T.-F. Guo, Y. (Michael) Yang, W.-H. Chang, Z. Hong, H.
1720 Chen, H. Zhou, Q. Chen, Y. Liu, N. De Marco, Y. Yang, *Nature Nanotechnology* **2016**,
1721 *11*, 75.
- 1722 [7] C. G. Granqvist, *Thin Solid Films* **2014**, 564, 1.
- 1723 [8] W. Gaynor, S. Hofmann, M. G. Christoforo, C. Sachse, S. Mehra, A. Salleo, M. D.
1724 McGehee, M. C. Gather, B. Lüssem, L. Müller-Meskamp, P. Peumans, K. Leo,
1725 *Advanced Materials* **2013**, 25, 4006.
- 1726 [9] K. Ellmer, *Nature Photonics* **2012**, 6, 809.
- 1727 [10] C. G. Granqvist, *Solar Energy Materials and Solar Cells* **2007**, 91, 1529.
- 1728 [11] H. J. Park, J. Kim, J. H. Won, K. S. Choi, Y. T. Lim, J. S. Shin, J.-U. Park, *Thin Solid*
1729 *Films* **2016**, 615, 8.
- 1730 [12] J. Gwamuri, A. Vora, J. Mayandi, D. Ö. Güney, P. L. Bergstrom, J. M. Pearce, *Solar*
1731 *Energy Materials and Solar Cells* **2016**, 149, 250.
- 1732 [13] M. Morales-Masis, S. De Wolf, R. Woods-Robinson, J. W. Ager, C. Ballif, *Advanced*
1733 *Electronic Materials* **2017**, 3, 1600529.
- 1734 [14] G. Rey, C. TERNON, M. Modreanu, X. Mescot, V. Consonni, D. Bellet, *Journal of*
1735 *Applied Physics* **2013**, 114, 183713.
- 1736 [15] V. Consonni, G. Rey, H. Roussel, B. Doisneau, E. Blanquet, D. Bellet, *Acta Materialia*
1737 **2013**, 61, 22.
- 1738 [16] K. Ellmer, A. Klein, B. Rech, Eds. , *Transparent Conductive Zinc Oxide*, Springer
1739 Berlin Heidelberg, Berlin, Heidelberg, **2008**.
- 1740 [17] A. Klein, *J. Am. Ceram. Soc.* **2013**, 96, 331.
- 1741 [18] D. Lincot, *MRS Bulletin* **2010**, 35, 778.
- 1742 [19] V. H. Nguyen, U. Gottlieb, A. Valla, D. Muñoz, D. Bellet, D. Muñoz-Rojas, *Materials*
1743 *Horizons* **2018**, 5, 715.
- 1744 [20] T. Sanniccolo, M. Lagrange, A. Cabos, C. Celle, J.-P. Simonato, D. Bellet, *Small* **2016**,
1745 *12*, 6052.
- 1746 [21] D. S. Hecht, L. Hu, G. Irvin, *Advanced Materials* **2011**, 23, 1482.
- 1747 [22] S. Hong, H. Lee, J. Lee, J. Kwon, S. Han, Y. D. Suh, H. Cho, J. Shin, J. Yeo, S. H. Ko,
1748 *Adv. Mater.* **2015**, 27, 4744.
- 1749 [23] S. Choi, J. Park, W. Hyun, J. Kim, J. Kim, Y. B. Lee, C. Song, H. J. Hwang, J. H. Kim,
1750 T. Hyeon, D.-H. Kim, *ACS Nano* **2015**, 9, 6626.
- 1751 [24] N.-S. Jang, K.-H. Kim, S.-H. Ha, S.-H. Jung, H. M. Lee, J.-M. Kim, *ACS Applied*
1752 *Materials & Interfaces* **2017**, 9, 19612.
- 1753 [25] S. Bae, H. Kim, Y. Lee, X. Xu, J.-S. Park, Y. Zheng, J. Balakrishnan, T. Lei, H. Ri
1754 Kim, Y. I. Song, Y.-J. Kim, K. S. Kim, B. Özyilmaz, J.-H. Ahn, B. H. Hong, S. Iijima,
1755 *Nat Nano* **2010**, 5, 574.
- 1756 [26] J. Zhao, Y. Li, G. Yang, K. Jiang, H. Lin, H. Ade, W. Ma, H. Yan, *Nature Energy*
1757 **2016**, 1, 15027.
- 1758 [27] Y.-H. Yoon, J.-W. Song, D. Kim, J. Kim, J.-K. Park, S.-K. Oh, C.-S. Han, *Adv. Mater.*
1759 **2007**, 19, 4284.

- 1760 [28] J. Du, S. Pei, L. Ma, H.-M. Cheng, *Advanced Materials* **2014**, 26, 1958.
- 1761 [29] Y. Sun, Y. Yin, B. T. Mayers, T. Herricks, Y. Xia, *Chem. Mater.* **2002**, 14, 4736.
- 1762 [30] A. R. Rathmell, S. M. Bergin, Y.-L. Hua, Z.-Y. Li, B. J. Wiley, *Advanced Materials*
- 1763 **2010**, 22, 3558.
- 1764 [31] A. R. Rathmell, B. J. Wiley, *Advanced Materials* **2011**, 23, 4798.
- 1765 [32] A. R. Rathmell, M. Nguyen, M. Chi, B. J. Wiley, *Nano Letters* **2012**, 12, 3193.
- 1766 [33] S. De, T. M. Higgins, P. E. Lyons, E. M. Doherty, P. N. Nirmalraj, W. J. Blau, J. J.
- 1767 Boland, J. N. Coleman, *ACS Nano* **2009**, 3, 1767.
- 1768 [34] S. De, P. J. King, P. E. Lyons, U. Khan, J. N. Coleman, *ACS Nano* **2010**, 4, 7064.
- 1769 [35] J. Liang, L. Li, X. Niu, Z. Yu, Q. Pei, *Nature Photonics* **2013**, 7, 817.
- 1770 [36] L. Li, Z. Yu, W. Hu, C. Chang, Q. Chen, Q. Pei, *Advanced Materials* **2011**, 23, 5563.
- 1771 [37] S. Ye, A. R. Rathmell, Z. Chen, I. E. Stewart, B. J. Wiley, *Adv. Mater.* **2014**, 26, 6670.
- 1772 [38] D. Bellet, M. Lagrange, T. Sanniccolo, S. Aghazadehchors, V. H. Nguyen, D. P.
- 1773 Langley, D. Muñoz-Rojas, C. Jiménez, Y. Bréchet, N. D. Nguyen, *Materials* **2017**, 10,
- 1774 570.
- 1775 [39] D. Chen, J. Liang, Q. Pei, *Sci. China Chem.* **2016**, 1.
- 1776 [40] J. Liu, D. Jia, J. M. Gardner, E. M. J. Johansson, X. Zhang, *Materials Today Energy*
- 1777 **2019**, 13, 152.
- 1778 [41] R. Zhang, M. Engholm, R. Zhang, M. Engholm, *Nanomaterials* **2018**, 8, 628.
- 1779 [42] C. Celle, C. Mayousse, E. Moreau, H. Basti, A. Carella, J.-P. Simonato, *Nano Research*
- 1780 **2012**, 5, 427.
- 1781 [43] S. Sorel, D. Bellet, J. N. Coleman, *ACS Nano* **2014**, 8, 4805.
- 1782 [44] O. Ergun, S. Coskun, Y. Yusufoglu, H. E. Unalan, *Nanotechnology* **2016**, 27, 445708.
- 1783 [45] T. Kim, Y. W. Kim, H. S. Lee, H. Kim, W. S. Yang, K. S. Suh, *Advanced Functional*
- 1784 *Materials* **2013**, 23, 1250.
- 1785 [46] M. Lagrange, T. Sanniccolo, D. Muñoz-Rojas, B. G. Lohan, A. Khan, M. Anikin, C.
- 1786 Jiménez, F. Bruckert, Y. Bréchet, D. Bellet, *Nanotechnology* **2017**, 28, 055709.
- 1787 [47] A. Khan, V. H. Nguyen, D. Muñoz-Rojas, S. Aghazadehchors, C. Jiménez, N. D.
- 1788 Nguyen, D. Bellet, *ACS Applied Materials & Interfaces* **2018**, 10, 19208.
- 1789 [48] C. Celle, A. Cabos, T. Fontecave, B. Laguitton, A. Benayad, L. Guettaz, N. Pélissier,
- 1790 V. H. Nguyen, D. Bellet, D. Muñoz-Rojas, J.-P. Simonato, *Nanotechnology* **2018**, 29,
- 1791 085701.
- 1792 [49] M. N. Gueye, A. Carella, N. Massonnet, E. Yvenou, S. Brenet, J. Faure-Vincent, S.
- 1793 Pouget, F. Rieutord, H. Okuno, A. Benayad, R. Demadrille, J.-P. Simonato, *Chemistry*
- 1794 *of Materials* **2016**, 28, 3462.
- 1795 [50] M. N. Gueye, A. Carella, R. Demadrille, J.-P. Simonato, *ACS Appl. Mater. Interfaces*
- 1796 **2017**, 9, 27250.
- 1797 [51] E.-H. Ko, H.-J. Kim, S.-J. Lee, J.-H. Lee, H.-K. Kim, *RSC Advances* **2016**, 6, 46634.
- 1798 [52] S.-H. Park, S.-M. Lee, E.-H. Ko, T.-H. Kim, Y.-C. Nah, S.-J. Lee, J. H. Lee, H.-K.
- 1799 Kim, *Scientific Reports* **2016**, 6, DOI 10.1038/srep33868.
- 1800 [53] H. Kim, Y. Kim, K. S. Kim, H. Y. Jeong, A.-R. Jang, S. H. Han, D. H. Yoon, K. S.
- 1801 Suh, H. S. Shin, T. Kim, W. S. Yang, *ACS Nano* **2013**, 7, 5769.
- 1802 [54] H. H. Khaligh, L. Xu, A. Khosropour, A. Madeira, M. Romano, C. Pradère, M.
- 1803 Tréguer-Delapierre, L. Servant, M. A. Pope, I. A. Goldthorpe, *Nanotechnology* **2017**,
- 1804 28, 425703.
- 1805 [55] G. Haacke, *Journal of Applied Physics* **1976**, 47, 4086.
- 1806 [56] X. Chen, S. Nie, W. Guo, F. Fei, W. Su, W. Gu, Z. Cui, *Advanced Electronic Materials*
- 1807 **2019**, 5, 1800991.
- 1808 [57] J. Kang, H. Kim, K. S. Kim, S.-K. Lee, S. Bae, J.-H. Ahn, Y.-J. Kim, J.-B. Choi, B. H.
- 1809 Hong, *Nano Lett.* **2011**, 11, 5154.

- 1810 [58] H. Askari, H. Fallah, M. Askari, M. C. Mohmmadieyh, *arXiv:1409.5293 [cond-mat]*
 1811 **2014**.
- 1812 [59] G. Giusti, V. Consonni, E. Puyoo, D. Bellet, *ACS Appl. Mater. Interfaces* **2014**, 6,
 1813 14096.
- 1814 [60] S. Ke, J. Xie, C. Chen, P. Lin, X. Zeng, L. Shu, L. Fei, Y. Wang, M. Ye, D. Wang,
 1815 *Applied Physics Letters* **2018**, 112, 031905.
- 1816 [61] Y. Kim, H. R. Lee, T. Saito, Y. Nishi, *Applied Physics Letters* **2017**, 110, 153301.
- 1817 [62] H. Choi, J. S. Choi, J.-S. Kim, J.-H. Choe, K. H. Chung, J.-W. Shin, J. T. Kim, D.-H.
 1818 Youn, K.-C. Kim, J.-I. Lee, S.-Y. Choi, P. Kim, C.-G. Choi, Y.-J. Yu, *Small* **2014**, 10,
 1819 3685.
- 1820 [63] P. Blake, P. D. Brimicombe, R. R. Nair, T. J. Booth, D. Jiang, F. Schedin, L. A.
 1821 Ponomarenko, S. V. Morozov, H. F. Gleeson, E. W. Hill, A. K. Geim, K. S. Novoselov,
 1822 *Nano Lett.* **2008**, 8, 1704.
- 1823 [64] M. Lagrange, D. P. Langley, G. Giusti, C. Jiménez, Y. Bréchet, D. Bellet, *Nanoscale*
 1824 **2015**, 7, 17410.
- 1825 [65] H. Yang, S. Bai, X. Guo, H. Wang, *Applied Surface Science* **2019**, 483, 888.
- 1826 [66] M. Bobinger, J. Mock, P. La Torraca, M. Becherer, P. Lugli, L. Larcher, *Advanced*
 1827 *Materials Interfaces* **2017**, 4, 1700568.
- 1828 [67] K. D. M. Rao, G. U. Kulkarni, *Nanoscale* **2014**, 6, 5645.
- 1829 [68] H. Hu, S. Wang, S. Wang, G. Liu, T. Cao, Y. Long, *Advanced Functional Materials*
 1830 **2019**, 1902922.
- 1831 [69] H. Wu, D. Kong, Z. Ruan, P.-C. Hsu, S. Wang, Z. Yu, T. J. Carney, L. Hu, S. Fan, Y.
 1832 Cui, *Nat Nano* **2013**, 8, 421.
- 1833 [70] B. W. An, E.-J. Gwak, K. Kim, Y.-C. Kim, J. Jang, J.-Y. Kim, J.-U. Park, *Nano Letters*
 1834 **2016**, 16, 471.
- 1835 [71] R. Gupta, K. D. M. Rao, K. Srivastava, A. Kumar, S. Kiruthika, G. U. Kulkarni, *ACS*
 1836 *Applied Materials & Interfaces* **2014**, 6, 13688.
- 1837 [72] D. Lordan, M. Burke, M. Manning, A. Martin, A. Amann, D. O'Connell, R. Murphy,
 1838 C. Lyons, A. J. Quinn, *ACS Applied Materials & Interfaces* **2017**, 9, 4932.
- 1839 [73] H. Wang, S. Lin, D. Zu, J. Song, Z. Liu, L. Li, C. Jia, X. Bai, J. Liu, Z. Li, D. Wang, Y.
 1840 Huang, M. Fang, M. Lei, B. Li, H. Wu, *Advanced Materials Technologies* **2019**,
 1841 1900045.
- 1842 [74] A. Khan, S. Lee, T. Jang, Z. Xiong, C. Zhang, J. Tang, L. J. Guo, W.-D. Li, *Small*
 1843 **2016**, 12, 3021.
- 1844 [75] S. An, H. S. Jo, D.-Y. Kim, H. J. Lee, B.-K. Ju, S. S. Al-Deyab, J.-H. Ahn, Y. Qin, M.
 1845 T. Swihart, A. L. Yarin, S. S. Yoon, *Advanced Materials* **2016**, 28, 7149.
- 1846 [76] H. S. Jo, S. An, J.-G. Lee, H. G. Park, S. S. Al-Deyab, A. L. Yarin, S. S. Yoon, *NPG*
 1847 *Asia Materials* **2017**, 9, e347.
- 1848 [77] N. Kim, H. Kang, J.-H. Lee, S. Kee, S. H. Lee, K. Lee, *Advanced Materials* **2015**, 27,
 1849 2317.
- 1850 [78] Y. Wang, C. Zhu, R. Pfattner, H. Yan, L. Jin, S. Chen, F. Molina-Lopez, F. Lissel, J.
 1851 Liu, N. I. Rabiah, Z. Chen, J. W. Chung, C. Linder, M. F. Toney, B. Murmann, Z. Bao,
 1852 *Science Advances* **2017**, 3, e1602076.
- 1853 [79] J. Li, J. Liang, X. Jian, W. Hu, J. Li, Q. Pei, *Macromol. Mater. Eng.* **2014**, 299, 1403.
- 1854 [80] B.-Y. Hwang, S.-H. Choi, K.-W. Lee, J.-Y. Kim, *Composites Part B: Engineering*
 1855 **2018**, 151, 1.
- 1856 [81] S. B. Singh, Y. Hu, T. Kshetri, N. H. Kim, J. H. Lee, *Journal of Materials Chemistry C*
 1857 **2017**, 5, 4198.
- 1858 [82] S. Kiruthika, R. Gupta, G. U. Kulkarni, *RSC Adv.* **2014**, 4, 49745.
- 1859 [83] J. J. Bae, S. C. Lim, G. H. Han, Y. W. Jo, D. L. Doung, E. S. Kim, S. J. Chae, T. Q.
 1860 Huy, N. Van Luan, Y. H. Lee, *Adv. Funct. Mater.* **2012**, 22, 4819.

- [84] A.-Y. Kim, K. Lee, J. H. Park, D. Byun, J. K. Lee, *physica status solidi (a)* **2014**, 211, 1923.
- [85] S. Duzyer, S. Sinha-Ray, S. Sinha-Ray, A. L. Yarin, *Macromolecular Materials and Engineering* **2017**, 302, 1700188.
- [86] D. Sui, Y. Huang, L. Huang, J. Liang, Y. Ma, Y. Chen, *Small* **2011**, 7, 3186.
- [87] S. Ji, J. Park, Y. Jo, Y.-B. Kim, J. Jang, S.-K. Kim, S. Jeong, J.-U. Park, *Applied Surface Science* **2019**, 483, 1101.
- [88] T. J. Kang, T. Kim, S. M. Seo, Y. J. Park, Y. H. Kim, *Carbon* **2011**, 49, 1087.
- [89] S. R. Das, A. M. S. Mohammed, K. Maize, S. Sadeque, A. Shakouri, D. B. Janes, M. A. Alam, *Nano Lett.* **2016**, 16, 3130.
- [90] D. P. Langley, M. Lagrange, G. Giusti, C. Jiménez, Y. Bréchet, N. D. Nguyen, D. Bellet, *Nanoscale* **2014**, 6, 13535.
- [91] K. Maize, S. R. Das, S. Sadeque, A. M. S. Mohammed, A. Shakouri, D. B. Janes, M. A. Alam, *Applied Physics Letters* **2015**, 106, 143104.
- [92] F. M. Smits, *Bell System Technical Journal* **1958**, 37, 711.
- [93] T. Sannicolo, N. Charvin, L. Flandin, S. Kraus, D. T. Papanastasiou, C. Celle, J.-P. Simonato, D. Muñoz-Rojas, C. Jiménez, D. Bellet, *ACS Nano* **2018**, 12, 4648.
- [94] N. Hoof, M. Parente, A. Baldi, J. G. Rivas, *Advanced Optical Materials* **2019**, 1900790.
- [95] S.-T. Zhang, M. Foldyna, H. Roussel, V. Consonni, E. Pernot, L. Schmidt-Mende, L. Rapenne, C. Jiménez, J.-L. Deschanvres, D. Muñoz-Rojas, D. Bellet, *J. Mater. Chem. C* **2016**, 5, 91.
- [96] T. Araki, J. Jiu, M. Nogi, H. Koga, S. Nagao, T. Sugahara, K. Suganuma, *Nano Res.* **2014**, 7, 236.
- [97] D. Toybou, C. Celle, C. Aude-Garcia, T. Rabilloud, J.-P. Simonato, *Environmental Science: Nano* **2019**, 6, 684.
- [98] P. R. N. Childs, in *Practical Temperature Measurement*, Elsevier, **2001**, pp. 98–144.
- [99] B. Liptak, Ed., *Instrument Engineers' Handbook, Fourth Edition, Volume One: Process Measurement and Analysis*, CRC Press, **2003**.
- [100] A. Rogalski, P. Martyniuk, M. Kopytko, *Reports on Progress in Physics* **2016**, 79, 046501.
- [101] Y.-A. Li, Y.-J. Chen, N.-H. Tai, *Materials Research Express* **2014**, 1, 025605.
- [102] D. Kim, L. Zhu, D.-J. Jeong, K. Chun, Y.-Y. Bang, S.-R. Kim, J.-H. Kim, S.-K. Oh, *Carbon* **2013**, 63, 530.
- [103] D. Pierścińska, *Journal of Physics D: Applied Physics* **2018**, 51, 013001.
- [104] T. Yagi, K. Tamano, Y. Sato, N. Taketoshi, T. Baba, Y. Shigesato, *Journal of Vacuum Science & Technology A: Vacuum, Surfaces, and Films* **2005**, 23, 1180.
- [105] O. Breitenstein, W. Warta, M. Langenkamp, *Lock-in Thermography: Basics and Use for Evaluating Electronic Devices and Materials*, Springer Science & Business Media, **2010**.
- [106] Ch. Schmidt, F. Altmann, O. Breitenstein, *Materials Science and Engineering: B* **2012**, 177, 1261.
- [107] T. Sannicolo, D. Muñoz-Rojas, N. D. Nguyen, S. Moreau, C. Celle, J.-P. Simonato, Y. Bréchet, D. Bellet, *Nano Letters* **2016**, DOI 10.1021/acs.nanolett.6b03270.
- [108] R. Gupta, A. Kumar, S. Sadasivam, S. Walia, G. U. Kulkarni, T. S. Fisher, A. Marconnet, *ACS Applied Materials & Interfaces* **2017**, 9, 13703.
- [109] H. Kim, H. Lee, I. Ha, J. Jung, P. Won, H. Cho, J. Yeo, S. Hong, S. Han, J. Kwon, K.-J. Cho, S. H. Ko, *Advanced Functional Materials* **2018**, 28, 1801847.
- [110] V. Zardetto, T. M. Brown, A. Reale, A. Di Carlo, *Journal of Polymer Science Part B: Polymer Physics* **2011**, 49, 638.

- 1911 [111] J. Jang, B. G. Hyun, S. Ji, E. Cho, B. W. An, W. H. Cheong, J.-U. Park, *NPG Asia*
 1912 *Materials* **2017**, 9, e432.
- 1913 [112] S. M. Lee, S. Oh, S. T. Chang, *ACS Applied Materials & Interfaces* **2019**, 11, 4541.
- 1914 [113] F. Oytun, O. Alpturk, F. Basarir, *Materials Research Bulletin* **2019**, 112, 53.
- 1915 [114] J.-G. Lee, J.-H. Lee, S. An, D.-Y. Kim, T.-G. Kim, S. S. Al-Deyab, A. L. Yarin, S. S.
 1916 Yoon, *Journal of Materials Chemistry A* **2017**, 5, 6677.
- 1917 [115] H.-J. Kim, Y. Kim, J.-H. Jeong, J.-H. Choi, J. Lee, D.-G. Choi, *Journal of Materials*
 1918 *Chemistry A* **2015**, 3, 16621.
- 1919 [116] M. Cao, M. Wang, L. Li, H. Qiu, Z. Yang, *ACS Applied Materials & Interfaces* **2018**,
 1920 10, 1077.
- 1921 [117] D. Doganay, S. Coskun, S. P. Genlik, H. E. Unalan, *Nanotechnology* **2016**, 27, 435201.
- 1922 [118] S. Xie, T. Li, Z. Xu, Y. Wang, X. Liu, W. Guo, *Nanoscale* **2018**, 10, 6531.
- 1923 [119] Y. Tang, H. Ruan, Z. Huang, D. Shi, H. Liu, S. Chen, J. Zhang, *Nanotechnology* **2018**,
 1924 29, 455706.
- 1925 [120] J. Kwon, H. Cho, Y. D. Suh, J. Lee, H. Lee, J. Jung, D. Kim, D. Lee, S. Hong, S. H.
 1926 Ko, *Advanced Materials Technologies* **2017**, 2, 1600222.
- 1927 [121] W. Lan, Y. Chen, Z. Yang, W. Han, J. Zhou, Y. Zhang, J. Wang, G. Tang, Y. Wei, W.
 1928 Dou, Q. Su, E. Xie, *ACS Applied Materials & Interfaces* **2017**, 9, 6644.
- 1929 [122] E. C. David Levy, Ed. , *TRANSPARENT CONDUCTIVE MATERIALS: From Materials*
 1930 *via Synthesis and Characterization to Applications.*, WILEY-VCH, Place of
 1931 Publication Not Identified, **2019**.
- 1932 [123] D. Ginley, H. Hosono, D. C. Paine, *Handbook of Transparent Conductors*, Springer
 1933 Science & Business Media, **2010**.
- 1934 [124] V. Consonni, G. Rey, H. Roussel, D. Bellet, *Journal of Applied Physics* **2012**, 111,
 1935 033523.
- 1936 [125] I. Hamberg, C. G. Granqvist, *Journal of Applied Physics* **1986**, 60, R123.
- 1937 [126] B. D. Ahn, S. H. Oh, D. U. Hong, D. H. Shin, A. Moujoud, H. J. Kim, *Journal of*
 1938 *Crystal Growth* **2008**, 310, 3303.
- 1939 [127] D. S. Y. Jayathilake, J. S. Sagu, K. G. U. Wijayantha, *Materials Letters* **2018**, DOI
 1940 10.1016/j.matlet.2018.11.092.
- 1941 [128] J. H. Kim, B. D. Ahn, C. H. Kim, K. A. Jeon, H. S. Kang, S. Y. Lee, *Thin Solid Films*
 1942 **2008**, 516, 1330.
- 1943 [129] M. K. Roul, B. Obasogie, G. Kogo, J. R. Skuza, R. M. Mundle, A. K. Pradhan, *Journal*
 1944 *of Applied Physics* **2017**, 122, 135110.
- 1945 [130] K. Im, K. Cho, J. Kim, S. Kim, *Thin Solid Films* **2010**, 518, 3960.
- 1946 [131] C. Kim, J.-W. Park, J. Kim, S.-J. Hong, M. J. Lee, *Journal of Alloys and Compounds*
 1947 **2017**, 726, 712.
- 1948 [132] K. Yang, K. Cho, K. Im, S. Kim, *Materials Research Bulletin* **2015**, 63, 194.
- 1949 [133] S. Ke, C. Chen, N. Fu, H. Zhou, M. Ye, P. Lin, W. Yuan, X. Zeng, L. Chen, H. Huang,
 1950 *ACS Applied Materials & Interfaces* **2016**, 8, 28406.
- 1951 [134] V. H. Nguyen, D. Bellet, B. Masenelli, D. Muñoz-Rojas, *ACS Applied Nano Materials*
 1952 **2018**, 1, 6922.
- 1953 [135] L. Li, S. K. Hong, Y. Jo, M. Tian, C. Y. Woo, S. H. Kim, J.-M. Kim, H. W. Lee, *ACS*
 1954 *Applied Materials & Interfaces* **2019**, 11, 16223.
- 1955 [136] X. Yao, S. C. Hawkins, B. G. Falzon, *Carbon* **2018**, 136, 130.
- 1956 [137] N. Karim, M. Zhang, S. Afroj, V. Koncherry, P. Potluri, K. S. Novoselov, *RSC*
 1957 *Advances* **2018**, 8, 16815.
- 1958 [138] H. Souri, D. Bhattacharyya, *ACS Applied Materials & Interfaces* **2018**, 10, 20845.
- 1959 [139] M. Yang, J. Pan, A. Xu, L. Luo, D. Cheng, G. Cai, J. Wang, B. Tang, X. Wang,
 1960 *Polymers* **2018**, 10, 568.

- 1961 [140] P. Liu, D. Zhou, Y. Wei, K. Jiang, J. Wang, L. Zhang, Q. Li, S. Fan, *ACS Nano* **2015**,
1962 9, 3753.
- 1963 [141] B. Zhou, X. Han, L. Li, Y. Feng, T. Fang, G. Zheng, B. Wang, K. Dai, C. Liu, C. Shen,
1964 *Composites Science and Technology* **2019**, 183, 107796.
- 1965 [142] H. Souri, S. J. Yu, H. Yeo, M. Goh, J.-Y. Hwang, S. M. Kim, B.-C. Ku, Y. G. Jeong,
1966 N.-H. You, *RSC Advances* **2016**, 6, 52509.
- 1967 [143] O. P. Morris, X. Zang, A. Gregg, B. Keller, B. Getachew, S. Ingersoll, H. A. Elsen, M.
1968 M. Disko, N. Ferralis, J. C. Grossman, *Advanced Materials* **2019**, 31, 1900331.
- 1969 [144] E. J. Spadafora, K. Saint-Aubin, C. Celle, R. Demadrille, B. Grévin, J.-P. Simonato,
1970 *Carbon* **2012**, 50, 3459.
- 1971 [145] H.-S. Jang, S. K. Jeon, S. H. Nahm, *Carbon* **2011**, 49, 111.
- 1972 [146] T. L. Chen, D. S. Ghosh, M. Marchena, J. Osmond, V. Pruneri, *ACS Applied Materials*
1973 *& Interfaces* **2015**, 7, 5938.
- 1974 [147] L. Hu, H. Wu, Y. Cui, *MRS Bulletin* **2011**, 36, 760.
- 1975 [148] B.-J. Kim, J.-S. Park, R. Yoo, J.-S. Park, *RSC Advances* **2017**, 7, 53025.
- 1976 [149] N. Kwon, K. Kim, J. Heo, I. Yi, I. Chung, *Nanotechnology* **2014**, 25, 265702.
- 1977 [150] P. Li, J. G. Ma, H. Y. Xu, D. Lin, X. D. Xue, X. Z. Yan, P. Xia, Y. C. Liu, *Journal of*
1978 *Alloys and Compounds* **2016**, 664, 764.
- 1979 [151] A. Khan, C. Liang, Y.-T. Huang, C. Zhang, J. Cai, S.-P. Feng, W.-D. Li, *Advanced*
1980 *Engineering Materials* **2019**, 1900723.
- 1981 [152] E. Thouti, C. Mistry, A. Chandran, D. K. Panwar, P. Kumar, H. Suman, J. Akhtar,
1982 *Journal of Physics D: Applied Physics* **2019**, DOI 10.1088/1361-6463/ab31dc.
- 1983 [153] T. Sannicolo, Transparent Electrodes Based on Silver Nanowire Networks: Electrical
1984 Percolation, Physical Properties, and Applications, PhD thesis, University of Grenoble
1985 Alpes (France), **2017**.
- 1986 [154] J. H. Park, D. Y. Lee, Y.-H. Kim, J. K. Kim, J. H. Lee, J. H. Park, T.-W. Lee, J. H.
1987 Cho, *ACS Appl. Mater. Interfaces* **2014**, 6, 12380.
- 1988 [155] Y.-Y. Zhao, M.-L. Zheng, X.-Z. Dong, F. Jin, J. Liu, X.-L. Ren, X.-M. Duan, Z.-S.
1989 Zhao, *Applied Physics Letters* **2016**, 108, 221104.
- 1990 [156] J. Kang, C.-G. Park, S.-H. Lee, C. Cho, D.-G. Choi, J.-Y. Lee, *Nanoscale* **2016**, 8,
1991 11217.
- 1992 [157] J. Xue, J. Song, Y. Dong, L. Xu, J. Li, H. Zeng, *Science Bulletin* **2017**, 62, 143.
- 1993 [158] H. Sohn, C. Park, J.-M. Oh, S. W. Kang, M.-J. Kim, *Materials* **2019**, 12, 2526.
- 1994 [159] C. G. da Rocha, H. G. Manning, C. O'Callaghan, C. Ritter, A. T. Bellew, J. J. Boland,
1995 M. S. Ferreira, *Nanoscale* **2015**, 7, 13011.
- 1996 [160] A. T. Bellew, H. G. Manning, C. Gomes da Rocha, M. S. Ferreira, J. J. Boland, *ACS*
1997 *Nano* **2015**, 9, 11422.
- 1998 [161] S. Coskun, E. Selen Ates, H. Emrah Unalan, *Nanotechnology* **2013**, 24, 125202.
- 1999 [162] Y. Goliya, A. Rivadeneyra, J. F. Salmeron, A. Albrecht, J. Mock, M. Haider, J. Russer,
2000 B. Cruz, P. Eschlwech, E. Biebl, M. Becherer, M. R. Bobinger, *Advanced Optical*
2001 *Materials* **2019**, 1900995.
- 2002 [163] M. Bobinger, J. Mock, M. Becherer, P. L. Torraca, D. Angeli, L. Larcher, P. Lugli,
2003 *IEEE*, **2017**, pp. 151–154.
- 2004 [164] I. E. Stewart, S. Ye, Z. Chen, P. F. Flowers, B. J. Wiley, *Chemistry of Materials* **2015**,
2005 27, 7788.
- 2006 [165] E. C. Garnett, W. Cai, J. J. Cha, F. Mahmood, S. T. Connor, M. Greyson Christoforo,
2007 Y. Cui, M. D. McGehee, M. L. Brongersma, *Nature Materials* **2012**, 11, 241.
- 2008 [166] Y. Huang, Y. Tian, C. Hang, Y. Liu, S. Wang, M. Qi, H. Zhang, J. Zhao, *ACS Applied*
2009 *Materials & Interfaces* **2019**, 11, 21850.
- 2010 [167] D. Chen, F. Zhao, K. Tong, G. Saldanha, C. Liu, Q. Pei, *Advanced Electronic*
2011 *Materials* **2016**, 2, 1600167.

- 2012 [168] H. H. Khaligh, I. A. Goldthorpe, *Nanoscale research letters* **2013**, 8, 1.
- 2013 [169] D. Tigan, S. P. Genlik, B. Imer, H. E. Unalan, *Nanotechnology* **2019**, 30, 325202.
- 2014 [170] M.-G. Kang, L. J. Guo, *Adv. Mater.* **2007**, 19, 1391.
- 2015 [171] B. Bessaire, M. Mathieu, V. Salles, T. Yeghoyan, C. Celle, J.-P. Simonato, A. Brioude, *ACS Applied Materials & Interfaces* **2017**, 9, 950.
- 2016 [172] L. J. Romasanta, P. Schäfer, J. Leng, *Scientific Reports* **2018**, 8, DOI 10.1038/s41598-018-34538-w.
- 2017 [173] M. N. Gueye, A. Carella, J. Faure-Vincent, R. Demadrille, J.-P. Simonato, *Progress in Materials Science* **2019**, 100616.
- 2018 [174] C. Shi, K. A. Owusu, X. Xu, T. Zhu, G. Zhang, W. Yang, L. Mai, *Small* **2019**, 1902348.
- 2019 [175] X. He, R. He, Q. Lan, W. Wu, F. Duan, J. Xiao, M. Zhang, Q. Zeng, J. Wu, J. Liu, *Materials* **2017**, 10, 220.
- 2020 [176] X. He, G. Shen, R. Xu, W. Yang, C. Zhang, Z. Liu, B. Chen, J. Liu, M. Song, *Polymers* **2019**, 11, 468.
- 2021 [177] J. Yan, Y. G. Jeong, *Materials & Design* **2015**, 86, 72.
- 2022 [178] S.-B. Yang, H. Choi, D. S. Lee, C.-G. Choi, S.-Y. Choi, I.-D. Kim, *Small* **2015**, 11, 1293.
- 2023 [179] L. Dou, F. Cui, Y. Yu, G. Khanarian, S. W. Eaton, Q. Yang, J. Resasco, C. Schildknecht, K. Schierle-Arndt, P. Yang, *ACS Nano* **2016**, 10, 2600.
- 2024 [180] H. J. Han, Y. C. Choi, J. H. Han, *Synthetic Metals* **2015**, 199, 219.
- 2025 [181] Y. Ahn, Y. Jeong, D. Lee, Y. Lee, *ACS Nano* **2015**, 9, 3125.
- 2026 [182] C. Wu, J. Jiu, T. Araki, H. Koga, T. Sekitani, H. Wang, K. Suganuma, *RSC Adv.* **2016**, 6, 15838.
- 2027 [183] Y. Tang, H. Ruan, Y. Chen, J. Xiang, H. Liu, R. Jin, D. Shi, S. Chen, J. Zhang, *Nanotechnology* **2020**, 31, 045704.
- 2028 [184] S. M. Lee, J. H. Lee, S. Bak, K. Lee, Y. Li, H. Lee, *Nano Research* **2015**, 8, 1882.
- 2029 [185] Y. Cai, X. Piao, X. Yao, W. Gao, E. Nie, Z. Zhang, Z. Sun, *Nanotechnology* **2019**, 30, 225201.
- 2030 [186] M. P. Gupta, N. Kumar, S. Kumar, *IEEE Transactions on Nanotechnology* **2018**, 17, 829.
- 2031 [187] S. Sadeque, Y. Gong, K. Maize, A. K. Ziabari, A. M. Mohammed, A. Shakouri, D. B. Janes, *IEEE Transactions on Nanotechnology* **2018**, 17, 276.
- 2032 [188] S. Wang, Y. Tian, C. Wang, C. Hang, Y. Huang, C. Liao, *Composites Science and Technology* **2019**, 174, 76.
- 2033 [189] K. Pyo, J.-W. Kim, *Current Applied Physics* **2016**, 16, 1453.
- 2034 [190] D. Han, Y. Li, X. Jiang, W. Zhao, F. Wang, W. Lan, E. Xie, W. Han, *Composites Science and Technology* **2018**, 168, 460.
- 2035 [191] K. Barros, P. L. Krapivsky, S. Redner, *Physical Review E* **2009**, 80, DOI 10.1103/PhysRevE.80.040101.
- 2036 [192] M. Žeželj, I. Stanković, A. Belić, *Physical Review E* **2012**, 85, DOI 10.1103/PhysRevE.85.021101.
- 2037 [193] J.-S. Bae, Y.-S. Lee, J. Li, J. Liang, D. Chen, Q. Pei, S.-B. Lee, *Advanced Materials Technologies* **2018**, 1700364.
- 2038 [194] S. Ji, W. He, K. Wang, Y. Ran, C. Ye, *Small* **2014**, 10, 4951.
- 2039 [195] K. Lee, J. Park, H. Kim, H.-S. Park, H.-K. Song, K.-H. Kim, K. Seo, *Journal of Materials Chemistry A* **2018**.
- 2040 [196] C.-Y. Chou, H.-S. Liu, G.-S. Liou, *RSC Advances* **2016**, 6, 61386.
- 2041 [197] M. Patel, K. R. Chauhan, J. Kim, J.-W. Kim, D. Lim, *Sensors and Actuators A: Physical* **2017**, 267, 8.
- 2042 [198] Y. Cai, X. Piao, X. Yao, E. Nie, Z. Zhang, Z. Sun, *Materials Letters* **2019**, 249, 66.

- [199] X. Shi, W. Xu, W. Shen, G. Wang, R. Wang, X. Li, W. Song, *Journal of Materials Science: Materials in Electronics* **2018**, DOI 10.1007/s10854-018-0480-4.
- [200] W.-R. Huang, Z. He, J.-L. Wang, J.-W. Liu, S.-H. Yu, *iScience* **2019**, *12*, 333.
- [201] P. Li, J. Ma, H. Xu, X. Xue, Y. Liu, *J. Mater. Chem. C* **2016**, *4*, 3581.
- [202] N. Tiwari, A. Ankit, M. Rajput, M. R. Kulkarni, R. A. John, N. Mathews, *Nanoscale* **2017**, *9*, 14990.
- [203] X. Shi, W. Xu, J. Zhang, R. Wang, X. Li, W. Shen, G. Chen, X. Fang, W. Song, *Materials Research Express* **2019**, *6*, 095069.
- [204] H.-Y. Lu, C.-Y. Chou, J.-H. Wu, J.-J. Lin, G.-S. Liou, *Journal of Materials Chemistry C* **2015**, *3*, 3629.
- [205] Z. R. Ramadhan, J. W. Han, D. J. Lee, S. A. N. Entifar, J. Hong, C. Yun, Y. H. Kim, *Materials Research Letters* **2019**, *7*, 124.
- [206] J. Li, S. Qi, J. Liang, L. Li, Y. Xiong, W. Hu, Q. Pei, *ACS Applied Materials & Interfaces* **2015**, *7*, 14140.
- [207] F. S. F. Morgenstern, D. Kabra, S. Massip, T. J. K. Brenner, P. E. Lyons, J. N. Coleman, R. H. Friend, *Applied Physics Letters* **2011**, *4*, 183307.
- [208] V. H. Nguyen, J. Resende, D. T. Papanastasiou, N. Fontanals, C. Jiménez, D. Muñoz-Rojas, D. Bellet, *Nanoscale* **2019**, *11*, 12097.
- [209] D. Muñoz-Rojas, V. H. Nguyen, C. Masse de la Huerta, S. Aghazadehchors, C. Jiménez, D. Bellet, *Comptes Rendus Physique* **2017**, *18*, 391.
- [210] V. H. Nguyen, J. Resende, C. Jiménez, J.-L. Deschanvres, P. Carroy, D. Muñoz, D. Bellet, D. Muñoz-Rojas, *Journal of Renewable and Sustainable Energy* **2017**, *9*, 021203.
- [211] S. Aghazadehchors, V. H. Nguyen, D. Muñoz-Rojas, C. Jiménez, L. Rapenne, N. D. Nguyen, D. Bellet, *Nanoscale* **2019**, *11*, 19969.
- [212] H.-G. Cheong, J.-H. Kim, J.-H. Song, U. Jeong, J.-W. Park, *Thin Solid Films* **2015**, *589*, 633.
- [213] H. Chen, L. Wang, J. Li, Y. Yu, X. Bi, *Materials Letters* **2018**, *217*, 52.
- [214] B. Sharma, J.-S. Kim, A. Sharma, *Microelectronic Engineering* **2019**, *205*, 37.
- [215] J. Kang, Y. Jang, Y. Kim, S.-H. Cho, J. Suhr, B. H. Hong, J.-B. Choi, D. Byun, *Nanoscale* **2015**, *7*, 6567.
- [216] H. Khachatryan, M. Kim, H.-J. Seok, H.-K. Kim, *Materials Science in Semiconductor Processing* **2019**, *99*, 1.
- [217] D.-H. Kim, K.-S. Cho, H.-K. Kim, *Scientific Reports* **2017**, *7*, DOI 10.1038/s41598-017-02711-2.
- [218] M. K. Roul, S. K. Pradhan, K. D. Song, M. J. Bahoura, *Journal of Materials Science* **2019**, *54*, 7062.
- [219] T.-W. Kang, S. H. Kim, C. H. Kim, S.-M. Lee, H.-K. Kim, J. S. Park, J. H. Lee, Y. S. Yang, S.-J. Lee, *ACS Applied Materials & Interfaces* **2017**, *9*, 33129.
- [220] G. Kim, J. W. Lim, C. Yeon, T. Kim, H. C. Lee, S. J. Yun, *Journal of Alloys and Compounds* **2019**, *774*, 1092.
- [221] H. Im, E. Y. Jang, A. Choi, W. J. Kim, T. J. Kang, Y. W. Park, Y. H. Kim, *ACS Applied Materials & Interfaces* **2012**, *4*, 2338.
- [222] C. Hudaya, B. J. Jeon, J. K. Lee, *ACS Appl. Mater. Interfaces* **2015**, *7*, 57.
- [223] K.-D. Kim, T. Pfadler, E. Zimmermann, Y. Feng, J. A. Dorman, J. Weickert, L. Schmidt-Mende, *APL Materials* **2015**, *3*, 106105.
- [224] Y. Cheng, H. Zhang, R. Wang, X. Wang, H. Zhai, T. Wang, Q. Jin, J. Sun, *ACS Applied Materials & Interfaces* **2016**, *8*, 32925.
- [225] R. Singh, R. Kuzhikkali, N. Shet, N. Sekarapandian, G. Kizhedath, M. Arumugum, SABIC Tech Center, **2016**, p. 9.

- 2113 [226] B. Vandecastelle, *Heated window for refrigerated showcase and method of*
 2114 *manufacturing same*, **1992**, EP0502775.
- 2115 [227] “Heater Circuits and LCD monitors,” can be found under
 2116 <https://www.allflexinc.com/blog/heater-circuits-and-lcd-monitors/>, **2015**.
- 2117 [228] “Transparent Heaters and LCD Heaters,” can be found under
 2118 [http://touchinternational.com/products/touch-display-enhancements/transparent-](http://touchinternational.com/products/touch-display-enhancements/transparent-heaters/)
 2119 [heaters/](http://touchinternational.com/products/touch-display-enhancements/transparent-heaters/), **n.d.**
- 2120 [229] S.-S. Yoon, D.-Y. Khang, *ACS Applied Materials & Interfaces* **2016**, 8, 23236.
- 2121 [230] L. Veeramuthu, B.-Y. Chen, C.-Y. Tsai, F.-C. Liang, M. Venkatesan, D.-H. Jiang, C.-
 2122 W. Chen, X. Cai, C.-C. Kuo, *RSC Advances* **2019**, 9, 35786.
- 2123 [231] S.-W. Kim, B. W. An, E. Cho, B. G. Hyun, Y.-J. Moon, S.-K. Kim, J.-U. Park, *Nano*
 2124 *Letters* **2018**, 18, 3865.
- 2125 [232] W. Cheong, Y. Kim, J. Lee, C. Hong, H. Choi, Y. Kwak, Y. J. Kim, Y. S. Kim,
 2126 *Advanced Materials Technologies* **2019**, 4, 1800550.
- 2127 [233] Y. Cheng, X. Zhang, C. Fang, J. Chen, Z. Wang, *Journal of Materials Science &*
 2128 *Technology* **2018**, 34, 2225.
- 2129 [234] Y. Gao, H. Luo, Z. Zhang, L. Kang, Z. Chen, J. Du, M. Kanehira, C. Cao, *Nano Energy*
 2130 **2012**, 1, 221.
- 2131 [235] Z. Shao, X. Cao, H. Luo, P. Jin, *NPG Asia Materials* **2018**, 10, 581.
- 2132 [236] P. Liu, L. Liu, K. Jiang, S. Fan, *Small* **2011**, 7, 732.
- 2133 [237] M. Li, S. Ji, J. Pan, H. Wu, L. Zhong, Q. Wang, F. Li, G. Li, *J. Mater. Chem. A* **2014**,
 2134 2, 20470.
- 2135 [238] Q. Huang, W. Shen, X. Fang, G. Chen, J. Guo, W. Xu, R. Tan, W. Song, *RSC*
 2136 *Advances* **2015**, 5, 45836.
- 2137 [239] S. Yao, J. Cui, Z. Cui, Y. Zhu, *Nanoscale* **2017**, 9, 3797.
- 2138 [240] Xing Liang, S. A. Boppart, *IEEE Transactions on Biomedical Engineering* **2010**, 57,
 2139 953.
- 2140 [241] Y. Liu, M. Pharr, G. A. Salvatore, *ACS Nano* **2017**, 11, 9614.
- 2141 [242] M. Amjadi, K.-U. Kyung, I. Park, M. Sitti, *Advanced Functional Materials* **2016**, 26,
 2142 1678.
- 2143 [243] S. Bagherifard, A. Tamayol, P. Mostafalu, M. Akbari, M. Comotto, N. Annabi, M.
 2144 Ghaderi, S. Sonkusale, M. R. Dokmeci, A. Khademhosseini, *Advanced Healthcare*
 2145 *Materials* **2016**, 5, 175.
- 2146 [244] R. C. Webb, A. P. Bonifas, A. Behnaz, Y. Zhang, K. J. Yu, H. Cheng, M. Shi, Z. Bian,
 2147 Z. Liu, Y.-S. Kim, W.-H. Yeo, J. S. Park, J. Song, Y. Li, Y. Huang, A. M. Gorbach, J.
 2148 A. Rogers, *Nature Materials* **2013**, 12, 938.
- 2149 [245] R. C. Webb, R. M. Pielak, P. Bastien, J. Ayers, J. Niittynen, J. Kurniawan, M. Manco,
 2150 A. Lin, N. H. Cho, V. Malyrchuk, G. Balooch, J. A. Rogers, *PLOS ONE* **2015**, 10,
 2151 e0118131.
- 2152 [246] J.-H. Park, J.-W. Lee, Y.-C. Kim, M. R. Prausnitz, *International Journal of*
 2153 *Pharmaceutics* **2008**, 359, 94.
- 2154 [247] S. F. Nadler, K. Weingand, R. J. Kruse, *Pain physician* **2004**, 7, 395.
- 2155 [248] H. Cramer, C. Baumgarten, K.-E. Choi, R. Lauche, F. J. Saha, F. Musial, G. Dobos,
 2156 *European Journal of Integrative Medicine* **2012**, 4, e371.
- 2157 [249] S. K. Barua, M. Z. A. Chowdhury, *Chattagram Maa-O-Shishu Hospital Medical*
 2158 *College Journal* **2014**, 13, 60.
- 2159 [250] H. Lee, *Medical Science Monitor* **2013**, 19, 661.
- 2160 [251] S. Michlovitz, L. Hun, G. N. Erasala, D. A. Hengehold, K. W. Weingand, *Archives of*
 2161 *Physical Medicine and Rehabilitation* **2004**, 85, 1409.
- 2162 [252] H. Zhai, R. Wang, X. Wang, Y. Cheng, L. Shi, J. Sun, *Nano Research* **2016**, 9, 3924.
- 2163 [253] T. Q. Trung, N.-E. Lee, *Journal of Materials Chemistry C* **2017**, 5, 2202.

- [254] W. Jiang, D. Niu, H. Liu, C. Wang, T. Zhao, L. Yin, Y. Shi, B. Chen, Y. Ding, B. Lu, *Advanced Functional Materials* **2014**, *24*, 7598.
- [255] R. H. Baughman, C. Cui, A. A. Zakhidov, Z. Iqbal, J. N. Barisci, G. M. Spinks, G. G. Wallace, A. Mazzoldi, D. D. Rossi, A. G. Rinzler, O. Jaschinski, S. Roth, M. Kertesz, *Science* **1999**, *284*, 1340.
- [256] T. Kimura, Y. Umehara, F. Kimura, *Soft Matter* **2012**, *8*, 6206.
- [257] R. V. Martinez, A. C. Glavan, C. Keplinger, A. I. Oyetibo, G. M. Whitesides, *Advanced Functional Materials* **2014**, *24*, 3003.
- [258] S.-E. Zhu, R. Shabani, J. Rho, Y. Kim, B. H. Hong, J.-H. Ahn, H. J. Cho, *Nano Lett.* **2011**, *11*, 977.
- [259] L. Chen, M. Weng, W. Zhang, Z. Zhou, Y. Zhou, D. Xia, J. Li, Z. Huang, C. Liu, S. Fan, *Nanoscale* **2016**, *8*, 6877.
- [260] W. Zhang, M. Weng, P. Zhou, L. Chen, Z. Huang, L. Zhang, C. Liu, S. Fan, *Carbon* **2017**, *116*, 625.
- [261] S. Walia, R. Gupta, K. D. M. Rao, G. U. Kulkarni, *ACS Applied Materials & Interfaces* **2016**, *8*, 23419.
- [262] K. C. Heo, S. H. Yu, J. H. Kwon, J. S. Gwag, *Appl. Opt., AO* **2013**, *52*, 8460.
- [263] P. Won, J. J. Park, T. Lee, I. Ha, S. Han, M. Choi, J. Lee, S. Hong, K.-J. Cho, S. H. Ko, *Nano Letters* **2019**, *19*, 6087.
- [264] L. Ou, B. Song, H. Liang, J. Liu, X. Feng, B. Deng, T. Sun, L. Shao, *Particle and Fibre Toxicology* **2016**, *13*, DOI 10.1186/s12989-016-0168-y.
- [265] M. Charehsaz, S. Coskun, H. E. Unalan, R. Reis, S. Helvacioğlu, A. K. Giri, A. Aydin, *Toxicological & Environmental Chemistry* **2017**, *99*, 837.
- [266] S. G. Lehmann, D. Toybou, A.-E. Pradas del Real, D. Arndt, A. Tagmount, M. Viau, M. Safi, A. Pacureanu, P. Cloetens, S. Bohic, M. Salomé, H. Castillo-Michel, B. Omaña-Sanz, A. Hofmann, C. Vulpe, J.-P. Simonato, C. Celle, L. Charlet, B. Gilbert, *Proceedings of the National Academy of Sciences* **2019**, *116*, 14893.
- [267] D. Mohanta, S. Patnaik, S. Sood, N. Das, *Journal of Pharmaceutical Analysis* **2019**, DOI 10.1016/j.jpha.2019.04.003.
- [268] Y. Tabei, A. Sonoda, Y. Nakajima, V. Biju, Y. Makita, Y. Yoshida, M. Horie, *Metallomics* **2015**, *7*, 816.